SISSA - SCUOLA
INTERNAZIONALE
SUPERIORE
DI STUDI AVANZATI
TRIESTE
Strada Costiera 11

ISAS - INTERNATIONAL SCHOOL FOR ADVANCED STUDIES

THESIS SUBMITTED FOR THE DEGREE

OF

"MAGISTER PHILOSOPHIAE"

THE LUMINOSITY-DIAMETER RELATION FOR ELLIPTICAL GALAXIES

Candidate:

Armando PISANI

Supervisor:

Prof. D.W. SCIAMA

October 1988

TRIESTE

The luminosity-diameter relation for elliptical galaxies

A. Pisani
SISSA-International School for Advanced Studies, Trieste

September 2, 1988

To my sisters Antonella and Sabrina

Contents

Acknowledgements

There are many people I have to thank for the help they continuously gave me. First I thank Professors D.W. Sciama, Giuliano Giuricin, Fabio Mardirossian and Marino Mezzetti both for their fundamental scientific support to my work and their friendly encouragement. Other S.I.S.S.A. students such as José Acosta, Phil Cuddeford, Mauro Orlandini and many others gave me some very useful suggestions and often they spent many hours in fruitful discussions. Finally the moral support of Antonella Diviacchi, my family and my friends has been the best *environment* for my work.

Introduction

The motivation for the present work aries from different considerations. I want mainly to discuss the well-known relation that exists between the total luminosity of elliptical galaxies and their diameter. [1] Any relation of this kind will have an important meaning in theories of galaxy formation and evolution. Besides this fact, the cosmological importance of ellipticals gives a good reason to study their reliability as standard candels.

I will attempt to throw more light upon the debated question of the dependence of the luminosity-diameter relation for elliptical galaxies on the environment. First of all, I am going to review what is generally taken as the indicator of the total luminosity and diameter of ellipticals, the problems related to the measurements and what the theory suggests about this question. Before discussing our results I will briefly consider the issues rised by previous studies. Finally we will discuss what I obtained and the possible future evolution of this work.

[1] For the moment, please accept these very usual words and guess their meaning. We will define them in a more precise way later.

Chapter 1

General properties of elliptical galaxies

In this chapter we [1] will briefly consider some of the main observational characteristics of elliptical galaxies in order to obtain an approximate picture of the information coming from these physical systems.

We will discuss the parameters indicating the dimensions and the energy output of the galaxies, since these are the quantities directly involved in the main part of this work.

1.1 Classification : qualitative morphology

When we speak of elliptical galaxies, we are naturally driven to consider first the morphological properties defining this class of objects. In the most widely used classification scheme due to Hubble (1936), we find the elliptical galaxies on the left side of this scheme, known as the tuning-fork diagram (see fig. 1.1). In fact elliptical galaxies are also known as early-type galaxies for this reason. These galaxies appear smooth, structureless and their shape varies from spheroidal to highly elliptical . Since ellipticals do not contain a fundamental plane (whereas disk galaxies do) we can not know the orientation of these galaxies and what we see is just the projected image on the sky. It is generally assumed that two of the three orthogonal axes of the ellipsoid are equal even though the possibility of a triaxial ellipsoid can not be ruled out (Bertola 1981). Denoting the semimajor and semiminor axes of the projected ellipsoid by a and b respectively, we can then use $n = 10(1 - b/a)$ to designate a sequence of ellipticals of different shape: E0 ... E7. For example an E0 galaxy appears spherical, while an E5 has the major axis twice as long as the minor axis. In practice this classification is somewhat approximate, since the ellipticity of galaxies is not strictly constant in radius. The most flattened galaxies have $b/a \simeq 0.3$ and are defined as E7 (see fig. 1.2). We must bear in mind that a galaxy that looks like an E0 may actually be an E7 seen along the direction of the symmetry axis. It is possible to estimate

[1] In the first two chapters the pronoun "we" will be used, whereas in chapter three which has an original content, it is more appropriate to use the singular "I".

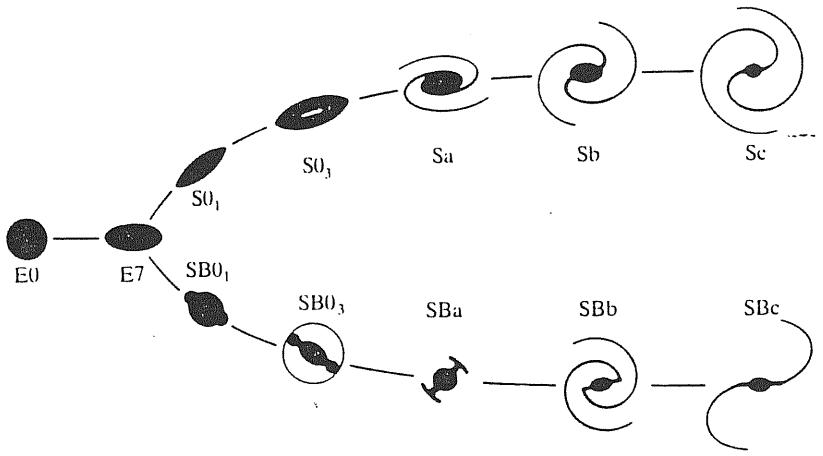

Figure 1.1: The Hubble turning-fork diagram. The diagram shown here differs from the Hubble's original in that it shows various stages of lenticulat galaxies interposed between the ellipticals and spirals (Mihalas and Binney 1981).

the likelihood of this phenomenon statistically by assuming that all ellipticals are randomly oriented; anyway, the most relevant observational fact to stress is the lack of structure in normal elliptical galaxies. In fig. 1.3 we can see the relative frequency of ellipticals compared with other types of galaxy.

1.2 Quantitative classification : the surface brightness distribution

A more quantitative approach to ellipticals starts from the observations and the study of the projected surface brightness distribution $\mathcal{I}(r,\theta)$ (generally given in $mag.arcsec^{-2}$) depending on the polar coordinates r and θ taking as origin the center of the galaxian image and referring the angle to a given direction. Studying this function we can obtain a lot of information on the physical state of these systems: the total light output, the shape and the dimension of the galaxies. We will consider some of the main features of different functions of this kind which are present in the literature.

1.2.1 Azimuthal brightness distribution

We will first consider the variation of the surface brightness $\mathcal{I}(r,\theta)$ with the angle θ around the nucleus. Unfortunately this kind of distribution is not as well known as the radial one. A crucial factor determining the angular distribution is the inclination of the galaxy's three dimensional form with

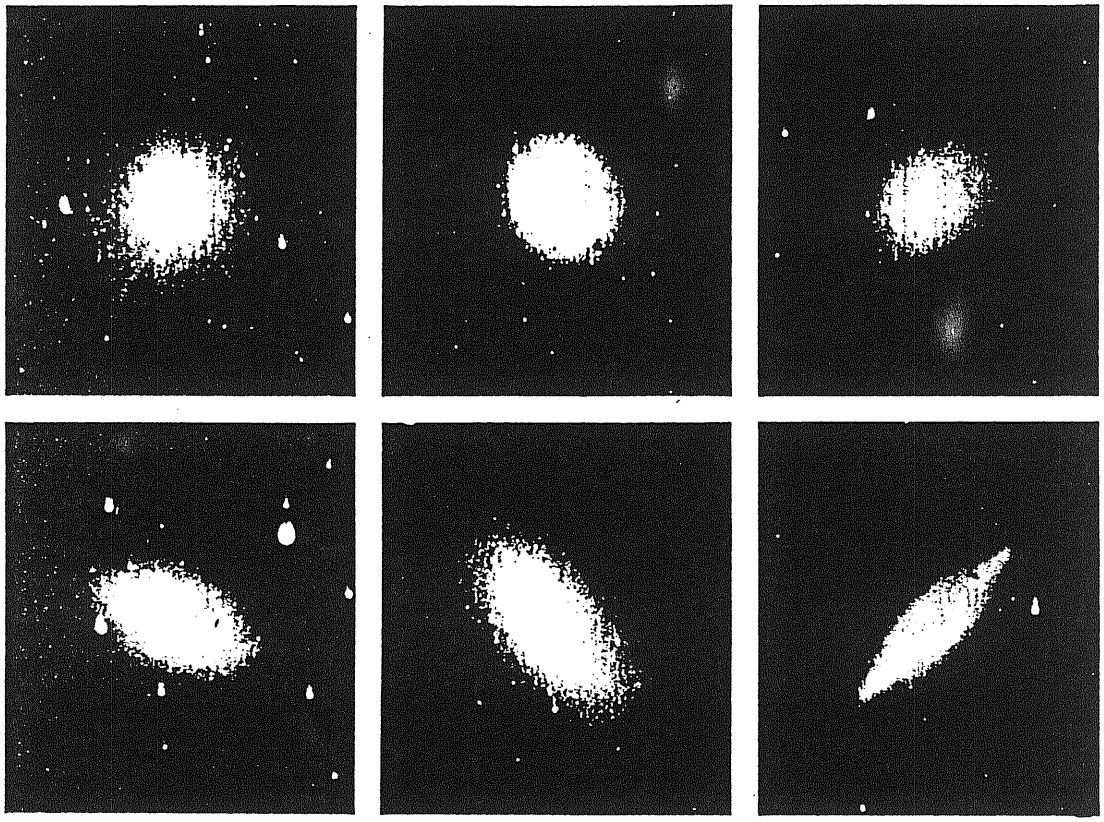

Figure 1.2: Elliptical galaxies: (from top left to bottom right) (a) NGC 4636, type E0/$S0_1$; (b) NGC 4271, type E1; (c) NGC 4406, type E3; (d) NGC 4697, type E5, (e) NGC 3377, type E6, (f) NGC 3115, type E7/$S0_1$. (Mihalas and Binney 1981)

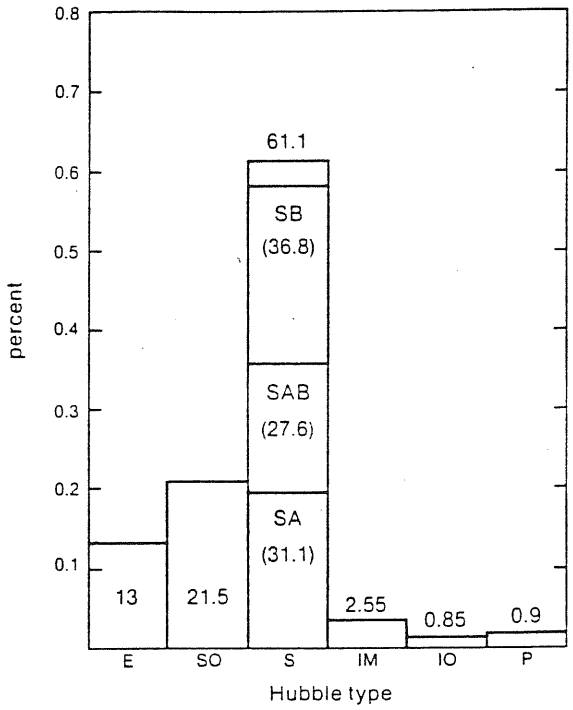

Figure 1.3: Frequancy distribution of galaxies among the Hubble types. The bin for spirals is devided into subclasses A, AB, B; numbers in paretheses are the percentages of class S (Bowers and Deeming 1984).

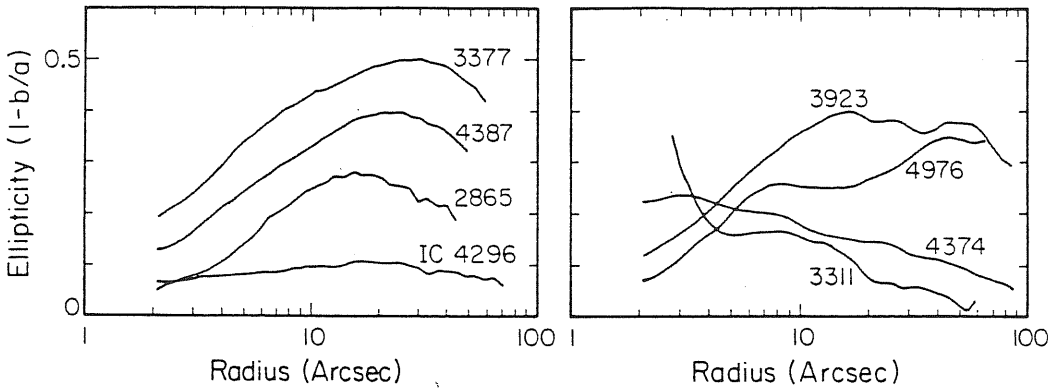

Figure 1.4: Ellipticity profiles for some NGC and IC galaxies (Jedrzejewski 1987).

the line of sight. For example, the image of a very flat galaxy can be either round or highly elongated, depending on whether the galaxy is seen face-on or edge-on. In general it is quite hard to distinguish between intrinsic and extrinsic components affecting the observed distribution. In any case, it is possible to say that the $\mathcal{I}(r,\theta)$ of elliptical galaxies is smooth and that their apparent isophotes (i.e.: contours of equal brightness on the sky) form a series of nested ellipses. In fact it is possible to fit the azimuthal distribution of brightness (given by an equation of the kind: $\mathcal{I}(r,\theta) = const$) with an equation such as:

$$\frac{1}{r^2} = C - A\cos(2\theta) - B\sin(2\theta) \tag{1.1}$$

as was done by Strom and Strom (1978) and Mihalas and Binney (1981). This is the polar equation of an ellipse having axial ratio $q = ((1-(A^2+B^2)/C)/(1+(A^2+B^2)/C))^{1/2}$, semimajor axis length $a = (C-(A^2+B^2)^{1/2})^{-1/2}$ and principal axis position angle $\phi = \arctan(B/A)$. There is more than one procedure to analyse the brightness measurements over the image of the galaxy allowing one to find the deviation of isophotes from perfect ellipses. It is possible to find that the actual isophotes are egg-shaped or box-like depending on the sign of the coefficients in the fitting equation. It has also been found that more or less all deviations from perfect ellipses are no larger than can be accounted for, by the noise in the data (Mihalas and Binney 1981).

Another quantity of dynamical interest is the dependence of ellipticity of isophotes $\varepsilon \equiv 1 - b/a = 1 - q$ with radius r. After having made the necessary correction for the seeing effect close to the center, ε is sometimes an increasing function of r, sometimes decreasing and sometimes constant (see fig. 1.4). The reason for such different kinds of behaviour has not yet been well understood. A subject of great interest is the major axis position

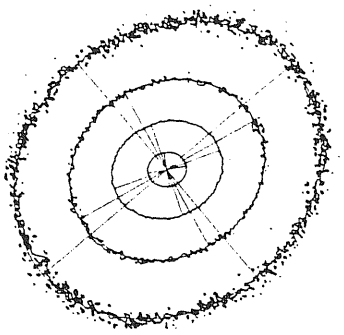

Figure 1.5: Contour map with major and minor axis (NGC 1549) (Jedrzejewski 1987).

angle, because, like the ellipticity, it often shows a significant variation with radius. This implies that the elliptical isophotes are frequently *twisted* with respect to one another on the sky (see fig. 1.5). The importance of this phenomenon is that it strongly suggests that the galaxy in question does not posseses an axis of rotational symmetry but is rather a triaxial body (not a figure of rotation). In this case and if the galaxy possesses an ellipticity gradient, then the twist of the isophote may result when the galaxy is seen in projection along an axis that does not coincide with one of the principal axes.

Finally the question of whether the ellipticals resemble more prolate or oblate spheroids is still under debate, even though several tests have been proposed (Marchant and Olsen 1979; Richstone 1979; Lake 1979; Bertola 1981). Two recent surveys show that elliptical galaxies populate a planar distribution in global logarithmic parameter space (R_e, σ_e, I_e). I_e is the effective surface brightness, σ_e is a globally averaged velocity dispersion and R_e is the effective radius (these quantities will be discussed later). The effect of other variables such as ellipticity, aspect angle and rotation seems to be small (Faber et al. 1986).

1.2.2 Radial brightness distribution

The surface brightness distribution is generally expressed in $mag.arcsec^{-2}$ as $\mathcal{I}(r,\theta) = I_c \cdot \mathcal{F}(r,\theta)$, where $I_c = \mathcal{I}(0,\theta)$ is the central value and $\mathcal{F}$ is an dimensionless function of the distance r from the center of the galaxy image, and θ is the azimuthal angle. When computing the total luminosity of a galaxy using eq. 1.6, a simpler version is adopted: the so called *circularized*

equivalent radial brightness profile $I(r) = I_c f(r)$ [2] In other words we consider the profile that an En galaxy would have if it were seen as $E0$ with the same total luminosity:

$$L_T = \int_0^{+\infty} \int_0^{2\pi} I_c \mathcal{F}(r,\theta) r dr d\theta = 2\pi I_c \int_0^{+\infty} f(r) r dr \tag{1.2}$$

so:

$$f(r) = < \mathcal{F}(r,\theta) >_\theta \equiv \frac{1}{2\pi} \int_0^{2\pi} \mathcal{F}(r,\theta) d\theta \tag{1.3}$$

and

$$I(r) = < \mathcal{I}(r,\theta) >_\theta \tag{1.4}$$

is the equivalent profile. We will now review some of the circularized functions.

The Hubble Law This was proposed by Hubble (1930) to describe the average of 15 ellipticals he measured:

$$I(r) = \frac{I_{0H}}{(1 + r/a)^2} \tag{1.5}$$

Here I_{0H} is the central value and a is a scale length at which I decreases by a factor 4. In the fits with observational data this law appears in logarithmic form as:

$$\mu(r) = B_{0H} + 5 \log(1 + r/a) \tag{1.6}$$

where $B_{0H} = -2.5 \log(I_{0H})$ and $\mu(r) = -2.5 \log(I(r))$.

While accurately describing the cores of ellipticals, this law breaks down at large radii where the galaxy surface brightness falls more rapidly than an r^{-2} power law. In fact Oemler (1976) found a gradient in the $\log I$ vs. $\log r$ plot that increased steadily with radius. The bad behaviour of this law at large radii is also indicated by the fact that when we try to compute the total amount of light coming from the galaxy we find a divergence:

$$L_T \equiv 2\pi I_{0H} \int_0^{+\infty} \frac{r dr}{(1 + r/a)^2} \tag{1.7}$$

so:

$$L_T = 2\pi a^2 I_{0H} [\frac{1}{1+x} + \log(1+x)]_0^{+\infty} \rightarrow +\infty \tag{1.8}$$

where $x = r/a$. Several attempts have been made to improve the Hubble law.

[2] Generally the introduction of a smoothed profile involves some problems as we are shall see in section 1.6

deVaucouleurs Law Like the Hubble law, this is a strictly empirical relation and has no theoretical grounds:

$$\log I(r) = \log I_e - 3.33((r/r_e)^{1/4} - 1) \tag{1.9}$$

Here r_e and I_e are two scale factors that in the ideal case of a perfect spherical E0 structure represent the radius containing half the total light, and the brightness at r_e, respectively. It is easy to compare this relation with observations since it is a straight line in a $\log I$ vs. $\log r^{1/4}$ plot and has no free parameters. As a first observation, we must note that in this case the computed total luminosity does not diverge, but:

$$L_T = \int_0^{+\infty} 2\pi I(r) dr = 7.22\pi r_e^2 I_e \tag{1.10}$$

Even if the fits with observational data are very good, some problems still remain.

As Holmberg (1958) and Oemler (1976) pointed out, the main weakness of this law is the lack of free parameters as it has just two scale factors and a fixed shape. A two-parameter law is not flexible enough to permit a complete description of the luminosity distribution in elliptical galaxies. In fact a comparison with observations shows that while this law fits the profiles of many galaxies fairly well, many others either have a too pronounced r^{-2} power law section or have envelopes which are too severely truncated by this law. A more succesful formula should be able to differentiate galaxies of different intrinsic oblateness (and different apparent ellipticity). A formula with at least three independent parameters seems to be indicated. Such a law may come from *King models* (King 1966).

King law The aim of these models was to describe the distribution of density in globular clusters; they give excellent fits to most small galaxies and also to large galaxies such as NGC 4816 and NGC 4841. However, the profiles of many large galaxies do have an extended r^{-2} segment described well by the Hubble law, but not by King models, which tend towards an isothermal r^{-1} projected light distribution.

An analytical expression for the King law (first obtained empirically) is:

$$I(r) = k[(1 + (r/r_c)^2)^{-1/2} - (1 + (r_t/r_c)^2)^{-1/2}]^2 \tag{1.11}$$

Two of the three constants in this expression, have the role of scale factors, say k and r_c, and the third r_t is a free parameter. The quantity r_c is referred to, as the *core radius*, while r_t is the *tidal radius* and is the distance from the centre to the point where the surface brightness drops to zero. Typical values of r_t/r_c range from 100 to 200 for giant ellipticals (Binggeli et al. 1984). We note that, the King model cannot fit all the observations: in fact r_c is in general quite small and then hard to measure because of the seeing effect, while r_t *may* depend on the gravitational interaction of the galaxy with its neighborhood.

Oemler's modified Hubble law A proposal due to Oemler (1976) looks like:

$$I(r) = I_0 \frac{\exp[-(r/\alpha)^2)]}{(1 + r/\beta)^2} \tag{1.12}$$

which is the Hubble law modified by an exponential cut off. As it is easily seen it has the main features of the King model: a finite central intensity, a core radius β, a cutoff radius α (Kormendy 1977; Binggeli et al. 1984).

The main advantage of this formula is that it can fit the brightest galaxies that are not fitted by the King model especially in the outermost parts. An extensive description of the features of this formula and of its relation with King parameters is nicely given by Binggeli et al. (1984). In relation to this expression it is often introduced a quantity $L_{rd} = I_0\,\beta^2$, called the reduced luminosity, which characterizes the power law section of the galaxy profile and is independent of core and envelope size (i.e.: $L_T = L_{rd} f(\alpha/\beta)$, with usually $1 < f < 25$). The relative reduced magnitude M_{rd} is obtained in the usual way and is related to the total magnitude by (Oemler 1976): $M_{V,tot} = -7.36 + 0.79 \cdot M_{V,rd}$.

1.3 Total luminosity

Once we know the function $\mathcal{I}(r, \theta)$ we can find the total luminosity of the galaxy as:

$$L_T \equiv \int_0^{+\infty} \int_0^{2\pi} \mathcal{I}(r, \theta) r d\theta dr \tag{1.13}$$

where in practice the integration on r is made until the background is reached. Then the definition of L_T will be better expressed as:

$$L_T \equiv \int_0^{R_{bg}} \int_0^{2\pi} \mathcal{I}(r, \theta) r d\theta dr \tag{1.14}$$

where $R_{bg}$is the smallest r for which $\mathcal{I}(R_{bg}, \theta)$ gives the value of the background sky. In general eq. 1.13 is used instead of eq. 1.14. If we are dealing with an E0 spherical galaxy, or using circularized profiles, then:

$$L_T = 2\pi \int_0^{+\infty} I(r) r dr \tag{1.15}$$

or if we have an elliptical galaxy with constant ellipticity ε, then, using elliptical coordinates:

$$L_T = 2\pi(1 - \varepsilon) \int_0^{+\infty} I(r) r dr. \tag{1.16}$$

If we consider a law for $I(r)$ such as the Hubble or deVaucouleurs law:

$$I(r) = I_0 f(r/r_0) \tag{1.17}$$

containing only two scale factors, we will obtain:

$$L_T = 2\pi I_0 r_0^2 \int_0^{+\infty} f(x) x dx \tag{1.18}$$

where $x \equiv r/r_0$. As an example, if we consider the deVaucouleurs law (eq. 1.2) we obtain: $L_T \propto I_e r_e^2$ or in a log – log plot:

$$\log L_T = 2 \log r_e + \log I_e + const \tag{1.19}$$

If our hypothesis is correct, we expect to find a straight line with slope 2 in the graph $\log L_T$ vs. $\log r$ if $I_e = const$. We will discuss this subject later.

In the case of an elliptical galaxy with non-zero eccentricity, the value of L_T will be slightly modified, from eqq. 1.2, 1.8, 1.10:

$$L_T = 2\pi(1-\varepsilon) I_e r_e^2 \int_0^{+\infty} f(x) x dx \tag{1.20}$$

so the shape of the galaxy does not affect the slope B_e,defined in general as:

$$B_0 = \frac{d \log L_T}{d \log r_0} \tag{1.21}$$

We must note that these quantities for the total luminosity of a galaxy are ill-defined from an observational point of view, since nobody can integrate a function over the whole sky. What we can actually deal with is an extrapolation of such an integral called *total magnitude*: $M_T = -2.5 \log L_T + const$. It is this number that we find in the catalogues. We will see later in this chapter how observers work out this quantity.

1.4 Diameter indicators

From observations it is easy to see that the density gradients in the outermost parts of galaxies are very small; this fact causes a difficulty in defining the the major and minor diameters of galaxies. The problem is somewhat simplified by deciding either to refer diameters to a given isophote or that the boundary defined by the diameter should enclose a certain portion of the total luminosity. The first definition applies to all diameters that are derived from the direct measurements of photographic images, provided that the plate material is homogeneous (constant limiting magnitude: a condition naturally satisfied in CCD images). The second definition requires a complete determination of the projected surface luminosity distribution out to quite large distances from the center of the galaxian image. One of the first diameters introduced by Holmberg (1958) satisfied the first definition and was really the isophotal diameter corresponding to the 26.5 $mag.arcsec^{-2}$.

In order to apply these definitions we must know the behaviour of $I(r)$ which can be derived directly from the corrected growth curve. Suppose that the background has been properly subtracted and that there is no contamination due to nearby objects. Then, from the observational multi-aperture photometry, we can obtain the so called *growth curve*: L_r i.e.: the

total luminosity enclosed within a distance r from the center of the projected image of the galaxy. In mathematical form:

$$L(r) = 2\pi \int_0^r I(a)ada \tag{1.22}$$

and:

$$I(r) = \frac{1}{2\pi r}\frac{dL(r)}{dr} \tag{1.23}$$

The growth curve will approach a horizontal asymptote which defines the total luminosity as:

$$L_T = \lim_{r\to+\infty} L(r) \tag{1.24}$$

We must stress that by using the growth curve to evaluate the total luminosity or the isophotal diameter some systematic errors can be introduced. Actually deVaucouleurs (RC2) proposed different *standard curves* for different morphological types of galaxies. If we have a spherical galaxy then an $r^{1/4}$ law will give the standard curve of growth for E0, but when we try to calculate the L_T for a very flattened galaxy such as $T = -5$ or $T = -7$ (T is the Hubble morphological number) we must remember eq. 1.8 and so, if we use the E0 standard curve (the $r^{1/4}$ law) then we overestimate L_T, and the error will increase with the flattening. In other words:

$$L_T(estimated) = \frac{L_T(true)}{(1-\varepsilon)} \tag{1.25}$$

In a similar way we overestimate the diameter of the galaxy by the factor $\sqrt{(1-\varepsilon)}$

Another cautionary tale, as pointed out by Binggeli et al (1984), is connected with the background subtraction that is often incorrect, so that the growth curve has no proper asymptote. A correction could always be applied to the background level to give a flat approach to total intensity (see fig. 1.6). They claim that such corrections never exceed 1 %. It is important to remember that any correction must be applied to the growth curve before the profile $I(r)$ is obtained by differentiation.

We can now apply the definition of diameters and say that if we fix a value of the surface brightness I_0, we can obtain an *isophotal diameter* by inverting the $I(r)$ law, i.e.:

$$I_0 = I(D_0/2) \tag{1.26}$$

or, since $\mu(r) \equiv -2.5 \log I(r)$, we can fix μ_0 to determine D_0.

One of the most widely used diameters of this kind is the *Standard Isophotal Diameter* of RC2: the diameter one estimates that the $25 mag.arcsec^{-2}$ contour would have if the galaxy was seen face-on and unobscured by dust. In a later section of this chapter we will see the necessary corrections to the observed angular diameters $\log D_{25}$ in order to obtain the absolute quantities.

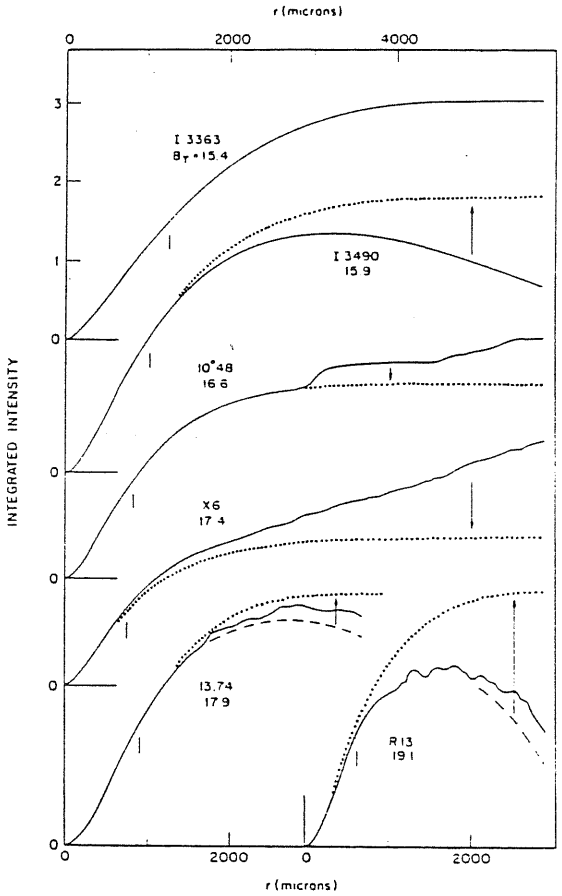

Figure 1.6: Selection of growth curves showing typical background problems. The solid lines are the measured growth curves. Dashed lines in the faintest examples show corrections due to overlapping star images. Arrows show final corrections to the adopted curve (dots) that has a proper horizontal asymptote. The ordinate is in direct intensity units (scale arbitrary). The effective radius containing half of the light is indicated by vertical ticks (Binggeli et al. 1984).

Following the second definition of diameter indicators, we will consider the *effective diameter* D_e $(= 2R_e)$ [3] as the diameter of the equivalent circular galaxy containing half of the total light emitted by the galaxy, mathematically:

$$L(D_e) = \frac{1}{2} L_T \tag{1.27}$$

It is worth noting that if we suppose a galaxy has a deVaucouleurs luminosity profile (eq. 1.2), then $R_e (= D_e/2)$ is exactly the length scale contained in that law.

We can measure R_e in essentially two ways: following Strom and Strom (1978), we can fit the observed brightness profile $I(r)$ with a deVaucouleurs law (eq. 1.2), adjusting the two scale factors I_e and r_e in order to have the best fit, and so we will call this the effective radius r_e. As was pointed out by Capaccioli (1987), what we actually measure in this way is $r_e^{1/4}$, so this kind of procedure gives an ill-defined quantity from the point of view of observations. This problem is generally avoided by adopting the general definition of R_e as the half effective aperture (i.e.: D_e), obtained via the growth curve (RC2). This parameter is not related to the fitting law and, from a methodological point of view, it is more suitable to seek correlations with other observed quantities like effective surface brightness, total luminosity and so on (Binggeli et al. 1984; Romanishin 1986). On the other hand, as Djorgovski and Davis (1987) pointed out, it would be better to deal with a radial scale length possibly independent of the magnitude or surface brightness. So these authors prefer to obtain the effective radius via a direct fit with the profile rather than via the curve of growth.

The last diameter indicator we want to mention is the so called D_n, which was introduced by Burstein et al. (1987). It is a new photometric diameter which can be measured, as they claim, with greater accuracy than other diameters from few observations. D_n is the diameter of the circular aperture within which the total mean surface brightness is chosen to be Σ_n. Mathematically:

$$\frac{L(D_n)}{\pi (D_n/2)^2} = \Sigma_n \tag{1.28}$$

Using data from CCD photometry, Burstein et al. (1987) claimed that $\log D_n$ can be measured with an accuracy ≤ 0.02, while for $\log D_e$ the best accuracy was ≤ 0.03.

A property characterizing D_n is that if σ is the velocity dispersion of the galaxy, then the correlation of $\log \sigma$ with D_n has a smaller scatter than the Faber and Jackson relation (Dressler et al.1987). Neglecting the cosmological effects on D_n, it was found that $\sigma^{4/3}/D_n$ scales directly with distance and so it provides us with a very good distance indicator.

Another useful property of D_n is the following. If we suppose that all our galaxies follow the same curve of growth, then it is possible to show that

[3] There is actually a good reason to distinguish between r_e and R_e, as we are going to see

the ratio D_n/D_e is just a function of D_e. Mathematically:

$$\frac{D_n}{D_e} = f(\Sigma(D_e)) \tag{1.29}$$

where $\Sigma(D)$ is the mean surface brightness within D:

$$\Sigma(D) \equiv \frac{4L(D)}{\pi D^2} \tag{1.30}$$

In fact, if the growth curve of every galaxy is the same, then:

$$L(D) = L_T \cdot f(D/D_e) \tag{1.31}$$

since, for the definition of $\Sigma(D)$:

$$\Sigma(D) = \frac{4L_T}{\pi D^2} f(D/D_e) \tag{1.32}$$

If we take $D = D_n$ and the corresponding Σ_n so that

$$-2.5 \log \Sigma(D_n) = 20.75\, mag.arcsec^{-2} \tag{1.33}$$

then:

$$const. = \frac{4L_T}{\pi D_n^2} f(D_n/D_e) = \frac{4L_T}{\pi D_e^2} \frac{D_e^2}{D_n^2} f(D_n/D_e) \tag{1.34}$$

where $\log(const.) = 20.75/(-2.5)$ and

$$\Sigma_e \equiv \Sigma(D_e) \tag{1.35}$$

then

$$const. = \Sigma(D_e) \frac{D_e^2}{D_n^2} f(D_n/D_e) \tag{1.36}$$

finally

$$\frac{const}{\Sigma(D_e)} = \frac{D_e^2}{D_n^2} f(D_n/D_e) \tag{1.37}$$

Or, in another form:

$$\frac{D_n}{D_e} = F(D_e) \tag{1.38}$$

only. So, for this hypothesis, if we know the relation $L_T = L_T(D_e)$ we can work out also $L_T = L'_T(D_n)$. In any case, we must bear in mind that the starting hypothesis may be not completely true as it has already been discussed in this section (see eq. 1.13).

Concluding this section we will recall that if a deVaucouleurs law is to hold at any distance from the centre of the galaxy, then we should find $L_T \propto I_e R_e^2$. Considering many different galaxies, we should expect to have a set of different pairs of parameters $(I_e; R_e)$, one for each galaxy. If we choose to characterize a galaxy by the pair $(L_T; R_e)$ then, from eqq. 1.10 and 1.2 results a dependence of I_e on R_e. In other words the exponent B in

the relation $L_T \propto R_e^B$ must also depend on the relation btween I_e and R_e. If we find that $B = 2$, then : $I_e = const(R_e)$.

From observations we have the measures of Σ_e, the mean surface brightness within R_e, and remembering that for eq. 1.2:

$$L(R_e) = 2\pi R_e^2 I_e \int_0^1 f(x) x dx \tag{1.39}$$

so that:

$$\Sigma_e = 2I_e \int_0^1 f(x) x dx \tag{1.40}$$

In this way:

$$I_e \propto R_e^n \Rightarrow \Sigma_e \propto R_e^n \tag{1.41}$$

we will observe:

$$L_T \propto I_e R_e^2 \propto R_e^{2+n} \tag{1.42}$$

In other words:

$$\frac{d \ln L_T}{d \ln R_e} = \frac{\partial \ln L_T}{\partial \ln R_e} + \frac{\partial \ln L_T}{\partial \ln \Sigma_e} \cdot \frac{d \ln \Sigma_e}{d \ln R_e} = 2 + \frac{d \ln \Sigma_e}{d \ln R_e} \tag{1.43}$$

since, *only for a perfect deVaucouleurs law*, we have:

$$\frac{\partial \ln L_T}{\partial \ln R_e} = 2; \quad \frac{\partial \ln L_T}{\partial \ln \Sigma_e} = 1. \tag{1.44}$$

1.5 Observed values

We must now concentrate our attention upon the observational problems, which are not typical only for elliptical galaxies, but with generally they affect any type of galaxy.

If we want to compare magnitudes of different galaxies, we must, of course, convert the individual magnitudes, obtained from aperture photometry, to a standard total magnitude, since the observed magnitude, as we have seen, varies with aperture in a way that depends both on the apparent diameter of the galaxy and on the variation of surface brightness with radius. A standard asymptotic magnitude B_T (deVaucouleurs 1976, RC2) must therefore be calculated for each galaxy in a sample. A wide bibliography on the photometry of galaxies is presented by Davoust and Pence (1982) and is updated by Pence and Davoust (1985).

In general, for each aperture A, a B magnitude can be calculated by adding the $B - V$ colour from that aperture (or the closest aperture for which a color is available) to the V magnitude. A plot of $B(A)$ vs $\log A$ is then made for each galaxy (generally A is in units of 0.1 *arcmin* as specified in RC2). Thanks to deVaucouleurs (1977) we have a set of standard curves of growth, each of these curves based on photographic surface photometry of a number of galaxies of the same morphological type. A general method used to convert the UBV aperture photometry to standard magnitudes and colors is described by deVaucouleurs (1977), deVaucouleurs and Corwin (1977) and

in RC2. The quantities to be derived are the asymptotic magnitude B_T and the effective aperture A_e, which is the same as D_e defined in eq. 2.15. Each standard curve is a plot of $\Delta m\,[= B_T - B(A)]$ vs. $\xi\,[= \log A/A_e]$. When the best fit of the curve with the observed data is determined, the value of $B(A)$ corresponding to $\Delta m = 0$ gives the value of B_T and the $\log A$ corresponding to $\xi = 0$ gives $\log A_e$ for the studied galaxy. The standard error on the observed B_T is generally $\leq 0.05\,mag.$ The relative error in $\log A_e$ is generally greater because of the small gradient in the standard curve approaching its horizontal asymptote: a small change in Δm causes a much larger change in $\log A_e$. The best values of $\log A_e$ are known within $0.05\,dex$ (RC2).

In RC2, deVaucouleurs gives an illustration of how it is possible to obtain the standard apparent isophotal diameter $\log D_{25}$ from the observed plate of galaxies. (See the catalog introduction for any further detail.) The apparent values of $\log D_n$ are obtained in a similar fashion to effective diameters (see Burstein et al. 1987, 7S.III).

For completeness, we will spent a few words about colour indices, necessary to obtain B_T from the V magnitudes usually observed. Since most early-type galaxies show a colour gradient (even if small) (Strom and Strom 1978), the observed $B-V$ and $U-B$ colours may vary with aperture for any of these galaxies. Actually in E0 and S0 the integrated light is generally redder in the centre and bluer in the outer parts of the galaxy. This is probably due to a variation in chemical abundance (Spinard, Smith and Taylor 1972; Strom et al. 1976). Then the $B-V$ and $U-B$ colours must be corrected for the aperture effect using the relation given by deVaucouleurs and Corwin (1977). Curves of ξ vs. $\Delta(B-V)$ and $\Delta(U-B)$ can be used to convert each observed colour $(B-V)_A$, $(U-B)_A$ to the value $(B-V)_e$, $(U-B)_e$ it would have if observed through a circular aperture with diameter equal to the effective diameter (i.e.: at $\xi = 0$). Some authors (like Sadler 1984) prefer to compute the effective colours rather than the total asymptotic colours $(B-V)_T$, $(U-B)_T$ also defined by deVaucouleurs and Corwin (1977), because the apertures used were generally close to A_e, so that only small corrections ($\leq 0.01\,mag.$ in $B-V$ and $\leq 0.03\,mag.$ in $U-B$) were necessary. In any case, the difference between effective aperture colours and total colours is given in RC2, and is $0.01 \ldots 0.02 mag.$ in $B-V$ and $0.04 mag.$ in $U-B$.

From observations we can have *apparent* quantities that must be corrected for some important effects to obtain *absolute* values. One of these effects is *galactic extinction.* The observed magnitudes can be corrected to extinction-free values by subtracting the galactic extinction in B, A_B which can be calculated using the formulae given in RC2.

The determination of galactic extinction has been the subject of many debates (RC2 and Sandage and Visvanathan 1978 both give discussions of this problem). The model of galactic absorption proposed by RC2 and adopted in the data used is based upon a combination of galaxy counts, bright galaxy colours and optical-to-radio emission ratios. It allows for the dependence of A_B on galactic longitude as well as galactic latitude. The

model proposed by Sandage (1973; Sandage and Visvanathan 1978) has absorption-free windows in the region of the galactic poles ($A_B = 0\, for \mid b \mid > 50°$), and is independent of galactic longitude. Since there is evidence that galactic extinction is patchy at all latitudes (Burstein and Heiles 1982), any general model is likely to be accurate to no more than $0.1 \ldots 0.2\, mag.$ in A_B and for galaxies below 15° galactic latitude ($A_B > 0.1\, mag.$), the calculated values of A_B must be regarded as tentative only (RC2). Griersmith (1980) points out that the difference between galaxy colours, corrected using models with and without reddening at the poles, is negligible; however, there will be an overall shift of $0.2 \ldots 0.3\, mag.$ in B_T depending on the model used.

The *K-effect* on the spectral energy distribution (Humason, Mayall and Sandage 1956; Pence 1976) acts to reduce the $B-$band fluxes, hence it must change the total magnitude and the isophotal diameter. The correction has the following form:

$$\Delta_2(z,T) = K'_B cz G_{25}^{-1} \tag{1.45}$$

where (RC2)

$$G_{25}^{-1} = (\partial \mu_B / \partial \log D_{25})^{-1} = 0.12 - 0.007 \cdot T \tag{1.46}$$

and T is the morphological type, cz is the heliocentric radial velocity red-shift.

Then we have the *red-shift effect* (Hubble and Tolman 1935). If the red-shift is a Doppler effect due to cosmological expansion (Weinberg 1972), then the surface brightness of an object will decrease with increasing red-shift according to:

$$I(z) = I(0)(1+z)^{-4} \tag{1.47}$$

so this correction to isophotal diameters will depend on the luminosity distribution within the outer isophotes of the galaxian image. For $z \ll 1$ RC2 proposes a simplified relation to take this fact into account:

$$\Delta_1(z,T) = 10 G_{25}^{-1} \log(1+z) \tag{1.48}$$

To give us an idea of the degree of this quantity: for $z = 0.037$ it ranges from 0.024, for $T = -5$, and to 0.012 for $T = 6$.

To conclude this section we can report the complete expression for fully corrected apparent galactic total B magnitude and angular diameter as they are given in RC2:

$$\log D_0 = \log D_{25} - 0.235 \log R_{25} + A_B G_{25}^{-1} \tag{1.49}$$

and

$$B_T^\circ = B_T - A_B - \alpha(T) \cdot \log R_{25} - K'_B cz \tag{1.50}$$

where R_{25} is the axial ratio of the isophote at $25\, mag.arcsec^{-2}$ and for $T \leq -4 \Rightarrow \alpha(T) = 0$. Finally: $10^4 \cdot K'_B = 0.15$.

1.6 Technical problems

Observations and measurements of diffuse and faint objects usually pose severe technical problems mainly related to faint surface photometry. We will consider here some of the basic problems, but for a wider discussion, see Capaccioli and deVaucouleurs (1983) and Capaccioli (1987).

1.6.1 Calibration

The introduction of CCD technology made the calibration problem not very difficult to avoid. In fact the individual pixels of CCD's are linear over a wide range, and sensitivity variations across the detector can be readily corrected. Photographic emulsions, on the contrary, are not linear. In any case, this fact does not prevent an accurate calibration, provided that the material is carefully processed and digitalized and that the external sensitometry is properly designed. Calibration errors weigh less at faint than at bright light levels, and what can be stressed is just that calibration is not the limiting factor in photometric surface photometry.

1.6.2 Sky background level

It is well-known that as the distance from the center of the image of the galaxy increases, the surface brightness of the galaxy fades smoothly into the diffuse light of the sky. Thus the most critical step in faint surface photometry is the removal of a noisy, low spatial frequency component, which is a hundred times stronger than the outermost part of the superimposed object. We should note that it is very important to stress that an error in the adopted sky level may have strong consequences on the apparent luminosity profiles. We have already seen the systematic errors induced by a false assumption in section 1.3. Here we must note also that depending on the sign of the systematic error, a pure $r^{1/4}$ law can mimic a tidal extension or a cutoff (Capaccioli and deVaucouleurs 1983). The background problem increases significantly whenever the blank sky can not be recorded simultaneously with the galaxy, since the luminosity of the night sky is not constant (random variations can occur up to 10 % in a few minutes ; deVaucouleurs (1958)). This is a typical difficulty faced in CCD photometry of galaxies with large angular diameters. A possible way to overcome this difficulty is to perform blank sky exposures preceding and following the galaxy exposure, but this procedure has the disavantage of being time consuming. Another way to estimate the low frequency component of the local background is given by some kind of interpolation of the signal from the blank sky areas surrounding the galaxian image. Nowadays, a lot of computer procedures, inspired by the 2-D mapping pioneered by Jones et al. (1967), are in use.

1.6.3 Scattered light

In addition to the classical seeing convolution affecting high frequency structure, the light of a galactic image is also re-distributed by telescopic, atmo-

spheric and Rayleigh scattering (acting at different scales: Capaccioli and deVaucouleurs 1983). It is mostly the energy of the brighter parts which is shed into the external regions, and it is possible to verify that the contamination of the galaxian profile by scattered light increases significantly with radius until the latter becomes the dominant signal.

1.6.4 Light profiles

As Capaccioli (1987) pointed out, it is generally not a good rule to adopt the so called *equivalent profile* (see eq. 1.1) in which the surface brightness is related to a radius $r_\star$ of the corresponding circularized isophote. For purely elliptical isophotes we have $r_\star = \sqrt{ab}$. Profiles determined by the ellipse-fitting technique fall in this category. Isophotes of actual galaxies, however, are often not pure ellipses, and equivalent profiles may obscure structural details and lead to false conclusions. In other words, experience suggests that, even for apparently *bona fide* elliptical galaxies, it is better to produce at least two distinct and unsmoothed luminosity profiles along the main axes. Anyway, we must remember that this problems mainly affects studies of the outermost parts of galaxies.

1.6.5 Photometric zero-point calibration

In photometric work the zero point of the photometric scale is usually set by a comparison with photoelectric measurements. In most cases only photoelectric integrated magnitudes within centred apertures are available. The comparison is straightforward, provided that the photographic photometry has no systematic scale error, especially near the galaxy center, where the luminosity gradient is steep. This is not the case for the limiting exposures used to map the faint outer parts of galaxies, due to saturation. Therefore, the outer profiles of galaxies can only be connected by matching to photoelectrically calibrated inner profiles, if available. This procedure, needed in any case to produce the complete light distribution from different exposures, may propagate systematic errors and modify the trend of the final luminosity profile. Often this problem is complicated by the use of heterogeneous materials(plates and CCD) without a proper allowance for color equations of the various devices. The quality of the result of this procedure can not be controlled easily with photoelectric photometry, first because the data at large apertures are often old and unreliable, and second since integration tends to absorb even large errors in luminosity gradients, transforming them into a shift of the photometric zero point.

In conclusion, it is possible to say that, while detections are still possible, it is difficult, if not impossible, to obtain reliable quantitative information at brightness levels fainter than $\mu \simeq 28.5\, mag.arcsec^{-2}$. Unfotunately, due to the nature of some sources of errors, this limit is unlikely to improve significantly from future technology.

1.7 Summary

To conclude this chapter, we should remember that elliptical galaxies are quite surprising objects in that they may appear very simple at first glance, but, as we study them in a deeper way, they show some quite peculiar features.

The aim of this chapter was to give a feeling for the problems which can be found when some quantities, like total magnitudes or diameters of galaxies, are measured. These parameters may seem very straightforward, but actually deserve a certain attention because of the fact that we are dealing with more or less ill-defined quantities. Moreover, every kind of interpretation of the measurements obtained must take into account the way in which the observers obtained their numbers.

Chapter 2

Environmental and evolutionary effects on elliptical structure

We would now like to see which are the processes that can affect the global structure of an elliptical galaxy and so must be taken into account when we consider the relation between different global parameters characterizing the galaxy as a whole. This chapter is a summry of a paper due to White (1982) about this subject, with some some new comments from later works in the literature. For further details see White (1982).

2.1 Introduction

The structure of galaxies may be intimately related to their environment both through ongoing interactions and through links to the processes which shaped them at their birth. The subject of this chapter is a qualitative review of these processes.

There are many possible effects of environment. Neighbours may steal some protogalactic material and may supply angular momentum to the material which is retained (Hoyle 1949; Peebles 1969; Efstathiou and Jones 1979); tidal effects may condition the overall shape of the final galaxy (Binney and Silk 1979). Galaxy formation may be triggered by energetic events happening nearby (Ostriker and Cowie 1981), or may be hindered by the photoionization of protogalactic gas by a strong UV-source like a quasar. If galaxies are formed by the aggregation of smaller objects (Tinsley and Larson 1979; Silk and Norman 1981; Struk-Marcell 1981) this process probably depends on the local conditions in which it takes place.

In most cases the role of environment cannot be easily separated from the formation process itself, hence it will not be discussed any further here. There are, however, a number of situations in which such a distinction is possible at least in some way. Actually, in some possible pictures for the growth of structures in the universe, the evolution of the dark halos of galaxies is particulary simple and can be considered independently of the process by

which their luminous cores are formed (White and Rees 1978; Blumenthal 1987). Some ellipticals may have achieved their present structure quite recently as a result of the mixing of two or more pre-existing objects (Toomre and Toomre 1972; Toomre 1977; White 1978; Aarseth and Fall 1980); the likelihood of such an event is clearly a strong function of the local conditions.

In general, any discussion of environmental influences on galaxies requires some understanding of how the large scale structure of the universe may have risen and to then produce the local conditions in which such environmental effects may occur. So we will briefly consider some current theories for the formation of the large scale structure, together with their implications for the composition and evolution of the environments of galaxies; on the other hand, the study of local dependence on galactic structure may have some implication for how to use galaxies as tracers of the large scale mass distribution (Dressler et al. 1987).

For any galaxy the influence of the environment lasts during its whole lifetime, given that it is not entirely isolated both from other galaxies and from the intergalactic medium (it is not clear that there exists any type of isolated system like this). Interactions with the intergalactic medium depend on the nature of the latter: if it is non-gaseous and effectively collisionless (e.g.: made of massive neutrinos, stellar remnants, or primordial black holes) then the only interaction is gravitational, resulting in an effective drag which removes energy from the motion of the galaxy. This energy loss can have important effects on the distribution of galaxies in clusters and may be responsible for the formation of cD galaxies (Larson 1975; Ostriker and Tremaine 1975; White 1976).

If the intergalactic medium is gaseous, it can exert pressure forces on the gas in a galaxy, and it is possible to have a heat exchange via thermal conduction (Gunn and Gott 1972; Cowie and Soneglia 1977).

Interactions will occur not only with a smoothly distributed medium in which galaxies are embedded, but also with nearby lumps such as other galaxies and galaxy clusters. The tidal field of the mass concentration in which a galaxy orbits may truncate the outermost parts of the galaxy at an effective Roche limit (King 1962). Mass loss and rearrangement of the outer regions of the galaxy may be due to encounters with other galaxies (Gallager and Ostriker 1972; Richstone 1975; Knobloch 1978; Merrit 1982). This rearrangement has particularly important consequences in slow encounters between galaxies which have highly ordered internal velocity fields (Toomre and Toomre 1972; Aguilar and White 1986), and the related loss of relative orbital energy may lead to tidal capture, followed by merging (Alladin 1965; Toomre and Toomre 1972; White 1978; Gerard 1981). In any case, collisions between galaxies may relieve them of their interstellar media even if they occur too rapidly to lead to a merger (Spitzer and Baade 1951) and moreover the structure and evolution of a given cluster will depend on such collisions (Merrit 1983). All these processes can have substantial effects on the observed structure of a galaxy, which we shall now discuss..

2.2 Some physical processes

2.2.1 Dynamical friction

Let us first consider a galaxy in a smooth background of collisionless massive particles. The galaxy then plays the role of a perturber of the background gravitational field. If the perturber is at rest, then it will cause a symmetric enhancement of the background density around itself. On the other hand, if it moves then the interaction between the background and the perturber particles will decelerate the latter. This kind of interaction is known as *dynamical friction.* It can be thought of as being caused by the collective response of the background to the perturber or as due to deflection of the background particles; these two points of view are physically identical if the self-gravity of the background response is negligible (White 1982).

According to Chandrasekhar (1942) and Henon (1973), collisional relaxation in stellar systems can be viewed as a competition between diffusion in velocity space, which tends to broaden the distribution of velocities, and dynamical friction, which tends to reduce all velocities. The two processes can balance each other and then produce a steady state in an infinite uniform system, so that at the end we will have each particle species with a Maxwellian velocity distribution with a root mean square velocity (r.m.s.) inversely proportional to its mass. In a more realistic situation we have a massive object moving through a background with a velocity of the same order as the background particles. The system is then very far from equipartition of energy, and dynamical friction dominates over diffusion, slowing down the motion of the perturber.

It is possible to show (Chandrasekhar 1942) that if all encounters between the perturber and background particles are treated as independent 2-body events, then an integration over all possible encounters lead to a momentum exchange equivalent to a frictional force:

$$F = -4\pi G^2 m^2 \rho(v) \ln(d_{max}/d_{min}) v^{-2} \tag{2.1}$$

where m is the mass of a perturbing particle moving at a speed v in a background of much lighter objects. The quantity $\rho(v)$ is the density of the background particles moving at a lower speed than v; d_{max} and d_{min} are the effective upper and lower limits for the impact parameter. White (1982) claims that for small speeds v, F is proportional to v as a normal viscous frictional force, but for large v, $F \propto v^{-2}$, in which case dynamical friction is quite ineffective. The m^2 dependence of F means that particles slow down at a rate that is proportional to the mass m, and it can be seen from the expression for the relaxation time scale of a stellar dynamical system that the most massive particles in any system are the most strongly affected by dynamical friction. Another point to stress is the dependence of F on the density only of the background and not on the mass of the single particle. This means that the effect of F does not change if we have a background of a few massive objects instead of many light particles.

As a value for d_{max} one can take the mean spacing between the background particles (Chandrasekhar 1942; Kendrup 1980) or the characteristic size of the entire system considered as the background (Spitzer 1962; Henon 1973; Farouki and Salpeter 1982), the second choice being the most widely adopted. In order to calculate d_{min} we can consider the collective response of the background to the perturber. The value obtained for d_{min} does not hold when it results smaller than the size of the background particles, as happens when the background is a galaxy cluster. In this case the corrected expression is given by White (1976b).

The given formula for dynamical friction is quite naive since it is obtained on the basis of highly unrealistic assumptions: rectilinear motion through an infinite uniform medium with an isotropic velocity distribution. Real astronomical systems are inhomogeneous, bounded and have anisotropic velocity distributions. Several modifications of eq. 2.1 have been proposed by Binney (1977), Kalnajs (1970) and Tremaine (1981); in any case Chandrasekhar's formula give quite a good expression.

As an example of dynamical friction at work, we will consider a very simple model of a galaxy orbiting in a cluster. Let us describe the cluster material (i.e.: galaxies and dark matter) as a single isothermal sphere with a one-dimensional velocity dispersion σ. Such a mass distribution has density, cumulative mass and gravitational potential given by:

$$\rho(r) = \sigma^2/2\pi G r^2; \;\; M(r) = 2r\sigma^2/G; \;\; \Phi(r) = 2\sigma^2 \ln(r/r_0) \qquad (2.2)$$

where r_0 is an arbitrary length scale which fixes the zero of the potential. Such a distribution has an infinite total mass and infinite central density, but is somehow a reasonable model for a cluster if we do not consider what happens close to the core or the outer boundary (r_0). If a galaxy is moving in a circular orbit at a distance r from the center with a velocity $\sqrt{2}\sigma$, from eq. 2.1 and the fact that the velocity distribution is Maxwellian we can obtain the rate of energy loss:

$$\frac{dE}{dt} = \sqrt{2}\sigma F = -0.6 G m^2 \sigma [\ln(d_{max}/d_{min})] r^{-2} \qquad (2.3)$$

For non circular orbits the formula is very similar to this, and angular momentum changes are such that non circular orbits tend to become more and more circular as the galaxy loses energy (Tremaine et al. 1975; White 1976a).

First we must note that $\frac{dE}{dt} \propto r^{-2}$, so that dynamical friction may affect quite weakly the massive galaxies orbiting in the outer parts of the cluster, while it modifies strongly the orbits of less massive galaxies in the inner regions. For this reason a model assuming that relaxation effects have everywhere produced the same degree of energy equipartition is not appropriate for a real cluster of galaxies. As a galaxy loses energy in its motion it will not slow down, but rather fall inwards to more tightly bound circular orbits and the energy loss will not produce a reduction of kinetic energy until the orbit is entirely within the uniform density core of the cluster (if it has one).

From eq. 2.2 and 2.3 we can obtain the time dependence of the orbit radius:

$$r/r_i = (1 - t/t_f)^{1/2};\ t_f/t_{0,i} = 0.18M(r_i)/[m\ln(d_{max}/d_{min})] \qquad (2.4)$$

where R_i and $t_{0,i}$ are the initial values for the radius and period of the orbit. So the galaxy will follow a spiral trajectory towards the centre of the cluster and from eq. 2.4 it is possible to compute the number of objects in the mass range $m, m + dm$ that fall to the cluster centre:

$$n(m,t)dm \simeq 1.9[\sigma^3 \ln(d_{max}/d_{min})t/Gm]^{1/2}\Psi(m)dm \qquad (2.5)$$

where $\Psi(m)dm$ is the fraction of the cluster mass in objects with mass in the range $m, m+dm$. Assuming that all objects in the cluster have the same initial distribution, and taking into account the eccentricity distribution by multiplying the evolution rate by a factor 1.5, it turns out that the central accumulation of material grows as $t^{1/2}$ and its composition is more strongly weighted towards high mass objects than is the general galaxy distribution (White 1982). Generalisations of these results are due to White (1976a).

In order to account for more realistic situations, one must also consider the interaction between massive galaxies and the stochastic change in the orbital properties they produce. Then the energy lost by the orbiting galaxies changes the distribution of the background by a non negligible amount. Finally the mass of a galaxy is not likely to be constant during the evolution of the cluster: in fact, if it has a massive halo, this can be stripped away by interactions with the mean cluster field or during collisions with other galaxies. All these processes can be described with diffusive equations assuming that changes in mass, orbital energy and orbital angular momentum are slow compared to the orbital period. The equations one obtains are coupling diffusion equations for galaxies in mass and phase space with a diffusion equation for the phase space evolution of the background. Poisson's equation is also required to ensure that the model is fully self consistent. This way of treating the problem is due to Merritt (1982, 1983). His results look very interesting for approaching knowledge of the cluster's evolution, but suffer the limitation due to the fact that he considers just the cluster in dynamical equilibrium, while the dominant effects of stripping and merging are likely to occur in the dynamic phase of cluster formation (White 1982).

2.2.2 Hydrodynamical effects

The interaction of a galaxy with a smooth gaseous background is complicated by the action of pressure, transport and radiation effects besides the gravitational interaction. All these processes can play a significant role in the galaxy's evolution. Actually, at the centre of a rich cluster the presence of hot intergalactic gas is clear from observations. Typically the number density and temperature of this gas are: $n \sim 10^{-3} cm^{-3}$, $T \sim 5 \times 10^7 K^\circ$ ($\sim T_\infty$) (White and Silk 1980), while the interstellar medium of our galaxy has $n \sim 3 \times 10^{-3} cm^{-3}$, $T \sim 5 \times 10^5 K^\circ$ (McKee and Ostriker 1977), thus giving a pressure 30 times lower.

If we put a galaxy at rest in a bath of hot gas, then the gas will respond to the new potential gradient by an opposite pressure gradient and so its temperature and density will increase around the galaxy. If conductive effects are important, the temperature gradient will soon be erased and a new isothermal equilibrium will be reached with the density of the gas given by:

$$\rho_{gas}/\rho_\infty = \exp\left[-\mu\Phi(r)/kT_\infty\right] \tag{2.6}$$

where $\Phi(r)$ is the gravitational potential of the galaxy and μ is the mean particle mass of the gas. Note that the gas will be strongly perturbed only if $\mu\Phi(r) \gg kT_\infty$, but this is not the case for galaxies in rich clusters or in a bath of $10^8 K^\circ$ gas.

Collisional processes can lead to radiative losses in a short time scale, mainly in the denser regions near the center of the galaxy instead of in the general medium. In this condition the evolution of the system depends on the prevalence of conduction or radiation. If radiation is dominant, then the central temperature drops and a radiative accretion flow is established onto the galaxy; if conduction is dominant, an inward heat flux balances the loss of energy at the galactic center and an isothermal steady state is reached (Fabian and Nulsen 1977; Cowie and Binney 1978; Binney and Cowie 1971). On the other hand, the galaxy has its own interstellar medium, the conductive flux will lead to its evaporation and so it will produce a mass outflow from the galaxy (Cowie and McKee 1977; Cowie and Sonaglia 1977). A simple estimate of the evaporation rate from the surface of the galaxy reads:

$$\dot{M}_{evap} = 4\pi r^2 \rho_h c_h F(\sigma_0)\ ; \quad \sigma_0 = 1.8\lambda_{h,e}/r \tag{2.7}$$

where ρ_h, c_h and $\lambda_{h,e}$ are the density, sound speed and effective electron mean free path in the hot gas, r is the galaxy radius and $F(\sigma_0) \simeq 2\sigma_0$ for $\sigma_0 \leq 1$, and increases more slowly for $\sigma_0 > 1$ (Cowie and McKee 1977). Unfortunately $\lambda_{h,e}$ depends strongly on the details of the magnetic field structure of the hot gas which is poorly known.

The situation becomes more complex if we allow the galaxy to move through the gaseous medium. In a galaxy cluster both gas and galaxies are in equilibrium in the same potential well, hence the motion of a galaxy is almost always transonic with respect to the hot gas. Then a weak shock wave forms ahead of the galaxy producing a density enhancement. These processes lead to a gravitational drag on the galaxy described similarly to eq. 2.1 for dynamical friction. But hot gas gives only a small fraction of the total mass of the cluster and then the gravitational drag it causes is only a small fraction of that caused by the other components. What is mostly affected by the intracluster gas is actually the interstellar medium of the galaxy moving through the cluster. The total dynamical force acting on the interstellar medium is given approximately by the ram pressure on its cross-section:

$$F_{rp} \sim \pi r^2 \rho_h V^2 \tag{2.8}$$

where V is the velocity of the galaxy. If this force exceeds the gravitational force which binds the gas into the galaxy, then the interstellar medium may

be removed (Gunn and Gott 1972). We can state a rough *stripping condition* by:

$$\pi r^2 \rho_h V^2 > fGm^2/r^2 \Rightarrow \frac{V^2}{v_c^2} > fm/(\pi r^3 \rho_h) \tag{2.9}$$

where f is the fraction of the mass of the galaxy in gaseous form and v_c is the circular velocity at r. Then we can expect this stripping to be more effective in the central regions of rich clusters than in the outer regions where the density is lower, or in groups with small velocity dispersion.

There are other processes that can remove the interstellar medium from a moving galaxy in a cluster. If the mean free path of the electrons in the hot gas is long, the evaporation phenomenon described by eq. 2.6 can occur regardless of the motion of the galaxy. In this case (Nulsen 1982) we will have viscous transport of momentum across the boundary layer between the gas and the interstellar medium, leading to a mass loss rate:

$$\dot{M}_{vis} \simeq 4\pi r^2 \rho_h c_h \frac{\lambda_{h,i}}{r} \tag{2.10}$$

where $\lambda_{h,i}$ is the effective ion mean free path in the hot gas, so

$$\dot{M}_{vis} \leq \dot{M}_{evap}. \tag{2.11}$$

To summarize, we can say that galaxies moving through a hot intergalactic gas in the center of a rich cluster will lose their interstellar medium quite rapidly as a result of pressure-induced star formation [1] and stripping of the residual gas by ram pressure, conductive and viscous boundary layer effects (White 1982). It is not clear how the intensity of these effects change with environmental conditions. One of the aims of the present work is to try to clarify this point.

2.2.3 Tidal truncation

The outermost parts of a galaxy moving through a cluster or around a companion are strongly affected by a tidal field depending on time. Let us consider a galaxy with a mass profile $m(r)$ in a circular orbit of radius R_0 about a cluster with a mass profile $M(R)$. If we equate the differential cluster force acting on a star at a distance r from the center of the galaxy with the force due to the galaxy itself, we can work out a *tidal radius* r_t as:

$$m(r_t) r_t^{-3} = \left(2 - \frac{d\ln M}{d\ln R}\right) \frac{M(R_0)}{R_0^3}. \tag{2.12}$$

Then the tidal cutoff is placed at the radius at which the mean density of the galaxy becomes equal to the mean density of the part of the cluster contained within the galaxy orbit. We can also say that the galaxy is limited at the radius at which the orbital period of a star becomes equal to the orbital period of the galaxy about the cluster centre. In this condition the

[1] This process is more likely to occur in spiral galaxies.

stars orbiting within r_t see a slowly varying tidal field and their orbital characteistics do not undergo a long term evolution. On the other hand, the stars orbiting outside r_t follow an orbit about the cluster centre almost independently of the core of the galaxy and thus are separated from it by phase mixing. This kind of process seems to be responsible for the limiting radii of globular clusters in our Galaxy and of dwarf galaxies in our group (King 1962).

If we consider a galaxy orbiting in a non circular trajectory with pericenter distance at R_p, assuming that both the galaxy and the cluster are isothermal spheres with one-dimensional velocity dispersions respectively σ_g and σ_c, then:

$$\frac{r_t}{R_p} = \frac{\sigma_g}{\sigma_c}. \tag{2.13}$$

Note that since a typical galaxy has R_p a factor 2 smaller than its distance from the center, then the mean cluster field is effective in truncating any massive halo that cluster members may posseses (White 1982). In any case it is unlikely to have a strong effect on the visible part of a galaxy! We should keep in mind that all these considerations are based on very crude arguments, so that the derived tidal radii are known within a factor of two or three. A better discussion of this effect is due to Keenan (1981) who uses a restricted three body method to derive the tidal radius.

2.2.4 Collisional stripping

A particularly interesting case of the previous phenomenon is the encounter of two galaxies, say in a cluster. The tidal effects of this interaction lead to an injection of energy mainly into the outer part of each galaxy which is generally studied adopting the so called *impulse approximation.* A recent simulation by Aguilar and White (1985) gives quite good agreement with full N-body expriments.

Let us consider a star characterized by a position $\vec{r^\star}$ and velocity $\vec{v^\star}$ relative to the centre of the galaxy. Then due to a perturber with mass m_p passing quickly at a velocity $\vec{V_p}$ in a relative orbit with pericenter $\vec{d}$, the star is affected by an impulse velocity change :

$$\Delta\vec{v}(\vec{r^\star}) = \int_{-\infty}^{+\infty} dt \cdot \vec{r^\star} \cdot \vec{\nabla} \left[-Gm_p(\vec{d} + \vec{V_p} \cdot t)/ \mid \vec{d} + \vec{V_p} \cdot t \mid \right] \tag{2.14}$$

then :

$$\Delta\vec{v}(\vec{r^\star}) = \frac{2Gm_p}{V_p d^2} \left[2(\vec{r^\star} \cdot \vec{d})\frac{\vec{d}}{d^2} + (\vec{r^\star} \cdot \vec{V_p})\frac{\vec{V_p}}{V_p^2} - \vec{r^\star} \right] \tag{2.15}$$

where $d \gg \mid \vec{r^\star} \mid$ and $V_p/d \gg v^\star/r^\star$ are assumed. The galaxy is thus stretched along the pericenter direction $\vec{d}$, and is compressed in the direction perpendicular to the orbital plane of the encounter. The change in energy per unit mass of the individual star is:

$$\Delta E^\star = \Delta(1/2\vec{v^\star})^2 = \vec{v^\star} \cdot \Delta\vec{v^\star} + 1/2\Delta v^2. \tag{2.16}$$

The first term is of first order in the velocity and can be either positive or negativem, so that by summing over a randomly oriented series of encounters we would obtain zero and the star would follow a random walk in energy space. The second term is always positive and will produce a net increase in the energy of the stars. Finally the net effect of a series of encounters on the stellar energy distribution will thus be the sum of a zero-mean diffusion process and a secular drift to less bound orbits (White 1982).

In order to have a significant change, because of the secular term in ΔE of a star with initial specific energy E, we must wait for a number of encounters N_{sec}:

$$N_{sec} = -\frac{\Delta E}{< E_{sec} >} = -\frac{2E}{< \Delta v^2 >} \tag{2.17}$$

where Δv^2 is averaged over the orbit and over all possible encounters. The change given by the diffusion term, is:

$$N_{diff} = \frac{E^2}{< \Delta E_{diff}^2 >} \simeq \frac{3E^2}{< v^{\star 2} >< \Delta v^2 >} \tag{2.18}$$

where $v^{\star 2}$ is averaged over all orbits.

So the mean specific energy change of stars in a shell of radius $\vec{r^\star}$ is easily shown to be:

$$\Delta E = \frac{4}{3}\frac{G^2 m_p^2 r^{\star 2}}{d^4 V_p^2} \tag{2.19}$$

(for details see Spitzer 1958). Considering shells in the outer parts of the galaxy we may estimate their binding energy by: $E \simeq -Gm(r^\star)/2r^\star$, and thus:

$$\frac{\Delta E}{E} = -\frac{8}{3}\frac{m_p/d^3}{m(\vec{r^\star})/r^{\star 3}}\frac{Gm_p}{dV_p} \tag{2.20}$$

We can define a truncation radius by $\Delta E/E = -1$ and reobtain the Roche criterion of eq. 2.9 apart from a factor of $4/3Gm_p/dV_p^2$, accounting for the fact that here the perturber is moving much faster than the orbiting companion of section 2.2.3. Note also that repeated encounters may affect deep regions of the target galaxy even if a single collision changes only the outermost orbits of its stars.

The linear term of eq. 2.11 that we have neglected can actually contribute in some cases to increase the energy of the outermost part of the target: if $\vec{v^\star}$ is parallel to $\Delta\vec{v}$ and $\vec{v^\star}$ is close to the escape velocity. This situation occurs mainly when the stars are in radial orbits in the outer regions. In many other cases there may be other effects like resonance and capture that cannot be treated within the impulsive approximation, but can cause significant escape of stars in encounters with realistic velocities (Richstone 1975; Dekel et al. 1980; Gerhard 1981).

Considering just the second term in eq. 2.11 and averaging the first to zero, the change in total binding energy of the galaxy is simply the integral of the second order energy change over the entire system minus the kinetic energy at infinity of the escaping stars. In numerical experiments it is generally found that the velocity of escaping stars is small compared to the

internal velocity of their parent galaxy. So neglecting the kinetic term, we have:

$$\Delta E_{tot} = \frac{4}{3}\frac{G^2 m_p^2 < \vec{r^\star}^2 >}{d^4 V_p^2} \tag{2.21}$$

where the r.m.s. radius of the stars in the initial galaxy is mass averaged. Taking the definition of the gravitational radius r_g from:

$$E_{tot} = -\frac{Gm}{4r_g} = -\frac{1}{2} < v^{\star\,2} > \tag{2.22}$$

we obtain:

$$\frac{\Delta E_{tot}}{E_{tot}} = -\frac{32}{3}\frac{m_p}{m}\frac{< v^{\star\,2} >}{V_p^2}\frac{r_g^2 < r^{\star\,2} >}{d^4}. \tag{2.23}$$

We must point out some of the consequances of this relation. Considering a galaxy in a cluster, we can say that most of the tidal damage to the galaxy will result from the closest encounters. Secondly, slow encounters are more effective in changing the galactic structure and more massive perturbers have a stronger influence on outer stars orbits. As a consequence of these facts we can say that the most important encounters for galactic evolution are those interpenetrating, relatively slow encounters for which the impulsive approximation and the assumption leading to eq. 2.12 are all invalid. Some assumptions such as the point-like mass perturber or the distant encounter are not difficult to relax (Alladin 1965; Alladin et al. 1975; Toomre 1977; Tremaine 1981). On the other hand it is quite difficult to relax the impulse approximation, mainly because the physical problem becomes very complex. Fortunately Toomre (1977) has pointed out that energy changes obtained by the impulsive approximation turn out to be quite accurate even in some situation where its validity is very dubious. In any case, the impulse approximation is up to now the most widely adopted framework within which to deal with tidal interaction of this kind (Aguilar and White 1985, 1986).

2.2.5 Merging processes

The enhancement of internal energy discussed in the previous section during the galaxy's encounters with other objects must of course come from their relative motion. So, if the motion is not too hyperbolic (total orbital energy not too positive) and the impact parameter is not too large, then we can have a tidal heating such that the post-collision orbit is bound, and then leading to other collisions, and finally to the possible merging of the two objects. From the impulse approximation of the tidal heating we can work out an estimate of the condition under which this capture will occur.

Let us consider two galaxies approaching at a relative velocity V_∞ and V_p at the pericenter distance d. The total change in internal energy (not specific energy) is obtained from eq. 2.12:

$$\Delta E = \frac{4}{3} G^2 m_1 m_2 \frac{m_2 < r_1^2 > + m_1 < r_2^2 >}{d^4 V_p^2} \tag{2.24}$$

Writing the initial energy of the pair in terms of the relative velocity at infinity:

$$E = \frac{1}{2}\frac{m_1 m_2}{m_1 + m_2} V_\infty^2 \tag{2.25}$$

then capture occurs for $E < \Delta E$, in other words:

$$V_\infty^2 < \frac{8}{3} G^2 (m_1 + m_2) \frac{m_2 < r_2^2 > + m_1 < r_1^2 >}{d^4 V_p^2}. \tag{2.26}$$

For nearly parabolic orbits: $V_p^2 = G(m_1 + m_2)/d$ and so:

$$V_\infty^2 = \frac{8}{3}\left(< v_2^2 > \frac{r_{g,2} < r_1^2 >}{d^3} + < v_1^2 > \frac{r_{g,1} < r_2^2 >}{d^3} \right). \tag{2.27}$$

Thus for similar galaxies the capture will occur for close encounters if the relative velocity at infinity is comparable to the internal velocity dispersion. For dissimilar objects, capture occurs just for very low energy orbits if mass and r.m.s. radius differ both in the same sense. When the collision leads to significant interpenetration then the basic assumption for eq. 2.14 breaks down. Fully self-consistent simulations of encounters between identical galaxies colliding head-on are due to Toomre (1977) and to Tremaine (1981).

After the encounter has captured two object in a bound orbit, subsequent collisions will cause further reduction in relative orbital motion and will finally cause the pair to merger into a single object. If our galaxy belongs to a cluster which initially contains no pairs, we can evaluate the merging rate using a simple $n \cdot \sigma \cdot v$ argument and taking into account the gravitational focusing effect, since capture occurs only for rather low energy orbits. This effect increases the merging rate by a factor V_∞^{-2}. The importance of this effect can be encreased by correlations in galaxy distribution and can lead to a high frequency of collisions between pairs of galaxies which have always been bound. This can explain the large number of colliding pairs seen in real galaxy catalogues (White 1982).

To conclude this section we can say that a great importance is attributed to the merging process in order to explain many observed features of the elliptical galaxies (Nieto 1987 and references therein), their formation and evolution; but this is still a question under debate, and there is no general agreement about it.

2.3 Evolutionary effects

The theories for the formation of large scale structure can be divided into three main groups. In the first, very large objects collapse and decouple from the general expansion with little substructure and, after collapsing, fragment into smaller units which must then evolve to form galaxies. The environments of galaxies are then highly structured when they form. Since the present density contrast of structures on large scales is quite small, all

non-linear evolution occurs at recent epochs in any such picture. The second groups of theories assumes that large scale structure is produced mainly by strong non-linear amplification of effects originating on smaller scales, then galaxies and clusters of galaxies will form as soon as bound objects can condense and the effective amplification factor becomes significantly greater than one. At the same time as galaxy formation the ambient medium is very active and strongly influenced by energetic non-gravitational processes. The third group of theories assumes that different-scale structures grow essentially independently of one another, and that fluctuations on all scales were present as the initial conditions at the recombination epoch. The typical formation time of different objects is then determined purely by the initial amplitude of the corresponding density perturbations, and although non-linear and highly dissipative processes may be important during the final stages of the formation of any system, these processes are assumed to have little effect on the evolution of large scale structure. The environment of a protogalaxy is only weakly non-linear and is relatively inactive in such theories.

Each of these pictures deals with the dark mass in a very different way and their predictions for the structure of galactic halos and for the evolution of the immediate environment of galaxies are very different (Blumenthal 1987).

2.3.1 Pancake theories

In the original pancake theory (Zel'dovich 1970) the matter content of the universe is purely gaseous, until the formation of the first caustic surfaces. Stars, galaxies and the missing mass must all form from fragmentation of the shocked gas in a pancake. Although this version of the theory encounters serious difficulties, it predicts that many properties of galaxies should be strongly related to their environment, since large scale structure regulates the galaxy formation processes. This picture runs into problems when considering the rather modest dependence of galaxy properties such as the luminosity function on the environment density: it is hard to see why coagulation should produce galaxies with the same characteristic luminosity both in dense and in sparse regions of a pancake. In addition to correlations with the environment engendered at galaxy formation, further correlations may arise from interactions of the interstellar medium in galaxies with the hot intergalactic gas predicted by the theory. A possible way out of the problems of the pancake theory is to consider a universe dominated by dark matter in the form of weakly interacting massive particles such as neutrinos or gravitinos. The new picture is in much better agreement with observations (Cowsik and Ghosh 1987). If massive neutrinos do indeed form dark matter, it seems likely that a large fraction of them will never become attached to any individual galaxy but will remain in a more uniform background. This property of the massive neutrino picture differs significantly from what would be expected if the dark matter were formed at the epoch of galaxy formation, and will cause some reduction in the efficiency of gravitational

interactions between galaxies thus reducing the environmental dependence of galactic characteristics.

2.3.2 Explosive galaxy formation

In this scenario, proposed by Ostriker and Cowie (1981), after a red-shift of about 100, relatively small seed perturbations are supposed to collapse giving rise to an explosive release of energy from the deaths of their first generation of massive stars. This energy drives a blast wave into the surrounding gas, thereby sweeping up a shell of shocked material which eventually cools, either by inverse Compton scattering or by gas-radiative processes at more recent epochs. This cool shell may then fragment to form a new generation of collapsing objects which will themselves explode. Then the process propagates like a detonation wave if the total mass of the shell fragments exceeds the mass of the initial seed. This kind of picture involves a lot of complications dealing with the efficiency of the star and galaxy formation process itself and with hydrodynamic effects of strong shock waves in an inhomogeneous star-forming mixture of gas and dark matter. Reliable predictions cannot be obtained until all these processes are carefully taken into account. In any case Ostriker and Cowie's picture would lead to a hot metal-rich intergalactic medium of high density; this medium may be directly observable and may have significant effects on the interstellar gas of the galaxies which are embedded in it (White 1982).

2.3.3 Hierarchical clustering

In this scenario the relative numbers of baryons and photons may vary giving rise to pure isothermal or entropy perturbations. For the details see Peebles (1980), White and Rees (1978), Eftathiou and Silk (1983). Then we can see that the ram pressure of the intergalactic gas acting on the interstellar medium of a galaxy would have been more effective in stripping galaxies in small clusters at early times than in a typical present day object. Similar estimates can be made for the frequency of interactions between galaxies. The collision rate for a galaxy is proportional to ρV and so the number of collisions suffered by a galaxy in the typical structures present at time t scales as $N_{coll} \propto \rho V t \propto M^{-2/3-n/3} \propto t^{-(8+4n)/(9+3n)}$ [2]; then most of the collisions that any galaxy had suffered will have occurred at the begining of its lifetime. Since collisions occurred at lower typical velocities at early epochs (for $n < 1$), most of the tidal damage done to any particular object was probably inflicted in an environment which differed considerably from the one which currently surrounds it and most mergers between galaxies probably happened in the period immediately following galaxy formation. Although all these scaling arguments are quite rough, they do indicate the danger of using the present environment of galaxies to estimate how much the effects of ram pressure stripping, tidal truncation and merging may

[2] The integer n is the spectral index of the density fluctuations: $\mid \delta_k \mid^2 \propto k^n$, typically $n = -1$.

have affected their structure. In all cases the total effect may be severely underestimated and the most significant structural damage may have been done very soon after galaxy formation. The spin and perhaps also the shape of galaxies were very probably determined by environmental influences right at galaxy formation (Hoyle 1949; Peebles 1969; Efstathiou and Jones 1979; Binney and Silk 1979) and may not have been modified since that epoch. This kind of study will stimulate further progress of the present work.

2.4 Summary

At this point we have a feeling of what may be the most relevant processes that have contributed in producing objects like galaxies as we observe them today. In a later chapter, using recent data, we will try to put upper limits on the magnitudes of these effects on elliptical structure. The hope is to provide people, who are more familiar with the theoretical aspects of the problem, with observational constraints to model the action of these processes.

Chapter 3

The luminosity-diameter relation for normal elliptical galaxies

3.1 Introduction

The family of elliptical-like stellar systems, to which we can say the normal elliptical galaxies belong, is by no means homogeneous. It rather spans a wide range in all the parameters characterizing these systems. If we want to obtain reliable results from this study, it is necessary to avoid any mixing of different members coming from different classes of elliptical-like galaxies (Wirth and Gallagher 1984). For this reason we are now going to consider briefly the main classes composing the crowded family of ellipticals and then try to isolate the class we are interested in.

3.2 The family of elliptical-like galaxies

A distinction between different classes was proposed by Binggeli, Sandage and Tarenghi (1984) in relation to the Virgo cluster. They examined a wide range of ellipticals from $M_B = -12$ to $M_B = -20$ and combined their data with other data present in teh literature on giant and dwarf ellipticals. They obtained the values of the total magnitudes and effective radii using the growth curve described in section 1.3 and 1.4. One of the main results is the evidence of a change in structure passing from ellipticals brighter than $M_B = -20$ ($H_0 = 50\ Km\ s^{-1} Mpc^{-1}$) to ellipticals fainter than that magnitude. They showed that the Hubble law (1926) $L \sim R^2$ fits none of the observed galaxies, rather two different laws fit the galaxy data in two different ranges of magnitude:

$$M_B \leq -20 \ \Rightarrow L \propto R_e^{1.3} \ ; \quad M_B > -20 \ \Rightarrow L \propto R_e^4 \qquad (3.1)$$

The proposed interpretation of this behaviour claims two different origins for these systems: the brighter, high mass galaxies probably formed by mergers,

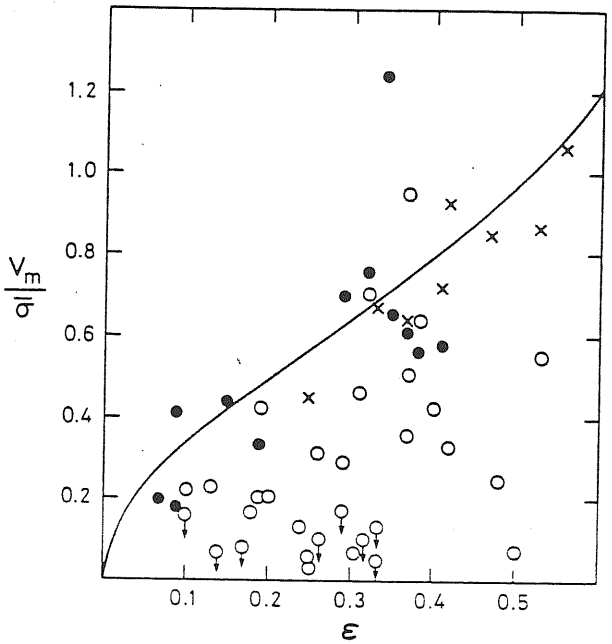

Figure 3.1: The $V_m/\bar{\sigma}$ vs. ellipticity; V_m is the maximum rotation velocity of galaxies, $\bar{\sigma}$ is the averaged value of the velocity dispersion within $1/2\, r_e$. Ellipticals with $M_B > -20.5$ are shown as filled circles, ellipticals with $M_B < -20.5$ are open circles and the bulges of disk galaxies as crosses. The solid line shows the $(V/\sigma, \varepsilon)$-relation for oblate galaxies with isotropic velocity distribution (Davies et al. 1983).

while fainter and less massive galaxies resisted the merging process evolving in a different way to populate the dE class of the family. Nieto (1987) is in agreement with this theory. Balcells and Quinn (1988) discussed it in relation to the alternative hypothesis that claims the same origin for all ellipticals with an inbuilt dynamical or hydrodynamical scale that is reflected in the change in properties observed today. Balcells and Quinn also performed numerical experiments to follow the evolution of an encounter remnant galaxy and check if its parameters scale as for ordinary ellipticals. Finally, their results showed a core-within-a-core structure (first proposed by Kormendy 1984) for the remnant and pointed out that cannibalized cores observed today may have suffered significant structural modification before they relaxed at the remnant core.

Another different sort of behaviour of ellipticals is related to rotation. Considering fig. 3.1 it is clear that faint ellipticals rotate more rapidly than most of the bright ellipticals.

Binggeli, Sandage and Tarenghi (1984) pointed out that neither a deVaucouleurs law (eq 1.2) nor an Oemler law (eq. 1.5) can fit the faint dwarfs, while a King model (eq. 1.4) offers a very good description of systems fainter than $M_B = -16$ while it is much worse in the range $-16 > M_B > -20$. An important fact is that the tidal radius r_t of these dwarf ellipticals does not have a *tidal meaning* in the usual sense. The authors don't believe, in fact, that tidal stripping occurs in Virgo cluster dwarfs, but rather that r_t is merely a convenient parameter to describe the galaxy. The striking thing is that I obtained the same results using the isophotal diameter (see section 1.4) and the total blue luminosity for a sample of bright galaxies ($M_B \leq -20$) comparing the $\log L \, vs. \log D_0$ relation for the inner and outer galaxies. As I will show later no difference was detected between the two sets of galaxies. Actually it would be expected that the environment affects more strongly the outermost tidal radius of a less tightly bound object such as a dwarf galaxy rather than a more internal length scale as the isophotal radius in a more massive galaxy. Binggeli and coworkers also gave an estimate of the timescale for tidal stripping in the Virgo cluster adopting Richstone's (1976) expression:

$$\tau_{dwarf} \geq 10^{12}\, yr. \; ; \; \tau_{giant} \geq 10^{11}\, yr. \tag{3.2}$$

for dwarf and giant elliptical galaxies. They argue that neither for dwarf nor for giant ellipticals can tidal stripping be effective in this cluster. They conclude by claiming that r_t is an intrinsic property of these galaxies not dependig on interactions with the environment (see also Oemler (1976)).

At the faintest end of the family of elliptical-like objects, as Wirth and Gallagher (1984) stressed, we can find the so called *compact classical ellipticals* like $M32$, and *diffuse dwarf ellipticals* like $NGC205$. The observations of $M32$-like galaxies do not show a distinct structural class of objects, but a natural extension of classical or normal luminous ellipticals to lower luminosities. On the other hand, diffuse dwarf ellipticals ($NGC205$-like objects) are a separate morphological and physical class of galaxies. Actually, diffuse dwarfs do not obey an $r^{1/4}$ law while compact dwarfs do, the former can be fit better by low central concentration (i.e. diffuse) King models. Binggeli et al. (1984) reached a similar conclusion for very faint objects in the Virgo cluster with $M_B \geq -16$. Both classes of dwarfs are present in the range $-18 \leq M_B \leq -15$, their relative luminosity function is shown in fig. 3.2 and is based on a sample of galaxies from the Fornax and Virgo clusters due to Sandage et al. (1982) which, unfortunately, suffered completeness problems. Wirth and Gallagher (1984) claim that probably the luminosity functions, for these classes of galaxies, depend on the galactic environment. It is worth noting that the existence of a small sample of isolated compact classical ellipticals ($M32$-like) lead Wirth and Gallagher to consider the possibility that the features of these systems are determined by their formation processes rather than by subsequent interaction with other galaxies.

At the brightest end of the family of elliptical-like galaxies we find the giant ellipticals (Thuan and Romanishin 1981) or bright cluster galaxies

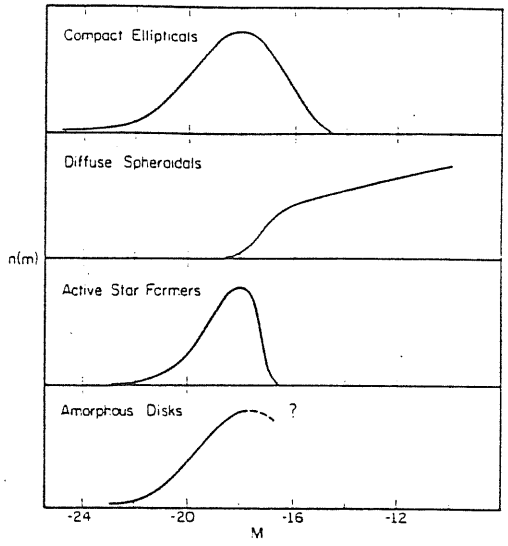

Figure 3.2: Schematic luminosity functions are shown for a variety of galactic structural families.(Wirth and Gallagher 1984).

(BCG), (Hoessel 1987) reaching quite high magnitudes ($M_{V,tot} \simeq -24.68, H_0 = 50\ Km\ s^{-1}\ Mpc^{-1}$). From the observations of the first brightest (FBCG) in clusters of different morphology present in the literature (Morgan, Kayser and White 1975; Albert, White and Morgan 1977), we can see that the profiles of FBCG are generally well fitted by an $r^{1/4}$ law within a wide range of magnitudes ($> 9\ mag.$) and so it is possible to use this law to derive structural parameters. It is then possible to see (Thuan and Romanishin 1981) that FBCG and cD galaxies in rich clusters are made up of two components: a main elliptical-like body and a large diffuse envelope [1]. On the other hand, FBCG's in poor clusters have only one component: the main elliptical-like central body, and so FBCG's are not cD galaxies in the Morgan sense[2] . Both rich and poor clusters show BCG having elliptical-like central bodies but more diffuse and brighter than normal ellipticals, that is to say with larger cores, larger effective radii and lower surface brightnesses. In poor clusters the FBCG have central bodies more diffuse than cD galaxies in rich clusters and are slightly brighter at a given luminosity. These observations suggest that FBCG in rich clusters are the result of two different processes: one responsible for the main central body and another process responsible for the envelopes of cD galaxies in rich clusters. The second process is probably given by accretion of tidal debris from collisions with other galaxies (see section 2.2.4). Thuan and Kormendy (1977) gave observational support to this interpretation. In poor clusters the collisional time scale is so long that such a process of envelope formation is not likely to occur. Many people suggest a merging process as responsible for the formation of the main elliptical-like body, but although all these facts are consistent with the

[1] Dressler (1980) suggests the presence of a third component of dark matter that is not detectable from surface photometry alone.

[2] Morgan defined the cD galaxy as a supergiant D galaxy, where a D galaxy has an elliptical-like nucleus surrounded by an extensive envelope (Mattews, Morgan and Schmidt 1964).

merger picture for the origin of the more massive elliptical galaxies, they do not prove it.

In order to postpone the discussion about normal ellipticals to the next section, we conclude here by just observing that it seems that a non negligible environmental effect is responsible for the envelopes of cD galaxies in rich clusters and that this effect actually seems absent in poor clusters. Hence we can say that the brightest galaxies in rich clusters are probably the best detectors of environmental effects both because of their sensitivity to the tidal field, and because we can observe them in quite a large number of clusters.

3.3 Normal elliptical galaxies

From the previous section it seems straightforward to define a normal elliptical galaxy as an object belonging to the elliptical-like family and occupying a position in parameter space going from $M32$-like galaxies to first brightest galaxies in poor clusters. I now consider different observations and resulting laws proposed as correlations between the parameters such as luminosity and diameter or radius characterizing this class of elliptical galaxies.

I am interested in testing the relation given by eq. 1.10. In the literature we find mainly two kind of laws connected with this relation. A first law relates parameters that are ideally obtained independently from the observation of the whole galaxy:

$$L_T = L(R_T) \tag{3.3}$$

and we will call this a *type G law* (G is for global). Another type of law relates the mean surface brightness μ_0 within a certain length scale R_0, and R_0:

$$\mu_0 = \mathcal{M}(R_0) \tag{3.4}$$

I will call this a *type C law* (C is for core). Now type C laws give good information about the behaviour of the inner part of the galaxy even if R_0 is obtained by a fit involving the profile of the whole galaxy (as is r_e, see section 1.4), although the situation gets better when we use the R_e from the growth curve. As far as the behavior of the whole galaxy is concerned, a type G law seems to be more reliable. In pratice this kind of law is not very easy to obtain. While L_T is measured by an extrapolation of the growth curve, it is very hard to measure the dimensions of a galaxy which generally appears to be an edgeless object, leading to serious problems of low intensity surface brightness (see section 1.6). What I can actually do is to correlate the extrapolated L_T with different fiducial diameters R_f and compare the behaviour of the different relations:

$$L_T = \mathcal{L}(R_f). \tag{3.5}$$

I will call this a *type g law* (g is again for global). The ideal situation would be reached when different R_f gave type g laws showing the same behaviour,

so that it is quite sure that this is proper for the set of galaxies we consider. That is the main aim of this work. Now let us try to separate the observed laws for the three types respectively.

3.3.1 Type G laws

From a study of normal ellipticals and cD galaxies fitted by eq. 1.12, Oemler (1976) obtained a relation between a cutoff radius called R_1, defined as the length scale at which the brightness profile of the galaxy reaches zero and determined visually from the plates of the galaxies, and the reduced luminosity L_{rd} from which one can estimate the total luminosity (see section 1.2.2). His relation reads:

$$\log R_1(Kpc) = -0.258\,(12.40 + M_{rd}) \tag{3.6}$$

with a dispersion of 0.14. Or in another form:

$$L_{rd} \propto R_1^{1.5}. \tag{3.7}$$

He used $H_0 = 50\,Kms^{-1}Mpc^{-1}$. His data were obtained from three clusters of galaxies and he claimed that the data showed no evidence that R_1 (although determined quite roughly by visual examination) was influenced by tidal interaction with other galaxies. He finally showed that for cD galaxies the envelope luminosity is a strong function of cluster luminosity (i.e.: $L_{env} \propto L_{cl}^{2.2}$). Hoessel (1976) agrees with these results.

3.3.2 Type C laws

The last expression of this kinds of law is due to Hoessel et al (1987) and to Romanishin (1986). Studying a sample of 372 normal and bright cluster galaxies (BCG) with $H_0 = 60Kms^{-1}Mpc^{-1}$ and $q_0 = 0$, they found that:

$$\mu_e = 19.42 \pm 0.08 + (3.09 \pm 0.08) \log R_e \tag{3.8}$$

with a dispersion in μ_e of $0.75mag.$ and using an $r^{1/4}$ fitting law to determine μ_e and R_e in the r band. The law they obtained is equivalent to $L_e \propto R_e^{0.76}$ and is consistent with Kormendy (1977, 1980) and Djorgowski and Davis (1987). Hoessel recommended to not use a mixed sample of BCG and non-BCG, since he found that the relation from such samples depends strongly on the relative population of the two kind of galaxies. Romanishin found essentially the same results for a sample of bright galaxies ($M_B < -20.5$ with $H_0 = 50\,Kms^{-1}Mpc^{-1}$).

3.3.3 Type g laws

The first relation of this kind is due to Strom and Strom (1978). They correlate the total visual magnitude M_V with the effective radius r_e obtained from an $r^{1/4}$ fitting law and with the $26\,mag.arcsec^{-2}$ isophotal radius for six clusters of different types: Coma, Perseus, A2199, A1367, A1288 and

Hercules. Comparing the least squares fitted relation $\log r_e = a - bM_V$ for different clusters, they claimed the presence of an environmental effect leading to more compact galaxies (i.e.: smaller radii at fixed magnitude) in denser regions both within anyone cluster and among different clusters. Strom and Strom interpreted this result as due to a tidal interaction between galaxies in a cluster and/or to genetic effects present at the time of cluster formation. Unfortunately, their analysis suffered many problems. As Kormendy (1980) pointed out, Strom and Strom used a sample of both E and S0 galaxies, and the $r^{1/4}$ law fits were made between a fixed inner radius and a fixed outer surface brightness cutoff without regard to the shape of the profile. Moreover the presence of S0 galaxies in the sample will modify the observed $\mu_e - r_e$ relation. Another complication is due to the presence in their sample of galaxies fainter than $M_V = -20$ ($H_0 = 50 Kms^{-1}Mpc^{-1}$) and we have already seen that this can be very dangerous. Other quite suspicious objects (they called them compact or underluminous galaxies) were also present in the sample. In order to compare the sizes of galaxies with a fixed visual magnitude at $M_V^* = -21.5$ or -20 in different clusters, they fixed the slope and compared quantities like $\log r_e^* = a - 0.21 M_V^*$. This too is quite a suspicious procedure.

Aguilar and White (1986) compared the results of Strom and Strom with their simulation of tidal interaction of spherical galaxies with a deVaucouleurs profile within an impulsive approximation. The results of these simulations were in qualitative agreement with the observations of Strom and Strom, but the effect measured was fainter than that claimed by Strom and Strom. Actually, in order to obtain the Strom and Strom observations one would have to wait for five times the Hubble time!

Vader (1986) analysed the data of a set of bright galaxies: 12 in Virgo, 12 in Coma and 23 field elliptical galaxies. Whenever the data were missing, she approximated the effective radii r_e as 1/6 times the standard isophotal diameter at 25 $mag.arcsec^{-2}$. Then she found a relation like: $r_e \propto L^{0.7}$, in agreeement with other results (Torny and Davis 1981; Torny 1981; Davis et al. 1983).

The first step in casting more light on this subject is to obtain a large homogeneous sample of E galaxies without undesired members coming from other morphological types or with a different physical structure. It is also better to deal with objects studied using in each case only one procedure, in other words all parameters should be obtained using only one technique (i.e.: $r^{1/4}$ fitting laws or growth curve etc.). Finally, we should not forget the technical problems considered in chapter one. Such a sample has been compiled by Dressler et al (1987, known as the Seven Samurai: 7S.I) and enriched by Burstein et al. (1987, 7S.III). In the next section we will summarize the main features of this sample.

3.4 A new sample of elliptical galaxies

The sample of galaxies giving the main input of this work is due to the 7S. They produced a deep survey ($B_T \leq 17.43$) of elliptical photometry in rich clusters (7S.I, 7S.III).

From the first paper of the series, we have taken the member list of the main body of input galaxies, then we enriched this list by some other members relying on other authors (Kent and Sargent 1983; Huchra 1985; Binggeli et al. 1987; Kent and Gunn 1982) in order to increase the statistics, but the main results do not depend strongly on the added members of each cluster. The complete list of the sample galaxies is given in appendix A and the extra members are listed after a horizontal line. All the photometric data come from the third paper 7S.III. In this way we have obtained a list of 27 galaxies for Virgo, 34 for Coma, 19 for Perseus, 14 for A2199, 11 for DC2345-28, and 8 for Fornax. Besides these clusters we have considered a list of 37 elliptical galaxies in groups and 13 in pairs, in order to span the largest possible range in density and environmental conditions. We have taken the list of E galaxies in the Huchra and Geller compilation from Mezzetti, Pisani, Giuricin and Mardirossian (1985) which also give the values of the *compactness* of each group as:

$$c = \log \frac{N_T}{4/3\,\pi\,R_p^3} \tag{3.9}$$

where N_T is an estimate of the total number of the galaxies in the group (i.e.: seen and unseen), and R_p is the mean pairwise distance of the group members. This parameter gives an indication of the number density in the group, on the assumption that the geometrical symmetry of the group is not too far from spherical. The list of E galaxies in pairs comes from White et al. (1983). The velocity of the galaxies in pairs has been taken as the mean of the pair in question, and as the velocity of the entire group for the group ellipticals.

Concerning the quality of the data we can say that photoelectric aperture photometry comes from the literature and 7S.III for Virgo, Fornax and some Perseus galaxies, while for the galaxies in Coma, A2199 and DC2345-28 the data come from the 60 inch (1.5 m.) RCA CCD camera or the 200 inches 4-Shooter TI CCD camera at the Palomar Observatory.

The aperture parameters were all obtained by fitting the observed growth curve with an $R^{1/4}$ standard curve of growth (see figg. 3.3, 3.4)
out to a level of 25 $B\ mag.arcsec.^{-2}$ or brighter, since fainter brightness levels may be strongly affected by sky subtraction problems (see sec. 1.6). For this reason some galaxies have only B_T and $\log D_n$ and the other two diameters are missing. In this way the authors of the survey obtained B_T, $\log D_n$, $\log D_e$,and $\log D_0$. Hence we have only considered galaxies with all the four data known in 7S.III in order to compare the behavior of different diameter indicators for the same galaxies. The authors of the survey gave a long discussion concerning the estimation of the growth curve fitting random errors and concluded that probably what they obtained were just lower limits

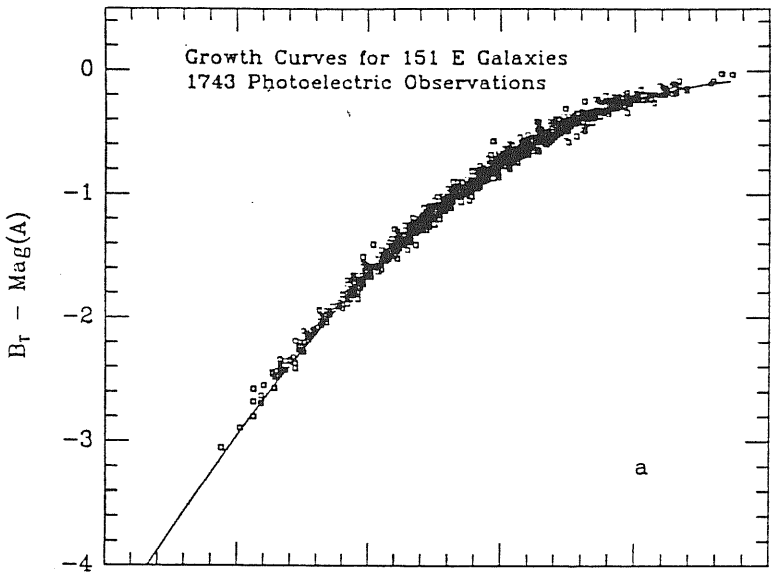

Figure 3.3: The average elliptical galaxy growth curve as defined by the individual photoelectric aperture growth curve of 151 galaxies. The average $R^{1/4}$ law growth curve used is plotted as a solid line(Burstein et al. 1987).

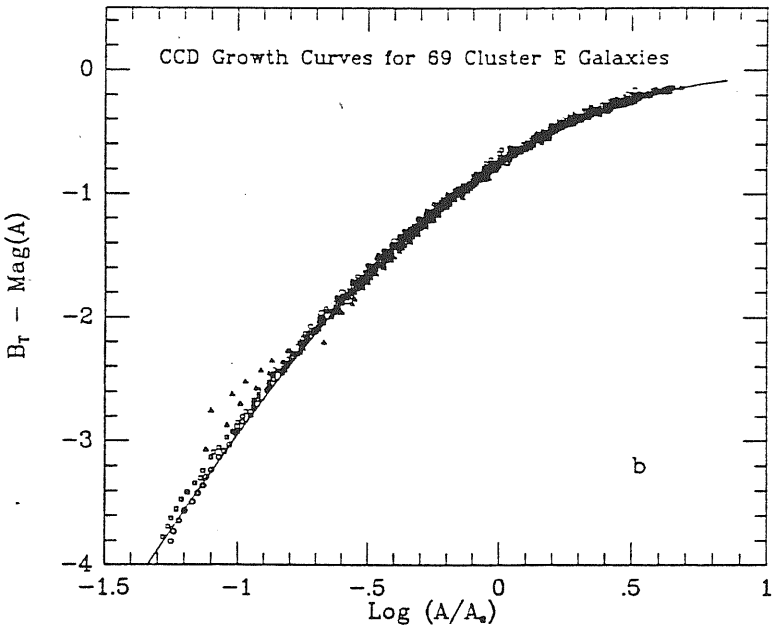

Figure 3.4: The average elliptical galaxy growth curve as defined by the individual CCD luminosity profiles of 69 cluster galaxies. The model growth curve is again plotted as a solid line. The smaller scatter among CCD growth curves is evident, indicating that much of the scatter in (a) is due to observational errors (Burstein et al. 1987).

Table 3.1

param.	$1\,\sigma$	$2\,\sigma$	$3\,\sigma$
$\log D_e$	≤ 0.05	≤ 0.10	> 0.10
$\log D_0$	≤ 0.05	≤ 0.10	> 0.10
$\log D_n$	≤ 0.02	≤ 0.05	> 0.05
B_T	≤ 0.15	≤ 0.30	> 0.30

to the true errors in D_e and B_T, but these problems are still not expected to affect the 70 cluster galaxies studied with CCD surface photometry. In the best (7S.I) cases of CCD data the accuracy is ~ 0.1 for B_T, 0.02 for $\log D_n$, and 0.03 for $\log D_e$. As a general evaluation of the random errors the authors of the survey gave the expected random errors for three different sigma levels in the case of the large survey composed not only of CCD data (table 3.1). In the large sample with 500 objects, a total of 400 galaxies have all parameters known to within or better than the $2\,\sigma$ level, for 478 galaxies $\log D_n$ is known within or better than the $2\,\sigma$ level. For these considerations and remembering that the sample used here contains 163 galaxies, half of which come from CCD photometry analysis, it seems to me that a good evaluation of the observational error σ_x averaging the CCD and photoelectric photometry uncertainty gives a value of 0.04 for all kinds of diameter. In any case, assuming the best values from the pure CCD sample, the general conclusion does not change. For further detail see the papers of 7S.

3.5 Absolute quantities

Since I want to compare the correlation in different objects at different distances, I need absolute quantities not affected by the distance. The parameter B_T is the measure of the blue magnitude and the diameters D_e, D_n, D_0 are in units of $0'.1$. All these values are corrected for K-effect, red-shift and absorption (see section 1.5). Here we will assume $H_0 = 100\,Km\,s^{-1}Mpc^{-1}$. The transformations to absolute quantities are then:

$$D(Mpc) = 2\,\frac{V}{H_0}\,\tan\left[\frac{1}{2}\,\frac{\pi}{180}\,\frac{D(0'.1)}{6}\right] \tag{3.10}$$

or equivalently:

$$\log D(Kpc) = \log(2.909) - 4 + \log[D(0'.1)] + \log V(Km/s) \tag{3.11}$$

and:

$$B_T = -2.5\,\log\left[L \cdot \left(\frac{H_0}{V(Km/s)}\right)^2\right] + const. \tag{3.12}$$

so that:

$$\log L/L_\odot = 0.4\,[5\log V(Km/s) - B_T + 20.48]\,. \tag{3.13}$$

Whenever the number of galaxies in a cluster was large enough (i.e.: $n \geq 20$), I divided the whole cluster into two regions: inner and outer. The distance of each galaxy from the center of the cluster was used to decide which of these regions the galaxy fell in. The limiting distance dividing the two regions was chosen in order to have more or less the same number of galaxies in each region. The coordinates of the centres come from the literature (7S.I). The number of galaxies in each group is so small that it is not possible to use the radial distance to distiguish regions with different density. So I used the compactness c instead of distance, and again the limiting compactness was chosen in order to have approximately the same number of dense and sparse group galaxies.

3.6 Analysis of the data

I will here describe the method adopted to study the behaviour of the sets of galaxies compared pairwise and the results I obtained. Then I will discuss the cases in which it was possible to split a set into two subsets, called inner and outer for the cluster galaxies and dense and sparse for the group galaxies. The limiting value of the radial distance r^* from the centre in the case of cluster galaxies and the limiting compactness c^* for the group are given in section 3.6.2.

3.6.1 Pairwise comparison

Now I have $r = 8$ sets of n^k $(k = 1, \ldots, r)$ couples of data $y_i^k = \log L_i^k / L_\odot$ and $x_i^k = \log D_{0,i}^k$ ([3]) (or $\log D_{e,i}^k$, or $\log D_{n,i}^k$ and $i = 1, \ldots, n^k$), with an error in the independent variable $\sigma_x = 0.04$ and spanning different intervals: Y^k, X_0^k, X_e^k, X_n^k. What I want to do is to correlate y_i^k with x_i^k in each set and check if the laws obtained change from one set to another. Guest (1963) gives a good description of a method which allows me to obtain an unbiased estimate of the error-free regression curve as a representation of the type g law for the sample:

$$y_i^k = B^k \cdot x_i^k + A^k \tag{3.14}$$

where (see eq. 1.12):

$$B^k = \frac{n^k(\Sigma_i x_i^k y_i^k) - (\Sigma_i x_i^k)(\Sigma_i y_i^k)}{n^k \Sigma_i (x_i^k)^2 - (\Sigma_i x_i^k)^2 - n^k(n^k - 1)\sigma_x^2} \tag{3.15}$$

with an error:

$$\sigma_{B^k} = \frac{B^k}{b^k} \cdot \sigma_{b^k} \tag{3.16}$$

where b^k and σ_{b^k} are the least squares values for the slope and its uncertainty:

$$b^k = \frac{n^k(\Sigma_i x_i^k y_i^k) - (\Sigma_i x_i^k)(\Sigma_i y_i^k)}{n^k \Sigma_i (x_i^k)^2 - (\Sigma_i x_i)^2} \tag{3.17}$$

[3] Do not worry: these are not tensors! An upper index k in the variables will indicate a particular set of galaxies, while a lower index i will indicate a particular galaxy in the $k-th$ set. So I have tried to avoid using three lower indices.

and:

$$\sigma_{b^k} = \sigma^k \cdot \left\{ \frac{n^k}{n^k \Sigma_i (x_i^k)^2 - (\Sigma_i x_i)^2} \right\}^{1/2} \tag{3.18}$$

where the quantity σ^k is the dispersion of the set:

$$\sigma^k = \left\{ \frac{1}{n^k - 2} \cdot \left[\Sigma_i (y_i^k)^2 - \frac{(\Sigma_i y_i^k)^2}{n^k} - (b^k)^2 \cdot \frac{n^k \Sigma_i (x_i^k)^2 - (\Sigma_i x_i^k)^2}{n^k} \right] \right\}^{1/2} . \tag{3.19}$$

The intercept reads:

$$A^k = \frac{\Sigma_i y_i^k}{n^k} - B^k \cdot \frac{\Sigma_i x_i^k}{n^k} = < y^k > - B^k \cdot < x^k > \tag{3.20}$$

and its uncertainty is:

$$\sigma_{A^k} = \left[\sigma_{B^k}^2 \cdot < x^k >^2 + (B^k)^2 \cdot \sigma_x^2 \right]^{1/2} . \tag{3.21}$$

When the regression line is known, it is possible to estimate the luminosity (y^k) of a galaxy with a given diameter (x^k) in a given set (k) just using eq. 3.13, the error in the estimated luminosity will be:

$$\sigma_y^k(x^k) = \left\{ (x^k - < x^k >)^2 \sigma_{B^k}^2 + (B^k)^2 \cdot \sigma_x^2 \right\}^{1/2} \tag{3.22}$$

Then the fitted relation $y^k \, vs \, x^k$ will cover a strip with upper $(+)$ and lower $(-)$ limits given by:

$$y_\pm^k = B^k \cdot x^k + A^k \pm \sigma_y^k(x^k). \tag{3.23}$$

Running this technique on the data of sample galaxies, we obtain the results listed in tables B.1,...,B.11. Some of these data were also discussed by Giuricin, Mardirossian, Mezzetti, Ramella and Pisani (1988). The first thing to note is the luminosity intervals spanned by galaxies. In section 3.2 we stressed the result of Binggeli et al. (1984) that one should not mix in the same sample elliptical galaxies brighter and fainter than $M^* = -20$, which corresponds in the units we used , to $\log L^*/L_\odot = 9.59$. Examining the table B.1 and the graphs C.1 to C.8 [4] , it is possible to see that in all sets the minimum luminosity falls below the $\log L^*/L_\odot$ value. In the case of Virgo there are 16 galaxies below this critical value, for Coma 8, for Perseus 4, for A 2199 5, for DC2345-28 3, for Fornax 2, for groups 4, and for pairs 4. Now we have run the computation on a subset of ellipticals brighter than L^* for the isophotal diameter and we have found no relevant difference with what we have obtained for the set of galaxies as a whole (compare tables B.1,...,B.7 with tables B.8,...,B.14). The same result was obtained applying the homogeneity test (described later in this section) to compare the regression lines of the whole $k-th$ set and its subset of bright galaxies

[4] For the sake of simplicity I preferred to put all the tables of sample data, results and graphs in appendices. The letters A, B and C refer to these appendices.

for the other two diameter indicators if, in the subset, the number of bright galaxies was larger than 10. In fact for poorer sets the estimated errors for the parameters were too high, mainly because of the poor correlation of the data. The conclusion was that in no case was the bright subset fit by a different regression line. This result also means that completeness problems do not affect the sample. Then I decided to keep all the galaxies in the sample.

I think that this fact can be interpreted by saying that probably the faint galaxies in this sample belong to the *classic compact ellipticals* or M-32-like objects described by Wirth and Gallagher (1984), while the faint Virgo galaxies of Binggeli et al. (1984) belong to the NGC-205-like objects also described by Wirth and Gallagher (1984). It must be noted that the group galaxies give one of the best correlations between $\log L$ and $\log D_0$ in a large sample. On a first examination of the values in table B.1 (case $x = \log D_0$) it is possible to note that the slopes are all the same within the given errors. The same holds for data in table B.2 (case $x = \log D_n$) except for the comparision between Coma with $B^C = 2.46 \pm 0.17$ and Fornax with $B^F = 1.71 \pm 0.20$. For data in table B.3 (case $x = \log D_e$) the largest difference results from the comparison between Perseus with $B^P = 1.19 \pm 0.18$ and pair galaxies with $B^p = 1.77 \pm 0.17$. To compare the fitted slopes of different sets we adopted the Welch method (Guest 1963). The following notes give a summary of this technique. If two different determinations of the slope are made: B^I and B^{II} with variances s_I^2 and s_{II}^2 on two samples of n^I and n^{II} values, then the quantity:

$$t = \frac{B^I - B^{II}}{(s_I^2 + s_{II}^2)^{1/2}} \tag{3.24}$$

will be distributed like the Student$-t$ with ν degrees of freedom:

$$\nu = \frac{(s_I^2 + s_I^2)^2}{\frac{s_I^4}{n^I - 1} + \frac{s_{II}^4}{n^{II} - 1}}. \tag{3.25}$$

So t and ν can lead to the estimate of the level of significance at which B^I and B^{II} are different. The method also can be applied to compare different estimates of the intercept.

In this way we obtained that the inequatity $B_n^C > B_n^F$ was significant at a level $> 99\%$, and the same holds for $A_n^C < A_n^F$. So comparing the two regression lines:

$$y^C(x_n) = B_n^C x_n + A_n^C \quad y^F(x_n) = B_n^F x_n + A_n^F \tag{3.26}$$

the difference between the ordinates never exceeds the estimated total error. Hence, for $x_n \in X_n^C \bigcap X_n^F : y^C(x_n) \pm \sigma_y^C(x_n) \simeq y^F(x_n) \pm \sigma_y^F(x_n)$.

In the case $x_e = \log D_e$ the most discordant parameters are obtained from Perseus and pair galaxies. The maximum difference between the ordinates $\mid y^P(x_e) - y^p(x_e) \mid$ for $x_e \in X_e^P \bigcap X_e^p$ has a value less than or equal to 1.8 ([5]) times the estimated total error $\sigma_y^P(x_e) + \sigma_y^p(x_e)$.

[5] This value reaches 1.98 if 0.03 is assumed to be the observational error for $log D_e$.

Continuing in this fashion we have compared pairwise all the 8 sets of galaxies. The comparison was performed by plotting eq. 3.23 for two different sets (k) and then checking if, and how, the estimated error bands overlapped in some region of the plot. In order to quantify the comparison we have performed the following procedure.

Considering a couple of sets k_1 and k_2 their regression lines are given by eq 3.13 with the appropriate parameters. The quantity:

$$\sigma(k_1, k_2) \equiv max \left\{ \frac{\mid y^{k_1}(x) - y^{k_2}(x) \mid}{\sigma_y^{k_1}(x) + \sigma_y^{k_2}(x)} \right\} \tag{3.27}$$

for $x \in X^{k_1} \bigcap X^{k_2}$ gives the maximum difference between the two estimated ordinates in units of the estimated total error. If $\sigma(k_1, k_2) < 1$ then the difference between the two regression lines amounts to less than the error, as happened for the case $x = \log D_n$ between Coma and Fornax. We are now considering all the possible pairs (k_1, k_2) for each diameter used and looking for the pair giving the greatest value, say $\tilde{\sigma}$. What we obtained is

$$\tilde{\sigma}_0 = 0.75 \tag{3.28}$$

for $x = log D_0$ resulting from the groups and pair galaxies. For $x = \log D_n$ we have

$$\tilde{\sigma}_n = 0.85 \tag{3.29}$$

from the pair: Coma and Fornax. For $x = \log D_e$ we have

$$\tilde{\sigma}_e = 2.21 \tag{3.30}$$

for the pair A 2199 and groups. Other relevant values are: $\sigma_e(C, p) = 1.97$ for Coma and pairs, $\sigma_e(P, D) = 1.65$ for Perseus and DC2345-28, $\sigma_e(D, G) = 2.02$ for DC2345-28 and groups, $\sigma_e(F, G) = 0.57$. If the best accuracy value is adopted (i.e.: 0.02 for $\log D_n$ and 0.03 for $\log D_e$), then $\tilde{\sigma}_n = 2.11$ for Fornax and pairs, $\tilde{\sigma}_e = 3.78$ for the same pair, $\sigma_e(C, p) = 2.13, \sigma_e(P, D) = 2.24, \sigma_e(D, G) = 3.15, \sigma_e(F, G) = 2.17$. Note that from table 3.3 it is possible to see that the higher values of $\sigma(k_1, k_2)$ are obtained in the case of lower correlation sets (as Perseus, DC2345-28, groups, Fornax) or member-poor sets (as pairs, Fornax, DC2345-28). Dropping the "bad-behavior" sets and keeping only Coma, Virgo, A 2199, groups and Perseus, then:

$$\tilde{\sigma}'_e = 1.82 \tag{3.31}$$

for Perseus and A 2199. Other values are: $\sigma_e(V, C) = 0.98$ for Virgo and Coma, $\sigma_e(V, G) = 1.23$ for Virgo and groups, $\sigma_e(C, A) = 1.42$ for Coma and A 2199.

Finally, no large difference between one set and another seems to result from these numbers as far as realistic values for observational errors are assumed. This fact leads me to suspect that all the regression lines are indicative of only one law valid for all galaxies no matter in which set (cluster or group) they fall. So the data we have represent only one parent population. The homogeneity test described by Guest (1963) is what is needed to

clarify this suspicion. I give here a summary of this test, further details are in the original Guest (1963) book. It tests the hypothesis that r different B^k and A^k with variances σ_{B^k} and σ_{A^k} come from only one distribution.

Taking a weighted mean of the slopes and intercepts as:

$$\bar{B} = \frac{\Sigma_k W_{B,k} B^k}{\Sigma_k W_{B,k}} \qquad W_{B,k} = \frac{\sigma^2}{\sigma^2_{B^k}} \tag{3.32}$$

$$\bar{A} = \frac{\Sigma_k W_{A,k} A^k}{\Sigma_k W_{A,k}} \qquad W_{A,k} = \frac{\sigma^2}{\sigma^2_{A^k}} \tag{3.33}$$

the quantity $\Sigma_k W_{B,k}(B^k - \bar{B})^2/\sigma^2$ will be distributed as χ^2 with $r-1$ degrees of freedom. A similar quantity is also computed using $A^k, \bar{A}, W_{A,k}$ and follows the same distribution. Also the $\Sigma_{k,i}(y_i^k - A^k - B^k x_i^k)^2/\sigma^2$ will be distributed, independently of the B^k, as χ^2 with $\Sigma_k(n^k - 2) = N - 2r$ degrees of freedom. Hence, under the assumption of the homogeneity of the slopes, intercepts and σ^2, the ratio:

$$F_B = \frac{\left[\frac{\Sigma_k W_{B,k}(B^k - \bar{B})^2}{r-1}\right]}{\left[\frac{\Sigma_{k,i}(y_i^k - A^k - B^k x_i^k)^2}{N-2r}\right]} \tag{3.34}$$

will be distributed like F with $(r-1, N-2r)$ degrees of freedom. This provides a test of the hypothesis of homogeneity of the slopes. A ratio F_A for the intercept similar to F_B is easy to obtain.

If the slopes pass the test, then $\bar{B}$ is an unbiased estimate of the true slope B, and the same holds if the intercepts pass the test. An unbiased estimate of σ^2 is:

$$s^2 = \frac{\Sigma_{k,i}(y_i^k - A^k - B^k x_i^k)^2}{N - 2r} \tag{3.35}$$

and then:

$$s^2(\bar{B}) = \frac{s^2}{\Sigma_k W_{B,k}} \tag{3.36}$$

gives an estimate of the variance of $\bar{B}$. A similar expression gives $s^2(\bar{A})$. Finally if both the slopes and the intercepts pass the homogeneity test, then the regression lines may be assumed to be all estimates of the same straight line.

Performing this test on the sample, we have found that in every case the fitted slopes and intercepts B^k and A^k pass the test and give:

$$\begin{aligned} \bar{B}_0 &= 1.91 \quad s(\bar{B}_0) = 0.02 \\ \bar{A}_0 &= 7.73 \quad s(\bar{A}_0) = 0.04 \end{aligned} \tag{3.37}$$

for the isophotal diameter;

$$\begin{aligned} \bar{B}_n &= 2.06 \quad s(\bar{B}_n) = 0.06 \\ \bar{A}_n &= 8.78 \quad s(\bar{A}_n) = 0.04 \end{aligned} \tag{3.38}$$

for the D_n diameter, and:

$$\begin{array}{ll} \bar{B}_e = 1.32 & s(\bar{B}_e) = 0.05 \\ \bar{A}_e = 8.95 & s(\bar{A}_e) = 0.04 \end{array} \tag{3.39}$$

for the effective diameter. Then putting together all the galaxies if they were all found in only one cluster and then performing once more the fitting to obtain the slope and intercept, the results were:

$$\begin{array}{ll} B_0 = 1.91 & \sigma_{B_0} = 0.02 \\ A_0 = 7.77 & \sigma_{A_0} = 0.08 \end{array} \tag{3.40}$$

for the isophotal diameter (see graph. C.9);

$$\begin{array}{ll} B_n = 2.07 & \sigma_{B_n} = 0.05 \\ A_n = 8.75 & \sigma_{A_n} = 0.09 \end{array} \tag{3.41}$$

for the D_n diameter (see graph. C.18), and:

$$\begin{array}{ll} B_e = 1.35 & \sigma_{B_e} = 0.05 \\ A_e = 8.95 & \sigma_{A_e} = 0.06 \end{array} \tag{3.42}$$

for the effective diameter (see graph. C.27), thus giving an excellent agreement with the estimates obtained by the homogeneity test.

Another useful test is as follows. Strom and Strom (1978) took the $M_V^{cfr} \equiv -21.5$ as a reference value of the galaxian magnitude at which they compared the fitted values of diameter. Such a magnitude corresponds, in the units we have used, to $\log L_{cfr}/L_\odot = 9.81$, and using the regression laws obtained by the homogeneity test (eqq. 3.37, 3.38, 3.39) we have fixed three values for the diameter $x_{cfr} = \log D_{0,cfr} \equiv 1.09$, $\log D_{e,cfr} \equiv 0.65$, $\log D_{n,cfr} \equiv 0.50$. Finally we have computed $y^k(x_{cfr})$ and $\sigma_y^k(x_{cfr})$ for each set and the results are listed in tables B.1...B.14 . As is easily seen, for $x_{cfr} = \log D_{0,cfr}$ all the estimated luminosities are equal to one another within the errors. The same holds for $x_{cfr} = \log D_{n,cfr}$. Once more I have found different behaviour for $x_{cfr} = \log D_{e,cfr}$. Here we list the inequalities with their significance levels:

$$\log L_{cfr}/L_\odot(A2199 < \log L_{cfr}/L_\odot(groups) \quad > 99\% \tag{3.43}$$

$$\log L_{cfr}/L_\odot(pairs) < \log L_{cfr}/L_\odot(groups) \quad \sim 99\% \tag{3.44}$$

$$\log L_{cfr}/L_\odot(pairs) < \log L_{cfr}/L_\odot(Perseus) \quad \sim 97\% \tag{3.45}$$

$$\log L_{cfr}/L_\odot(DC2345-28) < \log L_{cfr}/L_\odot(groups) \quad > 99\% \tag{3.46}$$

Also for this test the largest differences result when we compare objects which have a small number of members or are poorly correlated. Dropping these sets (namely: groups, Perseus and Fornax) only a marginally significant difference is found comparing Coma and pairs:

$$\log L_{cfr}/L_\odot(pairs) < \log L_{cfr}/L_\odot(Coma) \quad \sim 93\% \tag{3.47}$$

Hence it is possible to conclude that: *the galaxies examined here, although they come from different environmental conditions, seem to behave almost as if they were all within the same cluster or group, for almost all diameters used.* From a purely numerical point of view this result may seem straightforward from an examination of table B.1. Actually using the isophotal radius the correlations are always good and the slopes and intercepts are never different from one another by more than 1 σ. On the contrary, this result may appear rather surprising for the effective diameter where the largest differences in slopes and intercepts are found (eq. 3.30 and eq. 3.31). The D_n diameter show a quite averaged behaviour. A possible explanation may come from the low correlation in data for group ellipticals and in member-poor clusters like Fornax and DC2345-28. Dropping these clusters I drop the pairs giving the largest values of $\sigma_e(k_1, k_2)$, nad the homogeneity test gives essentially the same estimates in this case for the true slope and intercept. This means that the bad-behaviour of these clusters is not dominant, and the above result is confirmed.

3.6.2 Inner-outer and dense-sparse comparison

In four cases, namely Coma, Virgo, Perseus and group galaxies, it has been found possible to split the set into two subsets. For group galaxies the limiting compactness (eq. 3.9) has been taken as $c^* = 1.4$ so that we had 18 sparse group and 19 dense group galaxies. For the cluster galaxies, having the values of the coordinates in right ascension (α_i^k) and declination (δ_i^k) it was possible to compute the linear distance of each galaxy from the centre of the cluster (α_c^k, δ_c^k taken from the literature: 7SI, Kent and Sargent 1983, Kent and Gunn 1982). The projected distance is then:

$$r_i^k = 2 \frac{V^k}{H_0} \tan\left(\frac{\phi_i^k}{2}\right) \tag{3.48}$$

where the ϕ_i^k are defined by: $\cos(\phi_i^k) = \sin(\delta_i^k)\sin(\delta_c^k) + \cos(\delta_i^k)\cos(\delta_c^k)\cos(\alpha_i^k - \alpha_c^k)$. Then a limiting value $r^*(k)$ has been chosen to have two subsets with more or less the same number of galaxies. So: $r^*(Virgo) = 0.55\ Mpc$ gives 14 inner and 13 outer galaxies, $r^*(Coma) = 0.21\ Mpc$ gives 17 inner and 17 outer galaxies, $r^*(Perseus) = 0.15\ Mpc$ gives 9 inner and 10 outer galaxies.

Now let me consider the result in tables B.4, B.5, B.6 and B.7. The final line gives the values of the maximum difference between the estimated regression lines in units of the total estimated error (eq. 3.27). As in the previous subsection, the Virgo galaxies show a marginally different behaviour in regions of different density (graphs C.43,...,C.45). The outer galaxies seem to have slightly larger effective diameters with respect to the inner galaxies. The same holds when I consider the D_n diameter, while the isophotal diameter does not change from the inner to the outer region. I must say that, by using eqq. 3.25, 3.25 to compare the slopes and the intercepts inthe two regions, I obtain that for the Virgo cluster (table B.4) the change of the slopes between the inner and the outer region is less significant than 95 %

for $\log D_n$, and less than 53 % for $\log D_e$; the change of the intercepts is less significant than 85 % for $\log D_e$, and has a significant level of $\sim$ 98 % for $\log D_n$. All the other sets of galaxies: Coma, Perseus and group galaxies show no change, whatever diameter we use, between the two regions. This result is rather surprising and probably deserves more work. In fact it seems quite strange that the outermost diameter (i.e.: D_0) is insensitive to the environment, while the more inner diameters (i.e.: $D_n < D_e < D_0$) are. In order to check the result obtained, I performed the inner-outer comparison for the bright subsets using the same r^* and the results are listed in tables B.11, B.12, B.13, B.14. It can be seen that, again, no relevant difference is present with regard to the result of the set as a whole (see also graphs C.43,...,C.54), thus confirming the conclusion of the previous subsection: the galaxies in this sample probably all belong to one family and no basic difference in structure between the bright and faint members is shown by these tests. Elliptical galaxies show the same luminosity-diameter relation in different environmental conditions. Virgo galaxies might be an exception, but the comparison between the cluster as a whole and the bright subset is not as accurate as the other sets, because the bright Virgo galaxies are fewer (see table B.11). In any case, the data show a good correlation, both in the inner and in the outer region, only using the isophotal diameter.

3.7 Summary and conclusion

I have found some evidence that the relation between the luminosity and the dimensions of normal elliptical galaxies is quite stable against the variation of environmental conditions. This suggests that by using these objects as tracers of the large-scale structure of the universe, we can obtain reliable conclusions (Dressler et al. 1987, Lynden-bell et al. 1988, 7S.IV, 7S.V). On the other hand, this result can throw some doubt on the conclusion of Strom and Strom (1978), although it was based on data obtained in a different spectral band (the visual V), which is probably more likely to show the outermost part of ellipticals. In order to check this point, we plan to run the procedure, adopted in this work, on the same data of Strom and Strom, dropping those galaxies which are definitely not ellipticals. Probably we will get a much poorer sample, but the results will be extremely interesting. Whitmore, Forbes and Rubin (1988) indicate that the inner cluster environment can strip away some fraction of the mass in the outer halos of spiral galaxies or, alternatively, it does not allow the halo to form. Hence the environment is likely to affect the outermost parts of spiral galaxies probably in the way discussed in chapter 2. In fact the outer regions of spiral galaxies, being bluer than in elliptical galaxies, can be observed more easily in the B band. The blue band observation seems to show no environmental effect, according to my analysis. This is probably the origin of the different conclusion reached by Strom and Strom (1978). The relative behaviour of the three diameter indicators deserves more attention, also from a theoretical point of view. A good hint may come from the simulations of Aguilar

and White (1986).

In the future I plan to focus my attention on similar studies of the environmental effect on the angular momentum of spiral galaxies. In this way, I hope to obtain a good test of theories about the origin and evolution of galaxies.

To summarize what have been, up to now, the main results of this work, I can say that using B-band data:

- the sample contains nearly normal elliptical galaxies with the same structure, shared by bright and faint objects, spanning quite a wide range of luminosity;
- estimating the dimensions of the galaxies by three different indicators, no relevant difference in their behaviour seems to result from this study of rich cluster and group galaxies, while marginally different behaviour seems to occur in poor clusters;
- there is evidence that the regression lines $\log L$ vs. $\log D$, for galaxies in different environments, indicate the existence of only one law valid for all galaxies, no matter in what environment they are and which diameter indicator is used;
- normal elliptical galaxies seem to share the same *universal* behaviour as far as the $\log L$ vs. $\log D$ relation is concerned;
- the slope of the $\log L$ vs. $\log D_e$ law is consistent with that found by Binggeli et al. (1984) for the Virgo cluster galaxies;
- if the environmental effect is present, it is probably covered by observational errors;

In the future I plan to pursue the following goals:

- a deeper analysis of old data in order to compare my results with previous results;
- a wider discussion of the relative behaviour of diameter indicators;
- the inclusion, in this analysis, of the angular momentum of spiral galaxies, mainly in relation to theories of galaxy formation and evolution.

I interrupt the discussion here by noting that at least one of the last three points will hopefully be the subject of the Ph. D. thesis.

To be continued....

Appendix A

The sample of elliptical galaxies.

We list hereafter all the data we used to get the result discussed in the text. For the richest sets as Virgo, Coma, Perseus and Groups, we give also the coordinates (α_i^k, δ_i^k) used to compute the projected distance from the centre (eq. 3.43). The coordinates of the centre and the assumed recession velocity of the entire set are given on the top of each table. For the groups the values of the compactness c are listed instead of the coordinates and the velocity is given for each galaxy. In the case in which the coordinates are not used, they are not listed. If additional members are present , they are listed after horizontal line. In the case of A 2199and DC2345-28, the series number of the 7S.III catalog are listed as the name of galaxies. For those galaxies see 7S.III.

VIRGO, $V = 1071\, Km\, s^{-1}$, $\alpha_c = 12^h27'.8$, $\delta_c = 10°33'$.

Name	α			δ			B_T	$\log D_e$	$\log D_n$	$\log D_0$
N 4239	12	14	42	16	48	00	13.58	0.73	0.49	1.10
N 4635	12	21	55	07	35	42	10.64	1.28	1.10	1.68
N 4374	12	22	31	13	09	48	10.13	1.26	1.25	1.75
N 4387	12	23	09	13	05	18	12.87	0.71	0.70	1.20
N 4406	12	23	39	13	13	24	09.87	1.48	1.24	1.84
N 4434	12	25	00	08	26	00	12.83	0.79	0.68	1.23
N 4458	12	26	26	13	31	06	12.78	0.95	0.61	1.27
N 4464	12	26	49	08	26	06	13.61	0.25	0.64	0.94
N 4472	12	27	14	08	16	42	09.32	1.54	1.36	1.94
N 4473	12	27	16	13	42	24	11.21	0.92	1.09	1.50
N 4478	12	27	45	12	36	18	12.14	0.67	0.92	1.29
N 4486	12	28	17	12	40	06	09.52	1.54	1.30	1.91
N 4489	12	28	18	17	02	00	12.71	1.03	0.58	1.29
N 4551	12	33	06	12	32	24	12.72	0.77	0.72	1.24
N 4552	12	33	08	12	50	00	10.84	1.00	1.15	1.57
N 4564	12	33	55	11	42	54	11.96	0.86	0.90	1.38
N 4621	12	39	31	11	55	12	10.65	1.19	1.13	1.66
N 4636	12	40	17	02	57	42	10.20	1.53	1.08	1.79
N 4649	12	41	09	11	49	30	09.77	1.39	1.30	1.84
N 4660	12	42	01	11	27	36	12.19	0.63	0.91	1.27
N 4261	12	16	50	06	06	06	11.32	1.11	0.98	1.54
N 4318	12	20	12	08	28	00	14.17	0.32	0.49	0.90
N 4339	12	21	01	06	21	36	12.29	1.01	0.73	1.36
N4486B	12	28	00	12	46	00	14.23	0.01	0.54	0.76
N 4581	12	35	36	01	44	00	13.15	0.77	0.60	1.18
N 4168	12	09	44	13	29	00	11.95	1.18	0.74	1.44
N 4467	12	26	57	08	16	12	14.81	0.51	0.23	0.86

COMA, $V = 6890\ Km\ s^{-1}$, $\alpha_c = 12^h\ 57'.18$, $\delta_c = 28^\circ\ 13'.8$

Name	α			δ			B_T	$\log D_e$	$\log D_n$	$\log D_0$
N 4899	12	54	59	27	46	00	13.21	0.98	0.46	1.20
N 4926	12	59	29	27	53	36	13.95	0.58	0.47	1.01
I 3959	12	56	43	28	03	12	15.07	0.31	0.27	0.77
I 3957	12	56	43	28	02	21	15.63	0.21	0.16	0.66
D 0087	12	57	06	28	03	45	16.58	0.10	-.07	0.49
N 4869	12	56	58	28	10	54	14.57	0.45	0.35	0.88
D 0107	12	56	56	28	09	25	15.90	0.40	-.04	0.65
N 4906	12	58	15	28	11	30	14.87	0.43	0.28	0.83
N 4876	12	57	19	28	10	54	15.22	0.30	0.23	0.75
D 0125	12	57	18	28	11	47	16.41	-.16	0.08	0.44
N 4874	12	57	10	28	13	48	12.31	1.31	0.51	1.38
N 4872	12	57	09	28	13	00	15.35	0.09	0.28	0.67
N 4867	12	56	50	28	14	24	15.28	0.15	0.28	0.70
D 0136	12	56	31	28	14	12	16.37	-.14	0.09	0.46
I 4051	12	58	28	28	16	30	14.01	0.83	0.30	1.04
N 4889	12	57	43	28	14	42	12.48	1.02	0.69	1.33
I 4011	12	57	42	28	16	18	15.74	0.28	0.09	0.66
N 4886	12	57	39	28	15	18	14.78	0.49	0.27	0.86
D 0153	12	57	19	28	15	57	15.97	0.16	0.08	0.60
N 4864	12	56	48	28	14	48	14.62	0.46	0.34	0.88
I 4045	12	58	24	28	21	30	14.96	0.28	0.32	0.78
I 4021	12	57	49	28	18	30	15.62	0.17	0.18	0.66
I 4012	12	57	43	28	20	48	15.68	0.07	0.20	0.62
D 0193	12	57	31	28	24	00	16.05	0.21	0.04	0.60
N 4860	12	56	39	28	23	36	14.43	0.46	0.39	0.91
D 0207	12	57	44	28	26	31	15.77	0.21	0.12	0.64
N 4881	12	57	33	28	31	00	14.43	0.58	0.33	0.93
N 4841A	12	55	07	28	44	48	13.67	0.73	0.47	1.08
N 4692	12	45	28	27	29	48	13.69	0.73	0.45	1.08
N 4957	13	02	48	27	50	12	14.01	0.69	0.40	1.02
N 4816	12	53	48	28	01	00	13.79	0.85	0.38	1.08
N 4841B	12	55	09	28	45	06	13.51	0.79	0.50	1.12
N 4923	12	59	07	28	06	54	14.59	0.45	0.35	0.88
N 4849W	12	57	53	28	13	35	14.34	0.37	0.50	0.90

GROUPS

Name	Vel.	B_T	$\log D_e$	$\log D_n$	$\log D_0$	c
N 0083	5649	13.32	0.95	0.45	1.18	6.72
N 0183	5089	13.49	0.69	0.55	1.11	0.62
N 0533	5143	12.26	1.20	0.63	1.36	1.52
N 0661	3593	12.77	0.76	0.72	1.23	1.12
N 0680	2803	12.44	0.79	0.80	1.29	2.25
N 0741	5069	12.05	1.24	0.68	1.43	1.01
N 1016	6191	12.43	1.12	0.64	1.35	1.10
N 1587	3452	12.46	0.90	0.75	1.31	3.60
N 1588	3452	13.85	0.47	0.53	1.00	3.60
N 2693	4576	12.55	0.94	0.71	1.31	1.39
N 2778	2014	13.30	0.74	0.57	1.15	0.94
N 3193	1432	11.81	0.90	0.93	1.41	1.26
N 3226	1432	11.93	1.25	0.69	1.46	1.26
N 3377	1188	11.13	1.05	1.06	1.55	0.94
N 3379	1188	10.43	1.07	1.24	1.65	0.94
N 4008	3716	13.03	0.68	0.68	1.17	2.02
N 3348	2995	11.96	0.93	0.88	1.40	1.11
N 3640	7422	11.24	1.04	1.03	1.53	1.95
N 3641	1803	13.89	0.61	0.46	1.03	1.95
N 3605	1316	13.24	0.76	0.57	1.16	1.80
N 3608	1316	11.68	1.07	0.89	1.47	1.80
N 4291	1956	12.42	0.69	0.84	1.26	0.95
N 4589	1956	11.59	1.14	0.88	1.50	0.95
N 4648	1956	12.74	0.71	0.74	1.22	0.95
N 5129	7357	12.90	1.00	0.57	1.26	1.43
N 5612	2693	13.55	0.87	0.41	1.12	0.99
N 5322	2693	11.07	1.07	1.06	1.56	0.99
N 5490	5483	12.99	0.81	0.64	1.21	1.91
N 5576	1784	11.75	0.81	0.98	1.39	1.91
N 5557	3837	11.90	0.98	0.87	1.42	0.80
N 5638	1883	12.05	0.97	0.83	1.39	0.79
N 5813	1966	11.39	1.21	0.90	1.54	1.75
N 5831	1966	12.29	0.95	0.77	1.35	1.75
N 5845	1966	13.35	0.13	0.73	0.90	1.75
N 5846	1966	10.67	1.44	0.99	1.70	1.75
N 5982	3147	11.98	0.92	0.88	1.39	1.79
N 7454	2086	12.57	0.91	0.71	1.30	1.95

PERSEUS; $V = 5470\ Km\ s^{-1}$; $\alpha_c = 3^h\ 16'.5$; $\delta_c = 41°\ 19'.9$

Name		α			δ		B_T	$\log D_e$	$\log D_n$	$\log D_0$
N 1260	03	14	09	41	13	18	13.65	0.62	0.54	1.06
N 1270	03	15	39	41	17	18	13.57	0.42	0.63	1.02
N 1272	03	16	02	41	18	30	12.23	1.18	0.65	1.40
N 1274	03	16	22	41	22	06	14.38	0.20	0.48	0.83
N 1278	03	16	35	41	23	00	12.83	0.90	0.65	1.25
N 1282	03	16	53	41	11	12	13.36	0.65	0.61	1.12
I 0310	03	13	24	41	08	36	13.12	0.83	0.59	1.19
CR 032	03	16	18	41	24	00	13.79	0.67	0.47	1.05
CR 036	03	16	18	41	24	00	14.59	0.36	0.37	0.86
Per101	03	14	09	41	12	30	15.48	0.30	0.15	0.71
Per152	03	16	42	41	18	00	15.80	0.16	0.12	0.63
Per153	03	16	42	41	18	00	16.21	0.15	0.01	0.56
Per163	03	16	48	41	10	00	15.36	0.16	0.24	0.69
Per164	03	17	00	41	10	00	14.72	0.45	0.30	0.86
Per195	03	16	00	41	58	00	14.20	0.73	0.30	0.99
Per199	03	16	00	41	58	30	13.75	1.05	0.33	1.10
N 1273	03	16	07	41	21	36	13.52	0.55	0.61	1.07
N 1283	03	16	57	41	13	06	13.75	0.71	0.47	1.07
N 1293	03	18	21	41	13	00	13.41	0.73	0.55	1.13

A 2199, $V = 9150\, Km\, s^{-1}$

S. Nr.	B_T	$\log D_e$	$\log D_n$	$\log D_0$
352	16.58	0.46	-.33	0.53
537	16.05	0.10	0.09	0.58
538	16.56	0.05	-.03	0.49
540	16.07	0.17	0.06	0.59
539	16.17	0.06	0.08	0.55
529	16.62	0.15	-.10	0.50
530	14.82	0.55	0.23	0.86
531	15.62	0.23	0.16	0.67
533	15.19	0.53	0.12	0.80
534	16.63	0.13	-.09	0.49
535	15.97	0.02	0.15	0.56
536	17.30	-.01	-.22	0.36
393	14.47	0.58	0.33	0.93
395	12.76	1.28	0.37	1.29

DC2345-28, $V = 8900\ Km\ s^{-1}$

S. Nr.	B_T	$\log D_e$	$\log D_n$	$\log D_0$
556	14.82	0.40	0.32	0.83
557	13.46	1.16	0.21	1.15
558	16.95	-.28	-.01	0.33
559	16.06	0.21	0.21	0.60
560	17.13	0.16	-.28	0.41
561	16.21	0.20	0.00	0.57
562	15.71	0.22	0.14	0.66
563	13.94	0.75	0.39	1.04
564	14.81	0.38	0.33	0.83
565	16.09	0.13	0.07	0.58
566	17.43	0.12	-.35	0.35

FORNAX, $V = 1261\ Km\ s^{-1}$

Name	B_T	$\log D_e$	$\log D_n$	$\log D_0$
N 1339	12.51	0.75	0.79	1.27
N 1344	11.11	1.12	1.03	1.57
N 1374	11.88	1.00	0.86	1.42
N 1379	11.66	1.15	0.85	1.49
N 1399	10.55	1.15	1.18	1.66
N 1404	10.89	0.95	1.16	1.55
N 1477	11.76	1.04	0.88	1.45
I 2006	12.17	0.98	0.79	1.37

PAIR GALAXIES

Name	Vel.	B_T	$\log D_e$	$\log D_n$	$\log D_0$
N 2778	1983	13.30	0.74	0.57	1.15
N 3226	1222	11.93	1.25	0.69	1.46
N 3873	6263	13.68	0.77	0.45	1.09
N 4125	1768	10.58	1.30	1.11	1.69
N 4339	4166	12.29	1.01	0.73	1.36
N 4458	1304	12.78	0.95	0.61	1.27
N 4551	813	12.72	0.77	0.72	1.24
N 4649	1272	9.77	1.39	1.30	1.84
N 4841A	6525	13.67	0.73	0.47	1.08
N 4841B	6525	13.51	0.79	0.50	1.12
N 5629	4441	12.96	0.93	0.58	1.24
N 5846	1971	10.67	1.44	0.99	1.70
N 7562	3681	12.32	0.90	0.79	1.33

Appendix B

Tables of results

In the following pages we list the values of the parameters resulting from the techique discussed in chapter 3. Each table contains a self-explicating title.

Table B.1a: $\log L/L_\odot$ vs. $\log D_0$

Param.	Virgo	Coma	Perseus	A 2199
N_g	27	34	19	14
r	0.99	0.99	0.99	0.99
B	1.87	1.87	1.93	1.97
σ_B	0.06	0.03	0.07	0.06
A	7.82	7.81	7.75	7.67
σ_A	0.09	0.08	0.11	0.10
$< \log D_0 >$	0.89	1.14	1.18	1.08
$< \log L >$	9.49	9.95	10.03	9.81
$\log D_{0,min}$	0.25	0.74	0.76	0.78
$\log D_{0,max}$	1.43	1.69	1.60	1.71
$\log L_{min}$	8.33	9.23	9.18	9.19
$\log L_{max}$	10.53	10.94	10.78	11.01
$\log L_{cfr}$	9.89	9.88	9.88	9.85
σ_{cfr}	0.08	0.07	0.08	0.08

Table B.1b: $\log L/L_\odot$ vs. $\log D_0$

Param.	DC2345-28	Fornax	Groups	Pairs
N_g	11	8	37	13
r	0.99	0.98	0.98	1.00
B	1..95	2.37	1.89	2.02
σ_B	0.08	0.21	0.06	0.04
A	7.70	7.31	7.82	7.61
σ_A	0.12	0.23	0.10	0.09
$< \log D_0 >$	1.08	1.04	1.22	1.22
$< \log L >$	9.81	9.77	10.12	10.08
$\log D_{0,min}$	0.74	0.83	0.66	0.61
$\log D0, max$	1.56	1.22	1.86	1.46
$\log L_{min}$	9.11	9.39	9.13	8.92
$\log L_{max}$	10.71	10.17	11.44	10.51
$\log L_{cfr}$	9.86	9.93	9.91	9.84
σ_{cfr}	0.08	0.10	0.08	0.08

Table B.2a: $\log L/L_{\odot}$ vs. $\log D_n$

Param.	Virgo	Coma	Perseus	A 2199
N_g	27	34	19	14
r	0.97	0.93	0.93	0.85
B	2.02	2.46	2.08	2.09
σ_B	0.10	0.17	0.19	0.37
A	8.76	8.51	8.72	8.80
σ_A	0.09	0.14	0.15	0.20
$< \log D_n >$	0.36	0.59	0.62	0.48
$< \log L >$	9.49	9.95	10.03	9.81
$\log D_{n,min}$	-.28	0.23	0.21	0.09
$\log D_{n,max}$	0.85	0.99	0.85	0.79
$\log L_{min}$	8.33	9.24	9.18	9.19
$\log L_{max}$	10.53	10.94	10.78	11.01
$\log L_{cfr}$	9.77	9.74	9.76	9.84
σ_{cfr}	0.08	0.10	0.09	0.08

Table B.2b: $\log L/L_{\odot}$ vs. $\log D_n$

Param.	DC2345-28	Fornax	Groups	Pairs
N_g	11	8	37	13
r	0.84	0.96	0.95	0.98
B	1.87	1.71	2.03	1.97
σ_B	0.40	0.20	0.11	0.12
A	8.87	8.90	8.78	8.89
σ_A	0.21	0.12	0.11	0.11
$< \log D_n >$	0.51	0.51	0.66	0.60
$< \log L >$	9.81	9.77	10.12	10.08
$\log D_{n,min}$	0.06	0.35	0.15	0.09
$\log D_{n,max}$	0.80	0.74	1.36	0.87
$\log L_{min}$	9.11	9.39	9.13	8.92
$\log L_{max}$	10.71	10.17	11.44	10.51
$\log L_{cfr}$	9.80	9.75	9.79	9.87
σ_{cfr}	0.07	0.07	0.08	0.08

Table B.3a : $\log L/L_\odot$ vs. $\log D_e$

Param.	Virgo	Coma	Perseus	A 2199
N_g	27	34	19	14
r	0.90	0.94	0.85	0.90
B	1.40	1.25	1.19	1.21
σ_B	0.14	0.08	0.18	0.17
A	8.88	9.03	9.11	8.92
σ_A	0.08	0.08	0.14	0.13
$< \log D_e >$	0.43	0.74	0.77	0.73
$< \log L >$	9.94	9.95	10.03	9.81
$\log D_{e,min}$	-.50	0.14	0.35	0.41
$\log D_{e,max}$	1.03	1.61	1.38	1.70
$\log L_{min}$	8.33	9.23	9.18	9.19
$\log L_{max}$	10.52	10.94	10.78	11.01
$\log L_{cfr}$	9.79	9.84	9.88	9.70
σ_{cfr}	0.07	0.05	0.05	0.05

Table B.3b : $\log L/L_\odot$ vs. $\log D_e$

Param.	DC2345-28	Fornax	Groups	Pairs
N_g	11	8	37	13
r	0.88	0.64	0.88	0.95
B	1.23	1.42	1.29	1.77
σ_B	0.22	0.69	0.12	0.17
A	8.92	8.94	9.08	8.54
σ_A	0.17	0.40	0.11	0.16
$< \log D_e >$	0.73	0.58	0.81	0.87
$< \log L >$	9.81	9.77	10.12	10.08
$\log D_{e,min}$	0.13	0.31	-.11	0.14
$\log D_{e,max}$	1.57	0.71	1.41	1.20
$\log L_{min}$	9.11	9.39	9.13	8.92
$\log L_{max}$	10.71	10.17	11.44	10.51
$\log L_{cfr}$	9.72	9.86	9.92	9.69
σ_{cfr}	0.05	0.07	0.05	0.08

Table B.4: Virgo inner-outer comparison.

	$\log D_0$		$\log D_e$		$\log D_n$	
Param.	in.	out.	in.	out.	in.	out.
N_g	14	13	14	13	14	13
r	0.99	0.99	0.94	0.82	0.99	0.96
B	1.84	2.05	1.45	1.52	2.12	1.80
σ_B	0.07	0.10	0.15	0.32	0.10	0.16
A	7.88	7.61	8.94	8.73	8.66	8.90
σ_A	0.10	0.12	0.08	0.19	0.09	0.06
$< \log D >$	0.84	0.95	0.33	0.55	0.36	0.37
$< \log L >$	9.42	9.56	9.42	9.56	9.42	9.56
$\log D_{min}$	0.25	0.59	-.50	0.12	-.28	-.02
$\log D_{max}$	1.43	1.33	1.03	1.02	0.85	0.79
$\log L_{min}$	8.33	8.82	8.33	8.82	8.33	8.82
$\log L_{max}$	10.52	10.34	10.52	10.34	10.52	10.34
$\log L_{cfr}$	9.89	9.85	9.88	9.71	9.72	9.80
σ_{cfr}	0.08	0.08	0.07	0.07	0.09	0.07
	$\tilde{\sigma}_0 = 0.87$		$\tilde{\sigma}_e = 1.44$		$\tilde{\sigma}_n = 1.34$	

Table B.5: Coma inner-outer comparison.

	$\log D_0$		$\log D_e$		$\log D_n$	
Param.	in.	out.	in.	out.	in.	out.
N_g	17	17	17	17	17	17
r	0.99	1.00	0.93	0.95	0.92	0.94
B	1.88	1.93	1.23	1.29	2.32	2.64
σ_B	0.05	0.04	0.13	0.11	0.26	0.25
A	7.82	7.73	9.04	8.99	8.56	8.41
σ_A	0.09	0.09	0.09	0.11	0.17	0.19
$< \log D >$	1.06	1.22	0.63	0.85	0.54	0.64
$< \log L >$	9.82	10.09	9.82	10.09	9.82	10.09
$\log D_{min}$	0.74	0.90	0.14	0.51	0.23	0.34
$\log D_{max}$	1.68	1.50	1.61	1.28	0.99	0.80
$\log L_{min}$	9.23	9.45	9.23	9.45	9.23	9.45
$\log L_{max}$	10.94	10.58	10.94	10.58	10.94	10.58
$\log L_{cfr}$	9.87	9.83	9.84	9.83	9.72	9.73
σ_{cfr}	0.07	0.08	0.05	0.06	0.09	0.11
	$\tilde{\sigma}_0 = 0.28$		$\tilde{\sigma}_e = 0.21$		$\tilde{\sigma}_n = 0.45$	

Table B.6: Perseus inner-outer comparison.

	$\log D_0$		$\log D_e$		$\log D_n$	
Param.	in.	out.	in.	out.	in.	out.
N_g	9	10	9	10	9	10
r	0.99	0.98	0.92	0.73	0.96	0.90
B	1.90	1.99	1.34	0.96	2.26	1.81
σ_B	0.10	0.13	0.21	0.32	0.24	0.31
A	7.79	7.67	9.02	9.28	8.60	8.91
σ_A	0.14	0.18	0.17	0.25	0.18	0.21
$< \log D >$	1.17	1.19	0.74	0.80	0.63	0.63
$< \log L >$	10.02	10.04	10.02	10.04	10.02	10.04
$\log D_{min}$	0.76	0.89	0.35	0.36	0.21	0.35
$\log D_{max}$	1.60	1.39	1.38	1.25	.0.85	0.83
$\log L_{min}$	9.18	9.48	9.18	9.48	9.18	9.48
$\log L_{max}$	10.78	10.48	10.78	10.48	10.78	10.48
$\log L_{cfr}$	9.87	9.85	9.89	9.90	9.73	9.81
σ_{cfr}	0.08	0.08	0.06	0.06	0.10	0.08
	$\tilde{\sigma}_0 = 0.22$		$\tilde{\sigma}_e = 0.82$		$\tilde{\sigma}_n = 0.67$	

Table B.7: Groups sparse-dense comparison.

	$\log D_0$		$\log D_e$		$\log D_n$	
Param.	sp.	d.	sp.	d.	sp.	d.
N_g	18	19	18	19	18	19
r	0.99	0.98	0.85	0.89	0.93	0.96
B	1.96	1.85	1.27	1.29	1.92	2.09
σ_B	0.07	0.08	0.19	0.16	0.19	0.15
A	7.72	7.87	9.09	9.08	8.86	8.74
σ_A	0.12	0.13	0.17	0.14	0.15	0.13
$< \log D >$	1.23	1.22	0.82	0.80	0.66	0.66
$< \log L >$	10.13	10.12	10.13	10.12	10.13	10.12
$\log D_{min}$	0.92	0.66	0.44	-.11	0.30	0.15
$\log D_{max}$	1.60	1.83	1.41	1.37	0.95	1.36
$\log L_{min}$	9.48	9.13	9.48	9.13	9.48	9.13
$\log L_{max}$	10.80	10.44	10.80	10.44	10.80	10.44
$\log L_{cfr}$	9.85	9.88	9.92	9.91	9.78	9.82
σ_{cfr}	0.08	0.07	0.06	0.06	0.09	0.08
	$\tilde{\sigma}_0 = 0.31$		$\tilde{\sigma}_e = 0.14$		$\tilde{\sigma}_n = 0.34$	

Table B.8: $\log L/L_\odot$ vs. $\log D_0$ for $\log L/L_\odot > 9.59$

Param.	Virgo	Coma	Perseus	Groups
N_g	11	26	15	33
r	0.98	1.00	0.97	0.99
B	1.88	1.84	1.82	1.96
σ_B	0.11	0.03	0.12	0.05
A	7.82	7.85	7.89	7.71
σ_A	0.15	0.08	0.17	0.10
$< \log D_0 >$	1.22	1.23	1.27	1.28
$< \log L >$	10.12	10.11	10.20	10.22
$\log D_{0,min}$	0.99	0.92	1.03	0.97
$\log D_{0,max}$	1.43	1.69	1.60	1.86
$\log L_{min}$	9.72	9.60	9.78	9.63
$\log L_{max}$	10.53	10.94	10.78	11.44
$\log L_{cfr}$	9.87	9.86	9.88	9.88
σ_{cfr}	0.08	0.07	0.08	0.12

Table B.9: $\log L/L_\odot$ vs. $\log D_n$ for $\log L/L_\odot > 9.59$

Param.	Virgo	Coma	Perseus	Groups
N_g	11	26	15	33
r	0.90	0.90	0.80	0.93
B	2.33	2.98	1.84	1.99
σ_B	0.37	0.29	0.38	0.14
A	8.56	8.14	8.91	8.82
σ_A	0.27	0.23	0.28	0.13
$< \log D_n >$	0.67	0.66	0.70	0.70
$< \log L >$	10.12	10.11	10.20	10.22
$\log D_{n,min}$	0.47	0.46	0.50	0.30
$\log D_{n,max}$	0.85	0.99	0.85	1.36
$\log L_{min}$	9.72	9.60	9.78	9.63
$\log L_{max}$	10.52	10.94	10.78	11.44
$\log L_{cfr}$	9.72	9.63	9.83	9.81
σ_{cfr}	0.11	0.13	0.11	0.08

Table B.10: $\log L/L_\odot$ vs. $\log D_e$ for $\log L/L_\odot > 9.59$

Param.	Virgo	Coma	Perseus	Groups
N_g	11	26	15	33
r	0.88	0.96	0.74	0.87
B	1.10	1.13	0.77	1.28
σ_B	0.19	0.07	0.19	0.13
A	9.26	9.17	9.53	9.10
σ_A	0.16	0.07	0.17	0.12
$< \log D_e >$	0.79	0.83	0.87	0.87
$< \log L >$	10.12	10.11	10.20	10.22
$\log D_{e,min}$	0.41	0.37	0.40	0.44
$\log D_{e,max}$	1.03	1.62	1.38	1.41
$\log L_{min}$	9.72	9.60	9.78	9.63
$\log L_{max}$	10.52	10.94	10.78	11.44
$\log L_{cfr}$	9.97	9.91	10.03	9.93
σ_{cfr}	0.05	0.05	0.05	0.06

Table B.11: Virgo inner-outer comparison for $\log L/L_\odot > 9.59$.

	$\log D_0$		$\log D_n$		$\log D_e$	
Param.	in.	out.	in.	out.	in.	out.
N_g	5	6	5	6	5	6
r	1.00	0.98	0.96	0.82	0.97	0.84
B	1.71	1.09	4.01	2.15	1.01	0.95
σ_B	0.09	0.19	0.63	0.76	0.15	0.31
A	8.06	7.79	7.26	8.69	9.41	9.30
σ_A	0.14	0.23	0.50	0.47	0.13	0.23
$< \log D >$	1.29	1.16	0.75	0.61	0.86	0.73
$< \log L >$	10.28	10.00	10.28	10.00	10.28	10.00
$\log D_{min}$	1.06	0.99	0.64	0.47	0.49	0.41
$\log D_{max}$	1.43	1.33	8.85	0.79	1.03	1.02
$\log L_{min}$	9.92	9.72	9.92	9.72	9.92	9.72
$\log L_{max}$	10.52	10.34	10.52	10.34	10.52	10.34
$\log L_{cfr}$	9.92	9.86	...	...	10.07	9.92
σ_{cfr}	0.07	0.08	...	...	0.05	0.04
	$\tilde{\sigma}_0 = 0.45$		$\tilde{\sigma}_n = 0.91$		$\tilde{\sigma}_e = 1.83$	

Table B.12: Coma inner-outer comparison for $\log L/L_\odot > 9.59$.

	$\log D_0$		$\log D_n$		$\log D_e$	
Param.	in.	out.	in.	out.	in.	out.
N_g	11	15	11	15	11	15
r	1.00	1.00	0.91	0.89	0.97	0.94
B	1.84	1.89	2.87	3.10	1.16	1.13
σ_B	0.05	0.04	0.44	0.44	0.09	0.11
A	7.87	7.78	8.17	8.08	9.17	9.15
σ_A	0.09	0.09	0.31	0.32	0.08	0.11
$< \log D >$	1.18	1.26	0.65	0.67	0.75	0.89
$< \log L >$	10.04	10.17	10.04	10.17	10.04	10.17
$\log D_{min}$	0.92	0.96	0.48	0.46	0.37	0.51
$\log D_{max}$	1.68	1.50	0.99	0.80	1.61	1.28
$\log L_{min}$	9.60	9.62	9.60	9.62	9.60	9.62
$\log L_{max}$	10.94	10.58	10.94	10.58	10.94	10.58
$\log L_{cfr}$	9.88	9.84	10.04	10.10	9.93	9.89
σ_{cfr}	0.07	0.08	0.11	0.12	0.05	0.05
	$\tilde{\sigma}_0 = 0.30$		$\tilde{\sigma}_n = 0.36$		$\tilde{\sigma}_e = 0.52$	

Table B.13: Perseus inner-outer comparison for $\log L/L_\odot > 9.59$.

	$\log D_0$		$\log D_n$		$\log D_e$	
Param.	in.	out.	in.	out.	in.	out.
N_g	7	8	7	8	7	8
r	0.99	0.94	0.89	0.83	0.94	0.34
B	1.69	2.23	3.16	1.27	0.97	0.35
σ_B	0.12	0.32	0.71	0.35	0.15	0.40
A	8.07	7.36	7.93	9.31	9.41	9.86
σ_A	0.16	0.41	0.54	0.24	0.14	0.36
$< \log D >$	1.28	1.26	0.73	0.68	0.85	0.89
$< \log L >$	10.23	10.18	10.23	10.18	10.23	10.18
$\log D_{min}$	1.03	1.06	0.57	0.50	0.40	0.62
$\log D_{max}$	1.60	1.39	0.85	0.83	1.38	1.25
$\log L_{min}$	9.83	9.78	9.83	9.78	9.83	9.78
$\log L_{max}$	10.78	10.42	10.78	10.42	10.78	10.42
$\log L_{cfr}$	9.92	9.80	...	...	10.04	10.09
σ_{cfr}	0.07	0.10	...	...	0.05	0.10
	$\tilde{\sigma}_0 = 0.73$		$\tilde{\sigma}_n = 1.3$		$\tilde{\sigma}_e = 1.7$	

Table B.14: Groups sparse-dense comparison for $\log L/L_{\odot} > 9.59$.

	$\log D_0$		$\log D_n$		$\log D_e$	
Param.	sp.	d.	sp.	d.	sp.	d.
N_g	17	16	17	16	17	16
r	0.99	0.99	0.92	0.94	0.84	0.84
B	1.94	1.98	1.90	2.06	1.20	1.35
σ_B	0.08	0.06	0.21	0.19	0.20	0.19
A	7.75	7.68	8.87	8.78	9.16	9.05
σ_A	0.12	0.11	0.16	0.16	0.17	0.18
$< \log D >$	1.25	1.31	0.68	0.73	0.84	0.92
$< \log L >$	10.17	10.28	10.17	10.28	10.17	10.28
$\log D_{min}$	0.97	1.00	0.30	0.47	0.44	0.47
$\log D_{max}$	1.60	1.86	0.95	1.36	1.41	1.35
$\log L_{min}$	9.63	9.73	9.63	9.73	9.63	9.73
$\log L_{max}$	10.80	11.44	10.80	11.44	10.80	11.44
$\log L_{cfr}$	9.86	9.85	9.82	9.81	9.94	9.92
σ_{cfr}	0.08	0.08	0.08	0.09	0.06	0.07
	$\tilde{\sigma}_0 = 0.11$		$\tilde{\sigma}_n = 0.28$		$\tilde{\sigma}_n = 0.40$	

Appendix C

Tables of graphs

Here I give the complete series of graphs showing the observational data for each set and each diameter indicator. These graphs are followed by some example of pairwise comparison in the most relevant cases. In each pairwise comparison, the graphic show the first regression line as a solid line bwtween two short-dashed lines, giving the estimated error band (at 1 σ); then the second regression line is plotted by a dot-dashed line between two dotted lines, again giving the estimated error band. By "groups" and "pairs" I mean individual galaxies which are members of groups or binaty systems.

A list of the graphics may be useful:

graph. C.1 Virgo data for $\log L/L_\odot$ vs. $\log D_0(Kpc)$

graph. C.2 Coma data for $\log L/L_\odot$ vs. $\log D_0(Kpc)$

graph. C.3 Groups data for $\log L/L_\odot$ vs. $\log D_0(Kpc)$

graph. C.4 Perseus data for $\log L/L_\odot$ vs. $\log D_0(Kpc)$

graph. C.5 A 2199 data for $\log L/L_\odot$ vs. $\log D_0(Kpc)$

graph. C.6 Pairs data for $\log L/L_\odot$ vs. $\log D_0(Kpc)$

graph. C.7 DC2345-28 data for $\log L/L_\odot$ vs. $\log D_0(Kpc)$

graph. C.8 Fornax data for $\log L/L_\odot$ vs. $\log D_0(Kpc)$

graph. C.9 All galaxies data for $\log L/L_\odot$ vs.$\log D_0(Kpc)$

graph. C.10 Virgo data for $\log L/L_\odot$ vs. $\log D_n(Kpc)$

graph. C.11 Coma data for $\log L/L_\odot$ vs. $\log D_n(Kpc)$

graph. C.12 Groups data for $\log L/L_\odot$ vs. $\log D_n(Kpc)$

graph. C.13 Perseus data for $\log L/L_\odot$ vs. $\log D_n(Kpc)$

graph. C.14 A 2199 data for $\log L/L_\odot$ vs. $\log D_n(Kpc)$

graph. C.15 Pairs data for $\log L/L_\odot$ vs. $\log D_n(Kpc)$

graph. C.43 Comparison between Virgo inner and Virgo outer galaxies for $\log L/L_{\odot}$ vs. $\log D_0(Kpc)$

graph. C.44 Comparison between Virgo inner and Virgo outer galaxies for $\log L/L_{\odot}$ vs. $\log D_e(Kpc)$

graph. C.45 Comparison between Virgo inner and Virgo outer galaxies for $\log L/L_{\odot}$ vs. $\log D_n(Kpc)$

graph. C.46 Comparison between Coma inner and Coma outer galaxies for $\log L/L_{\odot}$ vs. $\log D_0(Kpc)$

graph. C.47 Comparison between Coma inner and Coma outer galaxies for $\log L/L_{\odot}$ vs. $\log D_e(Kpc)$

graph. C.48 Comparison between Coma inner and Coma outer galaxies for $\log L/L_{\odot}$ vs. $\log D_n(Kpc)$

graph. C.49 Comparison between Perseus inner and Perseus outer galaxies for $\log L/L_{\odot}$ vs. $\log D_0(Kpc)$

graph. C.50 Comparison between Perseus inner and Perseus outer galaxies for $\log L/L_{\odot}$ vs. $\log D_e(Kpc)$

graph. C.51 Comparison between Perseus inner and Perseus outer galaxies for $\log L/L_{\odot}$ vs. $\log D_n(Kpc)$

graph. C.52 Comparison between sparse and dense Groups galaxies for $\log L/L_{\odot}$ vs. $\log D_0(Kpc)$

graph. C.53 Comparison between sparse and dense Groups galaxies for $\log L/L_{\odot}$ vs. $\log D_e(Kpc)$

graph. C.54 Comparison between sparse and dense Groups galaxies for $\log L/L_{\odot}$ vs. $\log D_n(Kpc)$

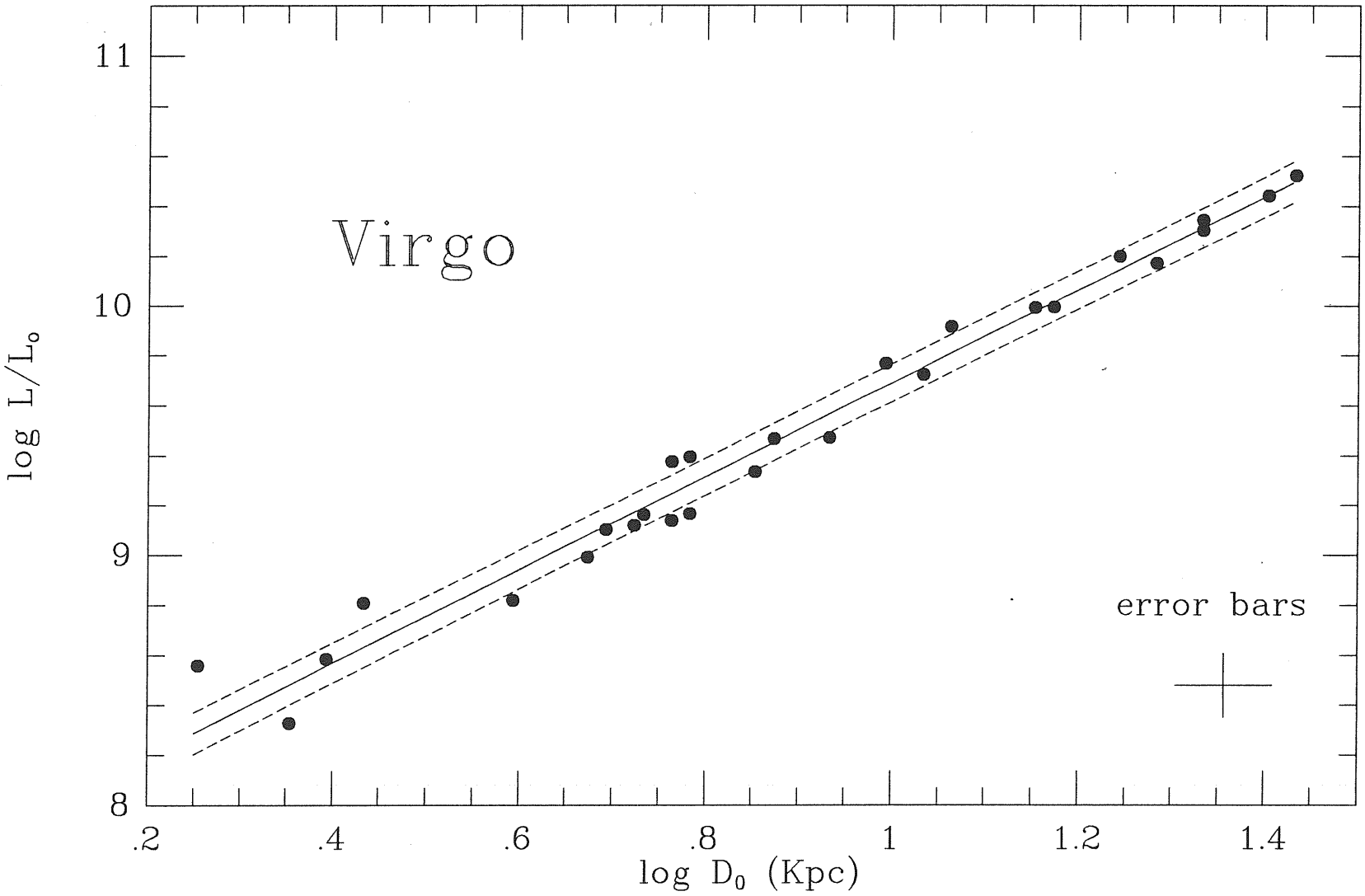

graph. C.1

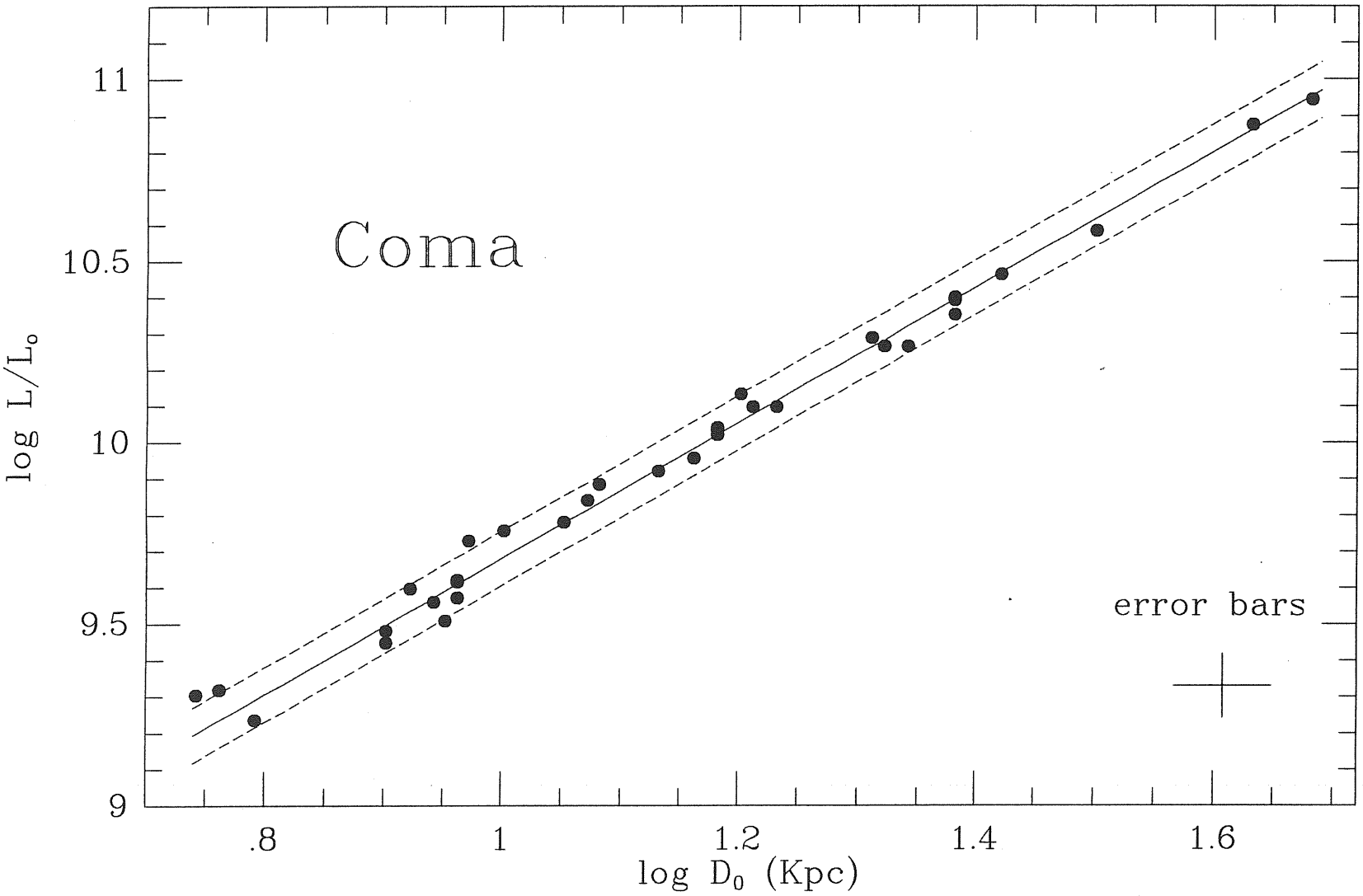

graph. C.2

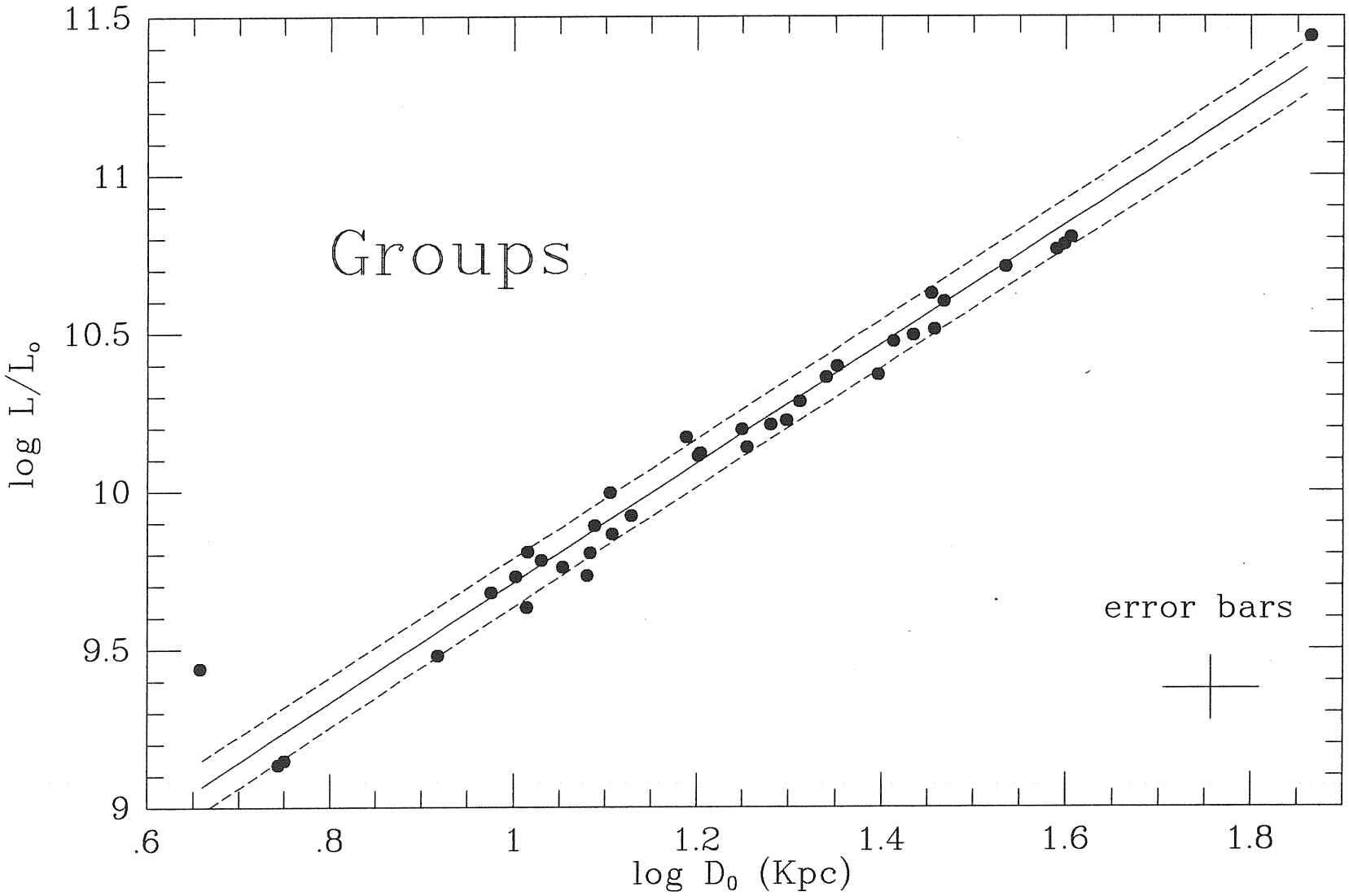
Groups
error bars
log L/L$_o$
log D$_0$ (Kpc)
11.5
11
10.5
10
9.5
9
.6
.8
1
1.2
1.4
1.6
1.8

graph. C.3

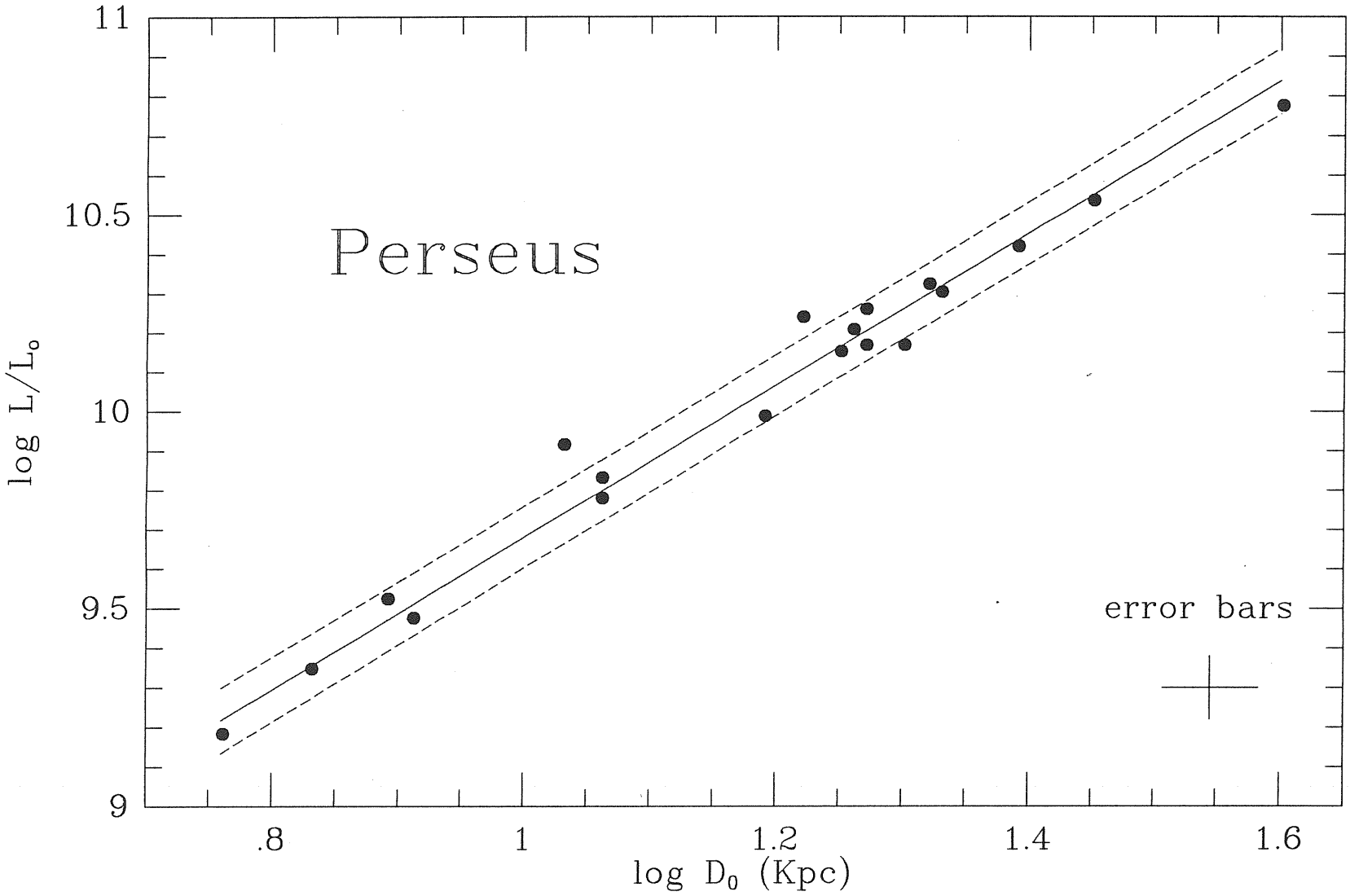
Perseus
error bars
log L/L$_\odot$
log D$_0$ (Kpc)
11
10.5
10
9.5
9
.8
1
1.2
1.4
1.6

graph. C.4

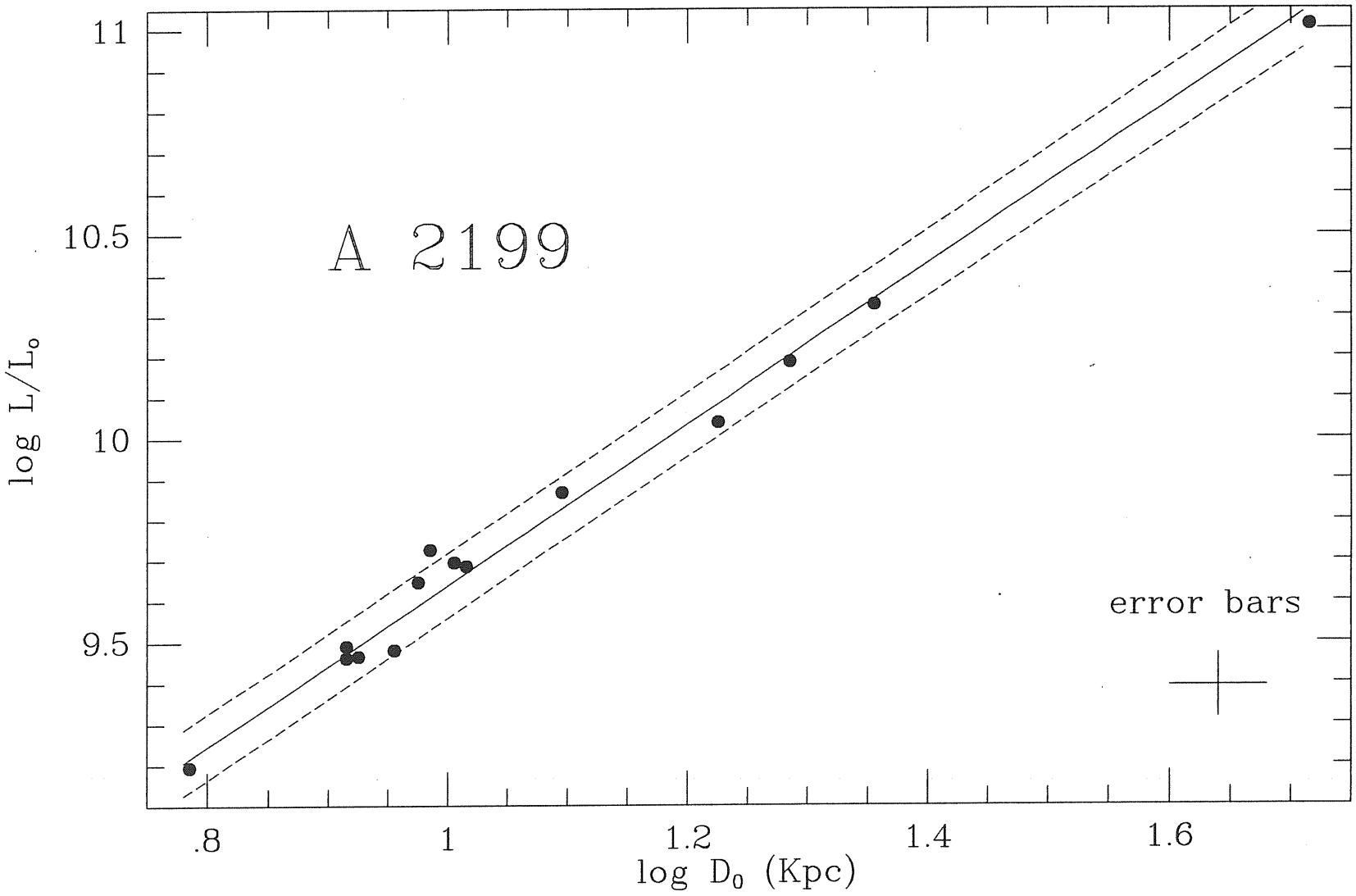

graph. C.5

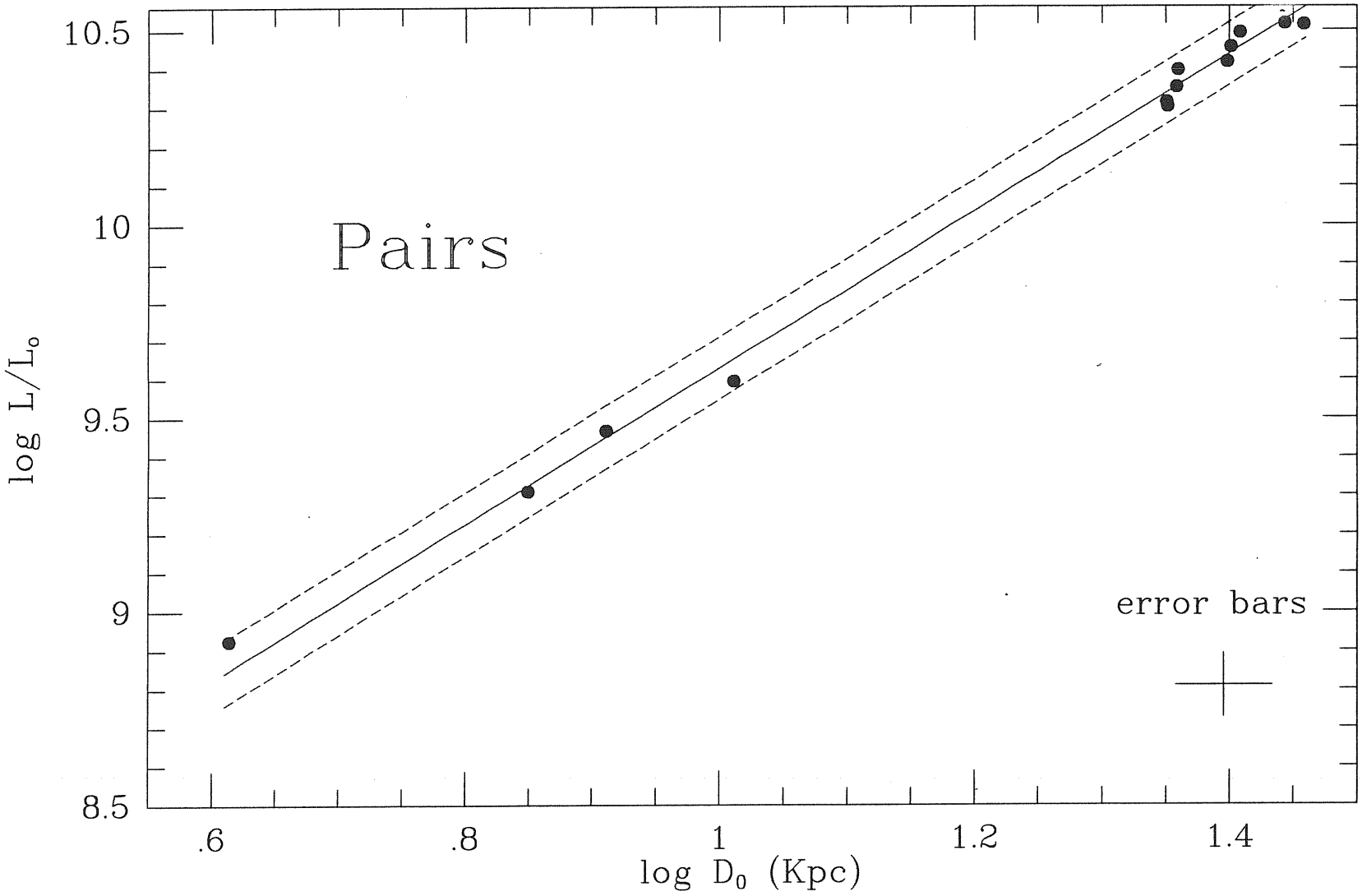

graph. C.6

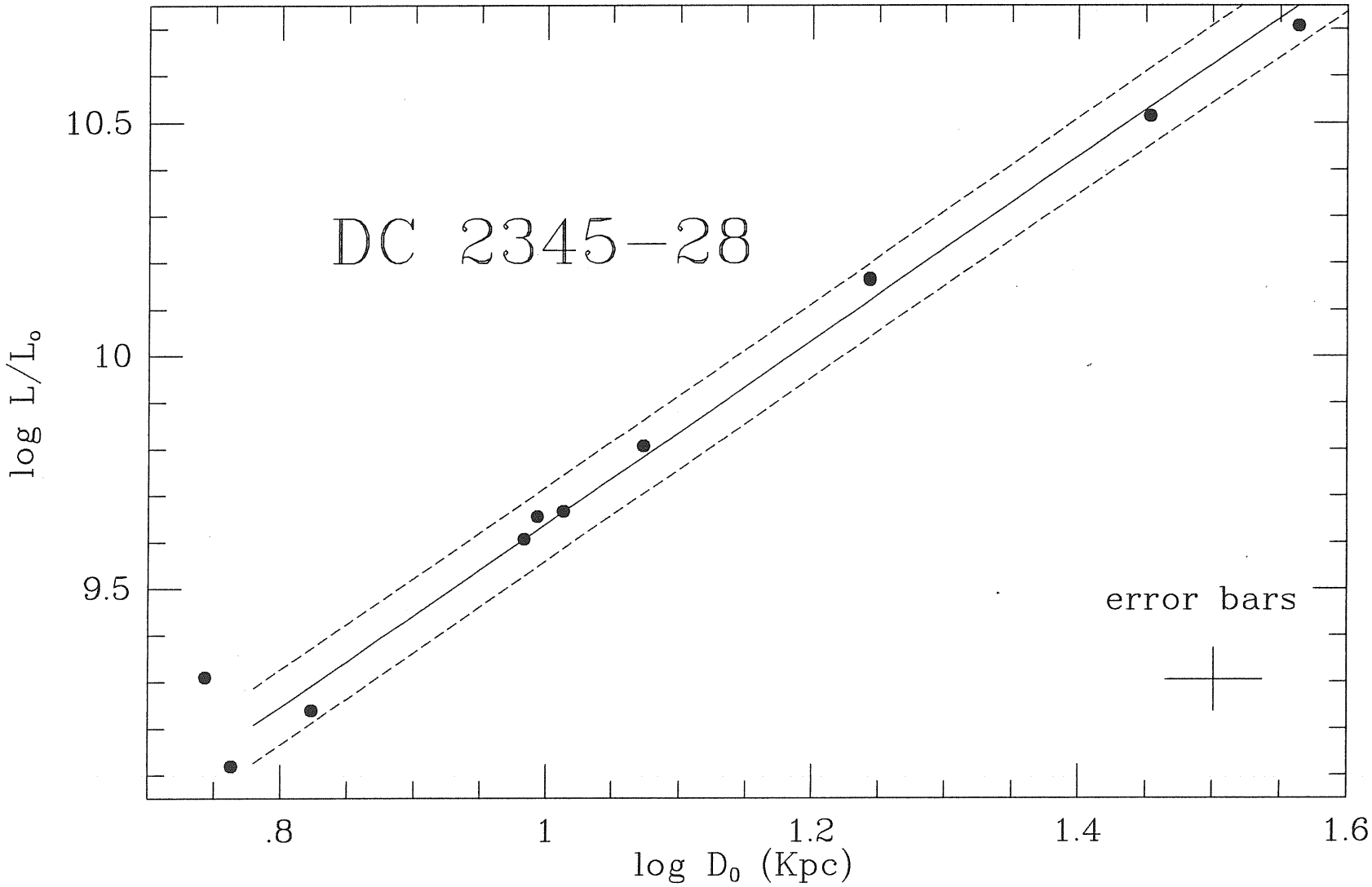

graph. C.7

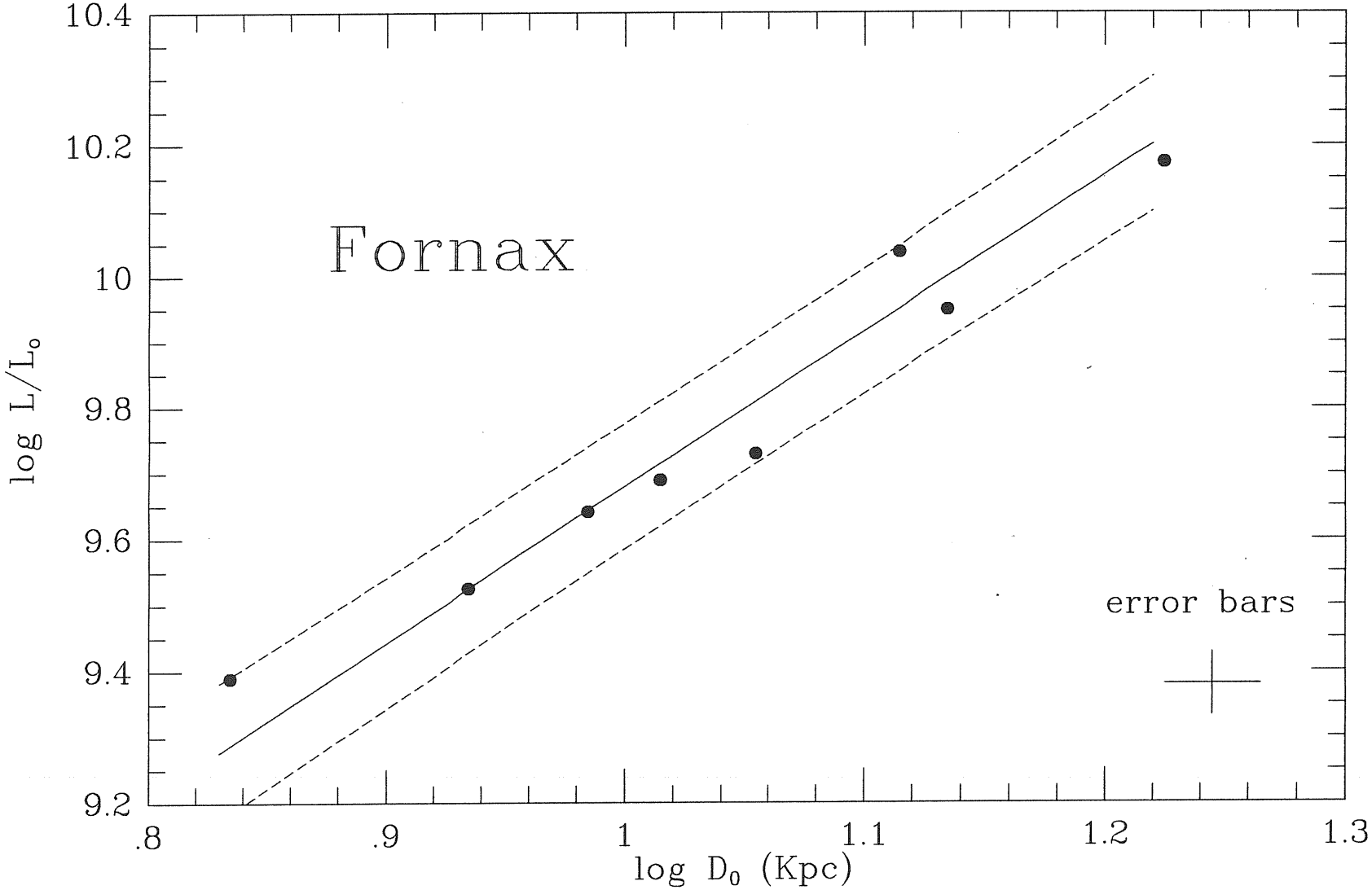
Fornax
10.4
10.2
10
9.8
9.6
9.4
9.2
log L/L$_o$
.8
.9
1
1.1
1.2
1.3
log D$_0$ (Kpc)
error bars

graph. C.8

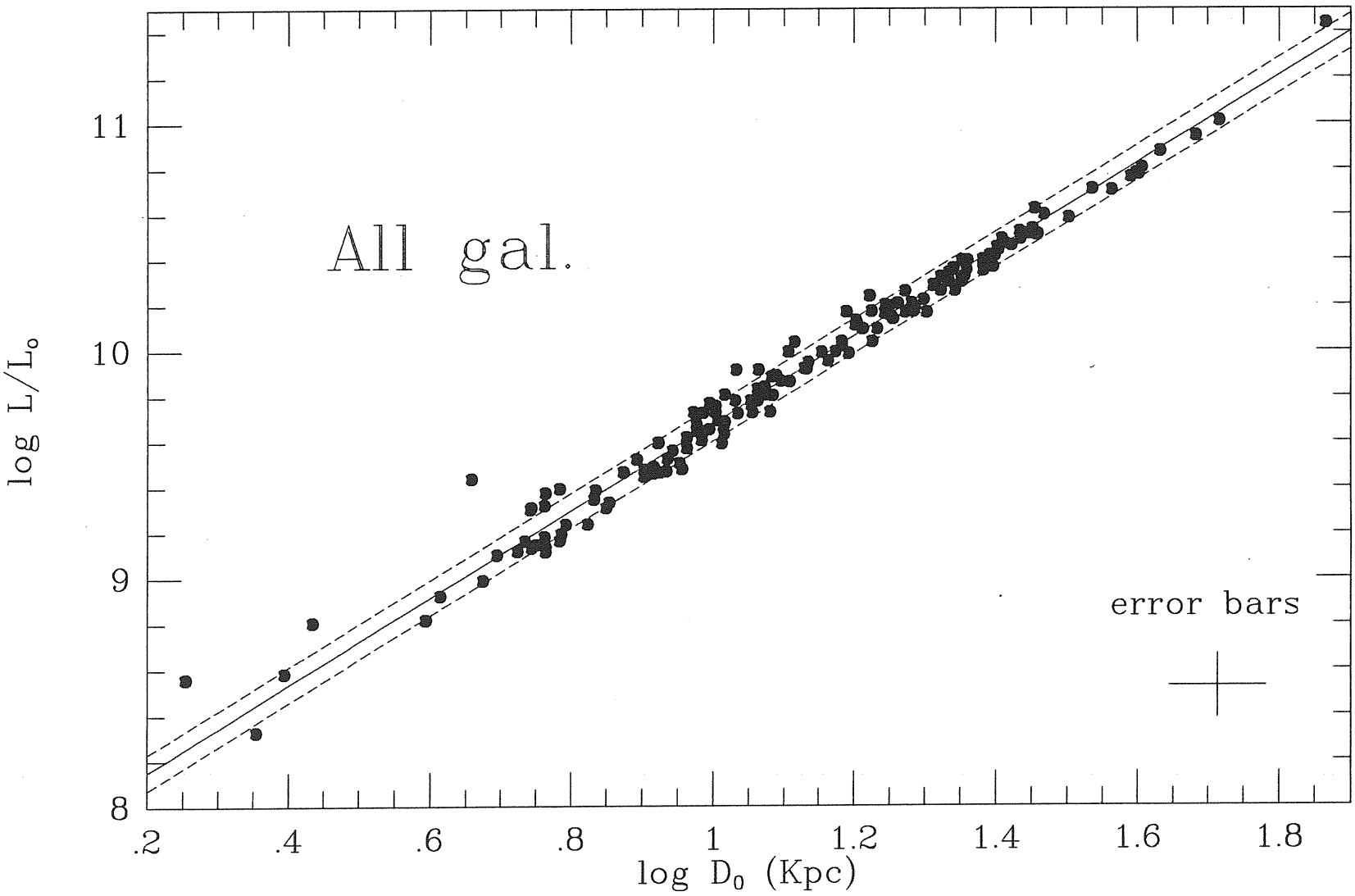

graph. C.9

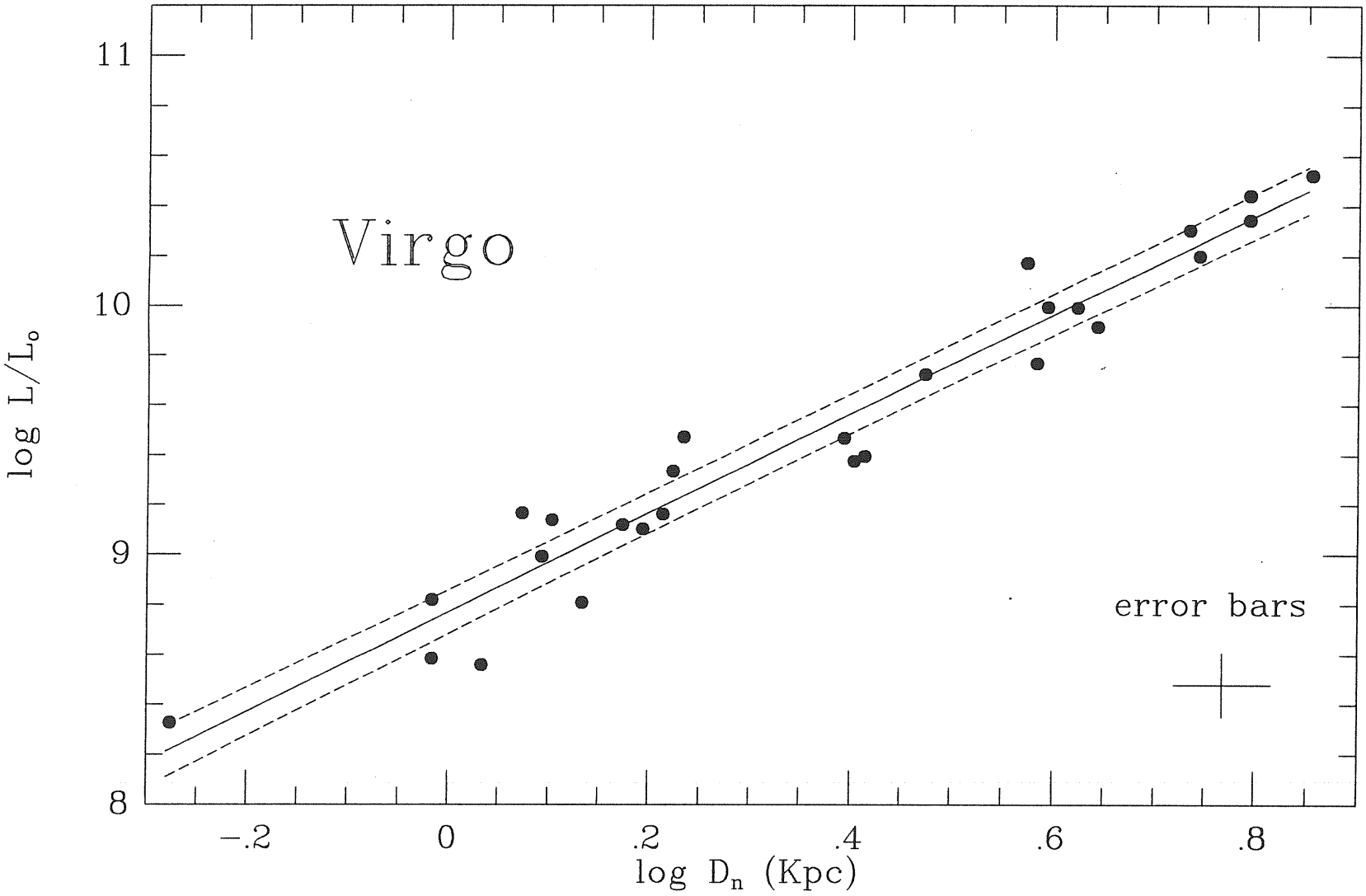

graph. C.10

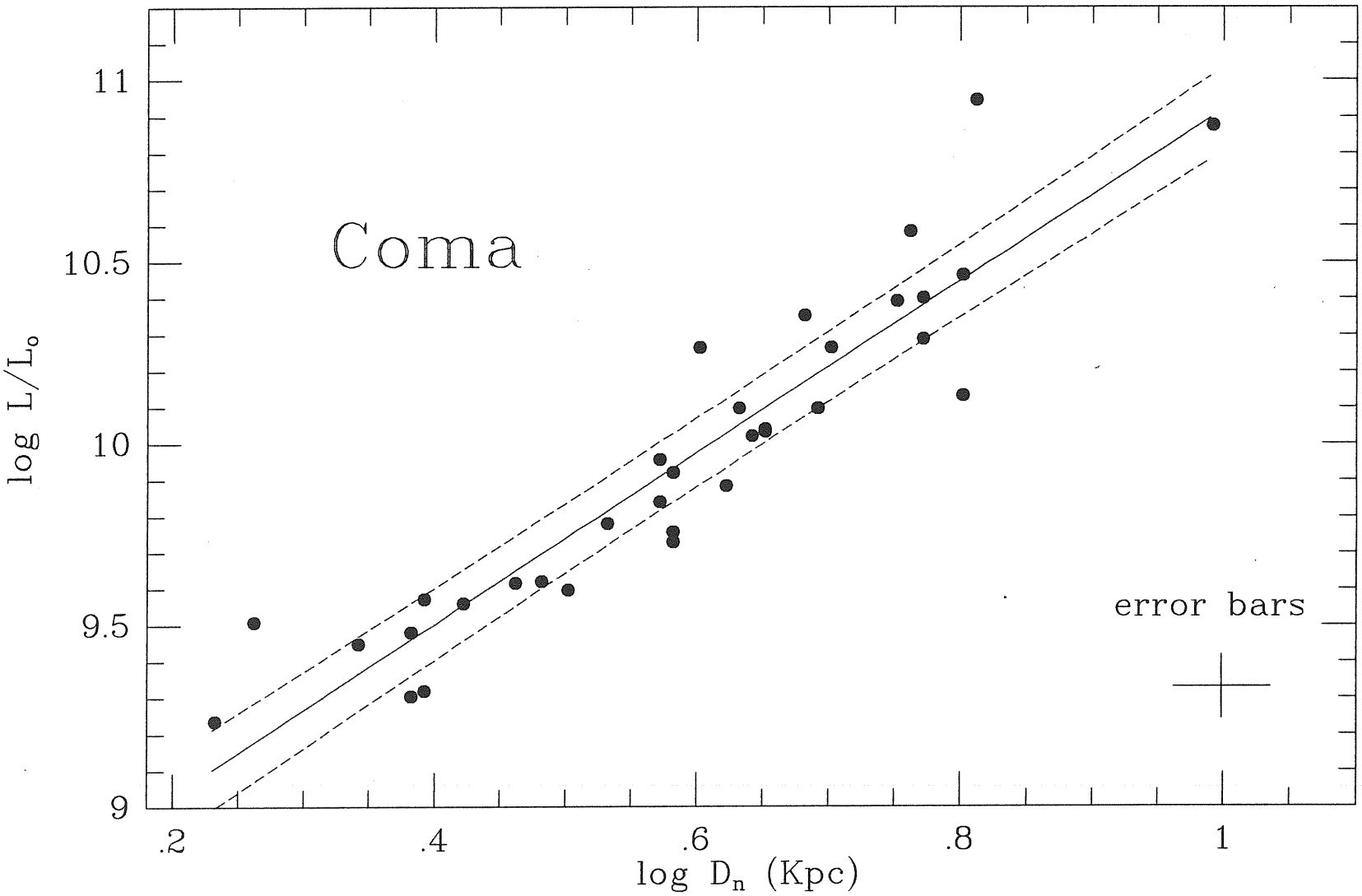

graph. C.11

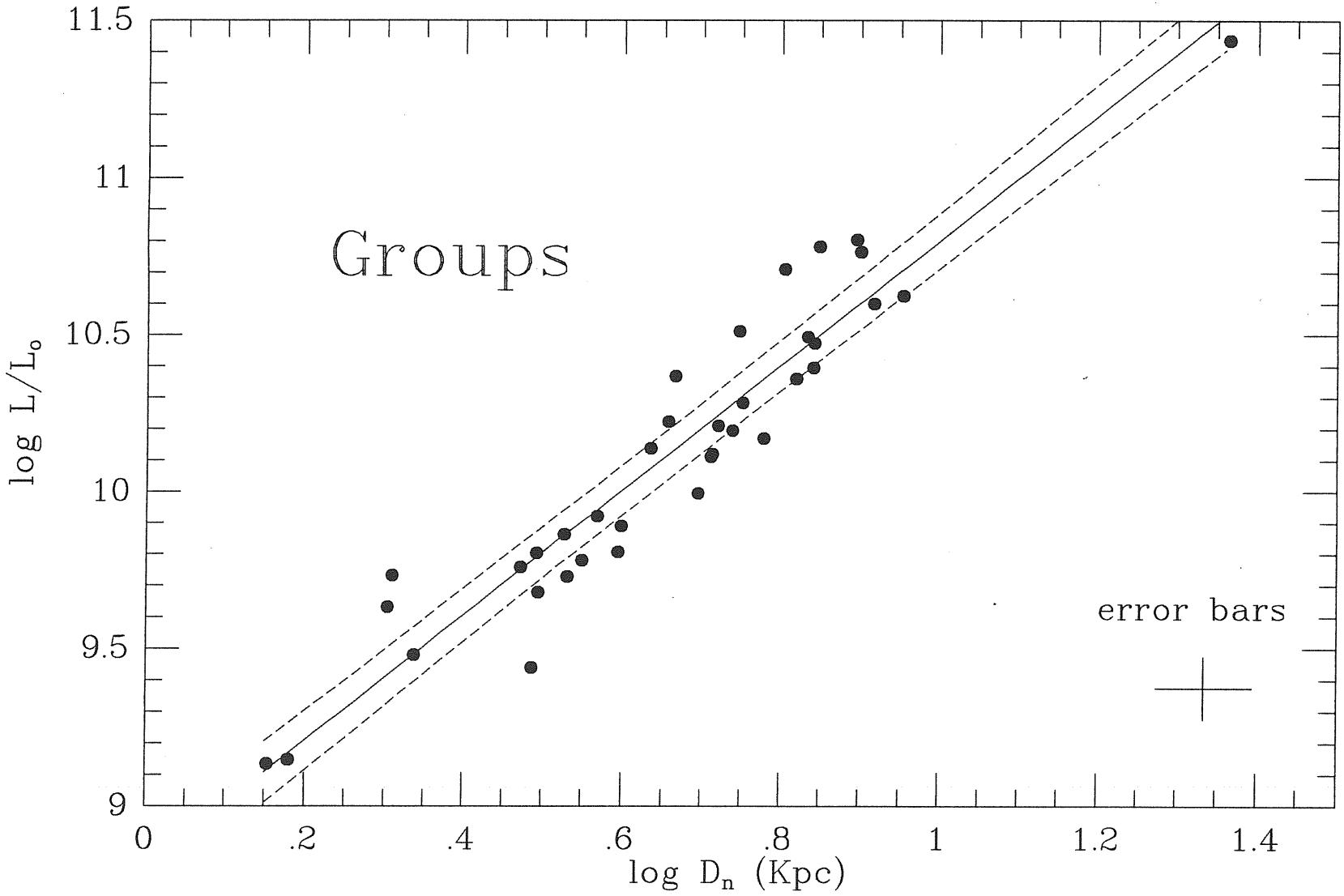
Groups
error bars
log L/L$_o$
log D$_n$ (Kpc)
11.5
11
10.5
10
9.5
9
0
.2
.4
.6
.8
1
1.2
1.4

graph. C.12

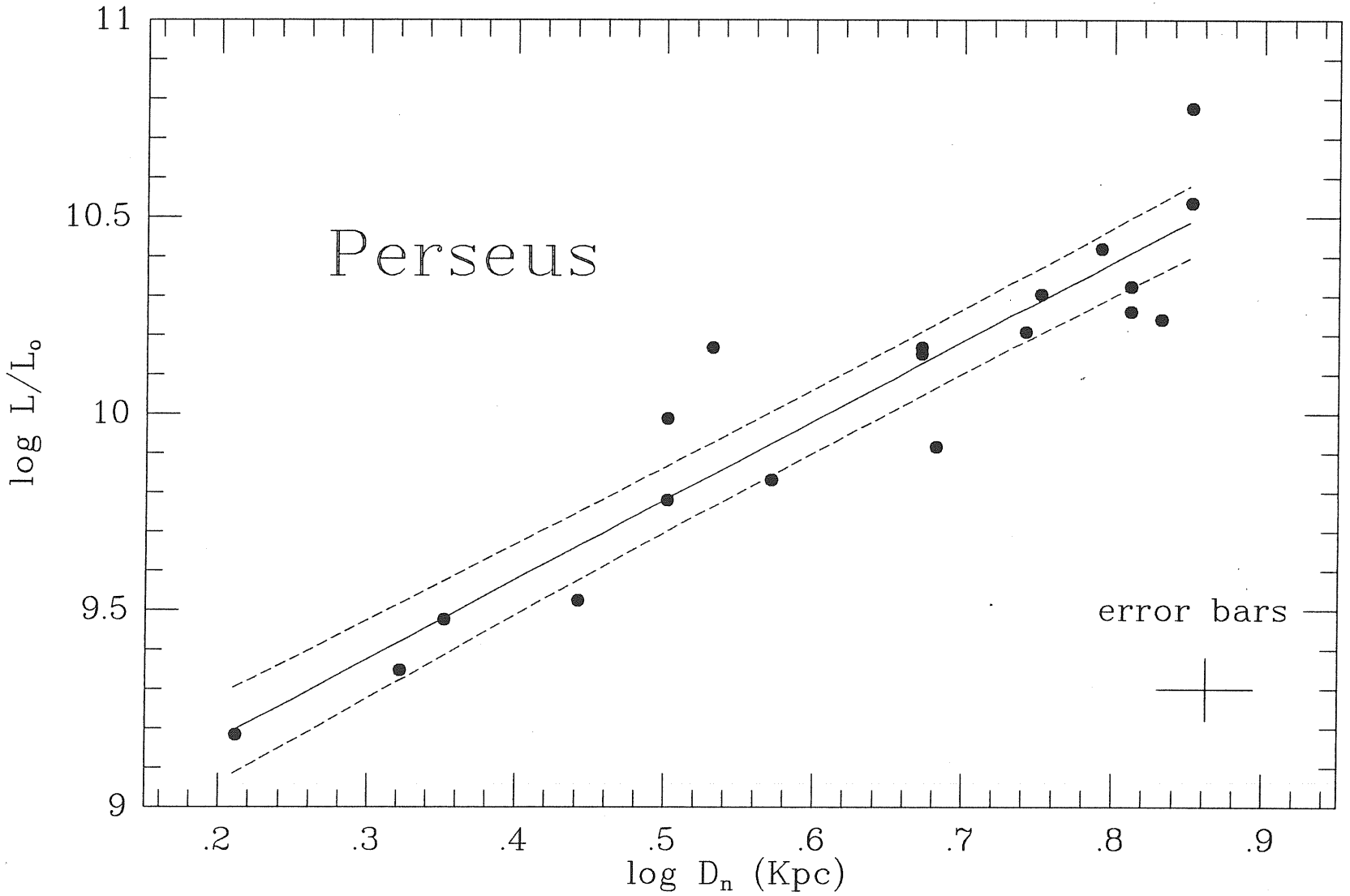

graph. C.13

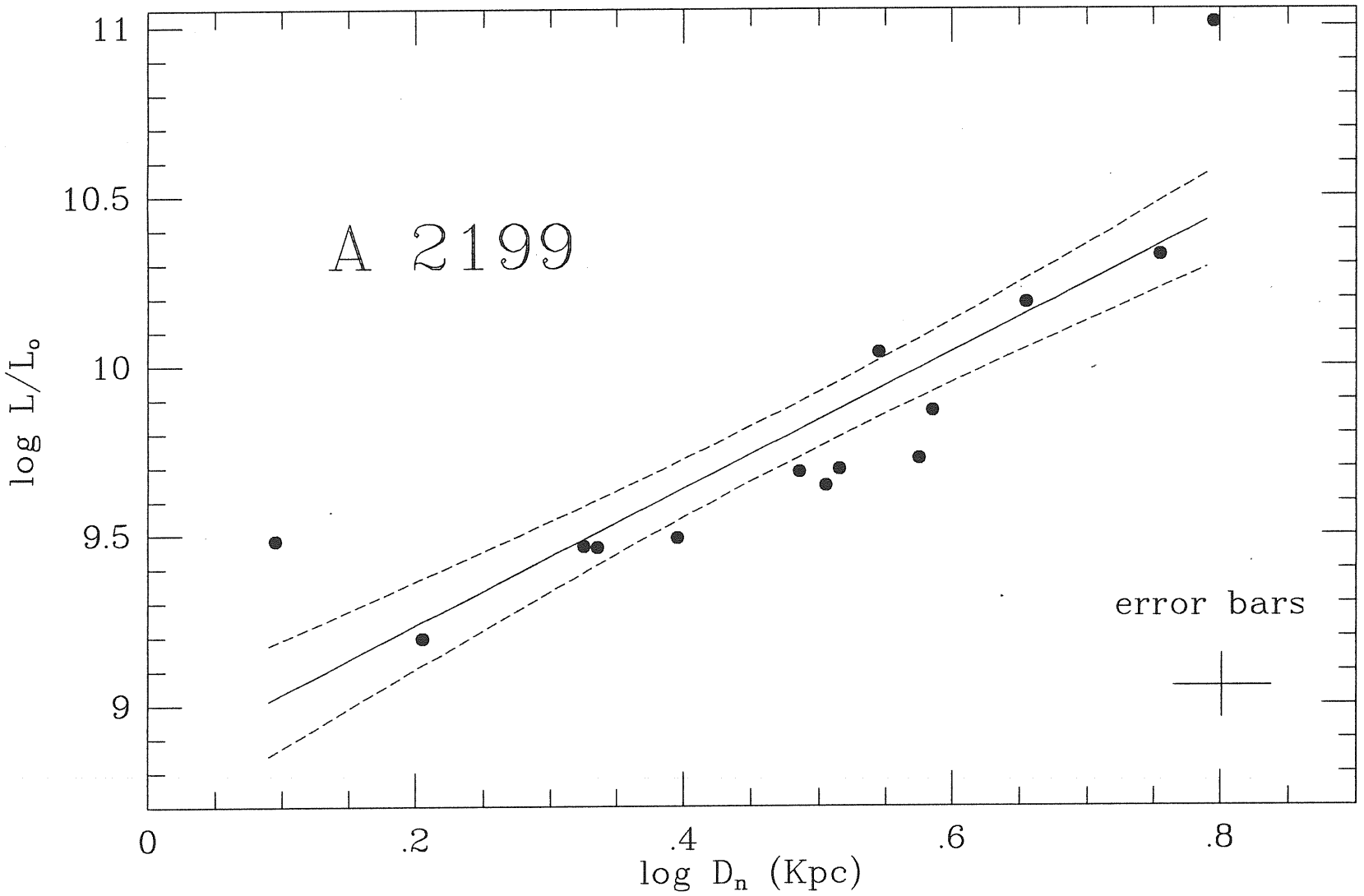

graph. C.14

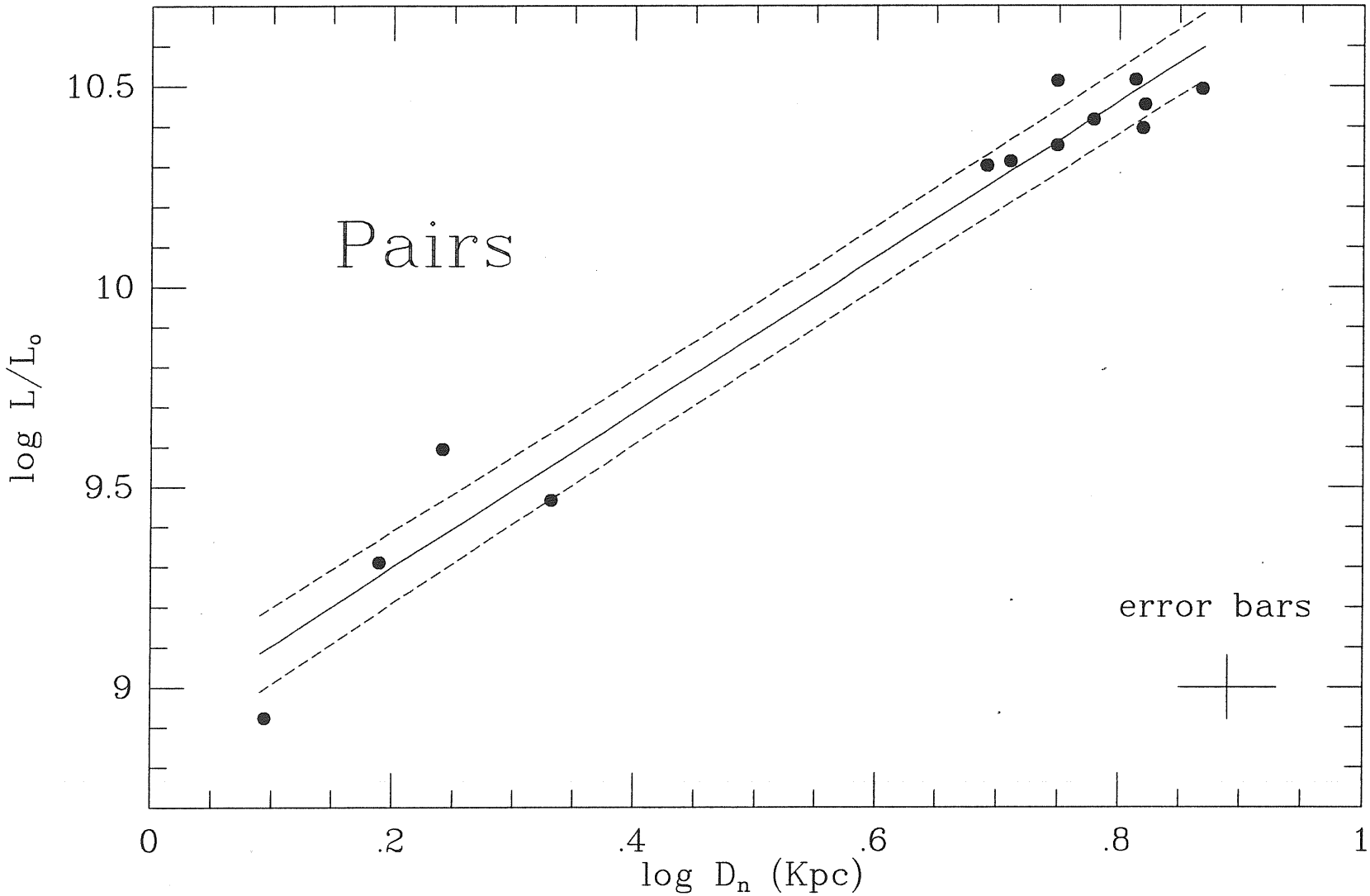

graph. C.15

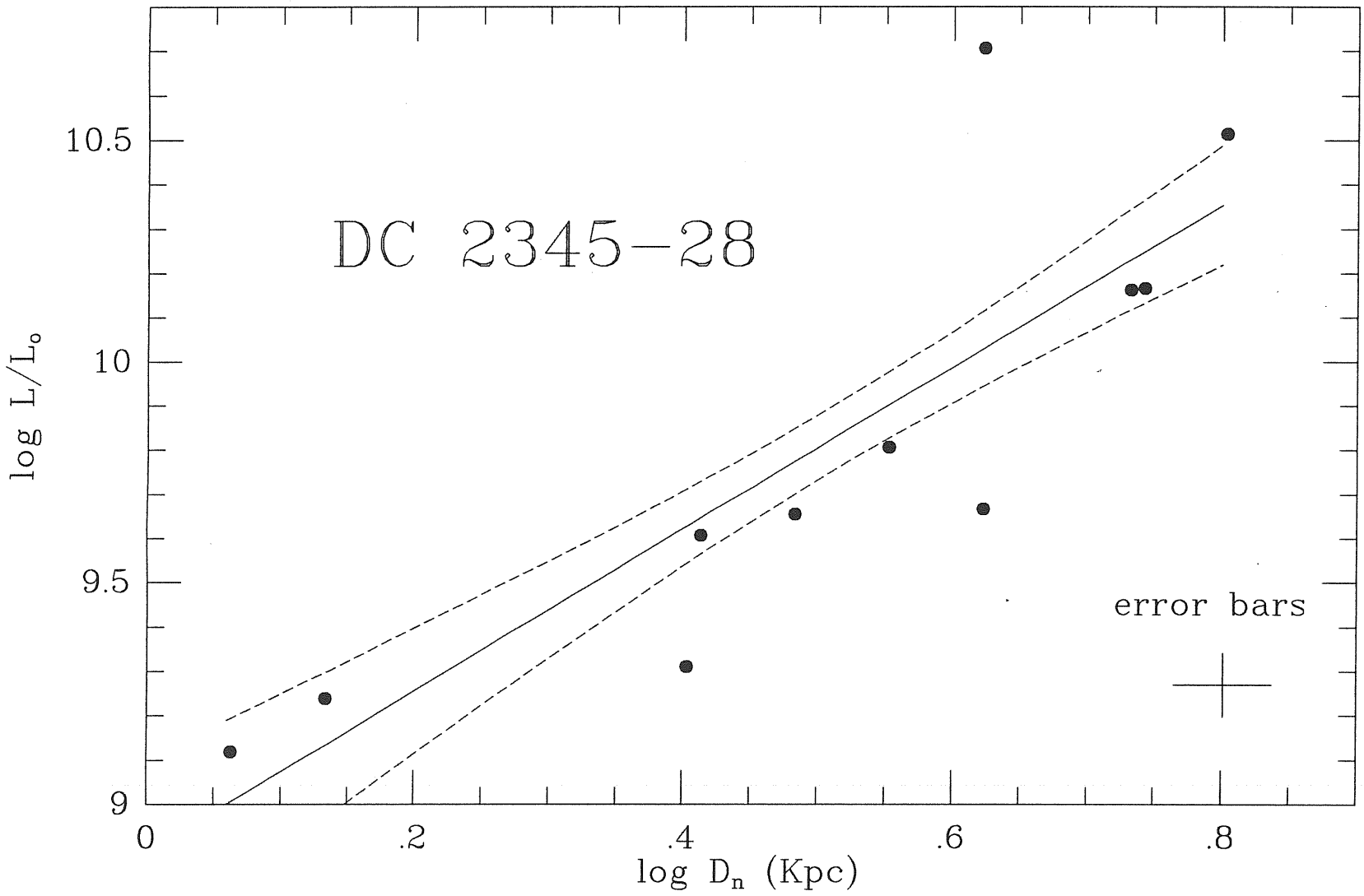

graph. C.16

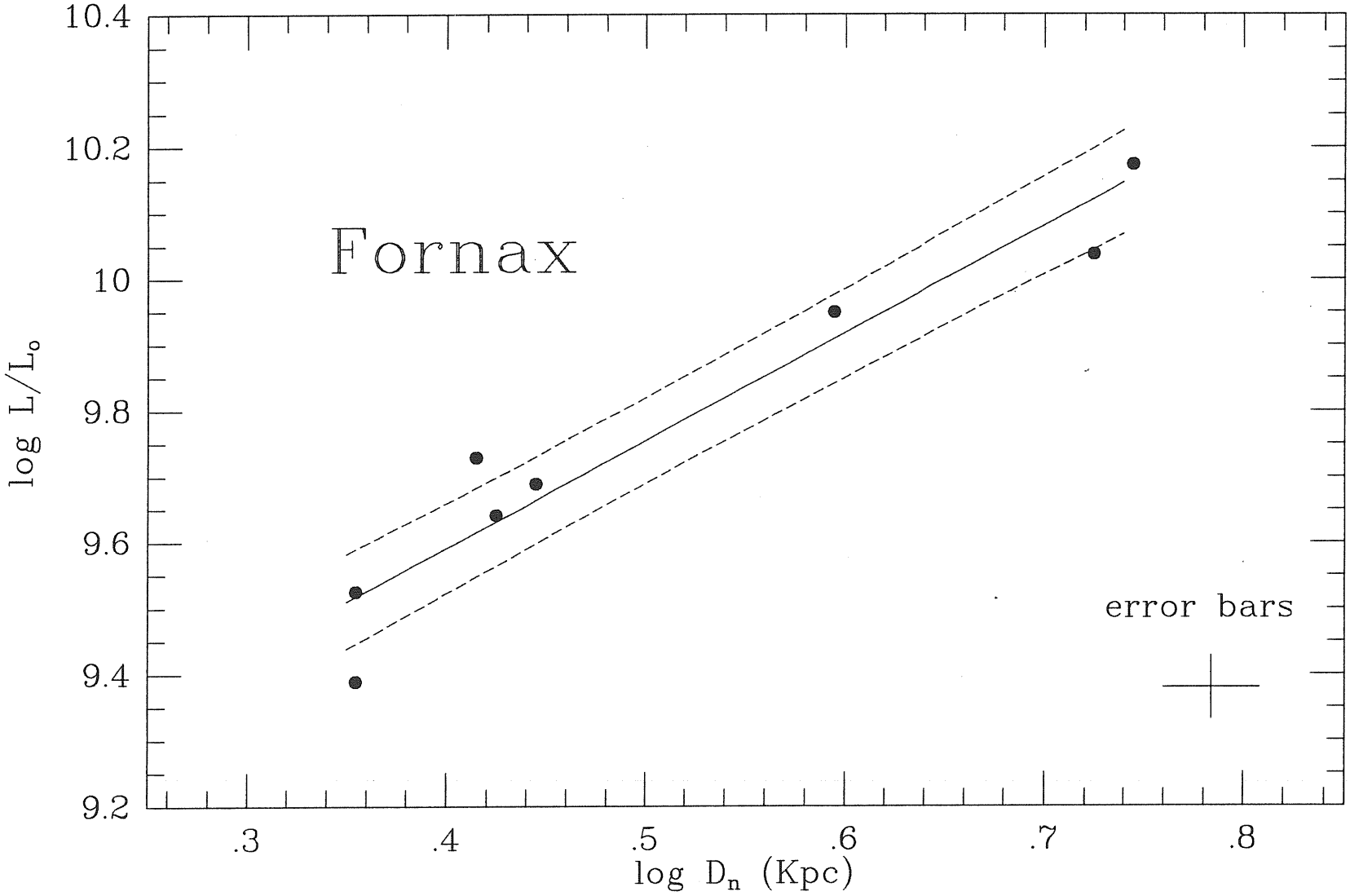
Fornax
10.4
10.2
10
9.8
9.6
9.4
9.2
log L/L$_o$
.3
.4
.5
.6
.7
.8
log D$_n$ (Kpc)
error bars

graph. C.17

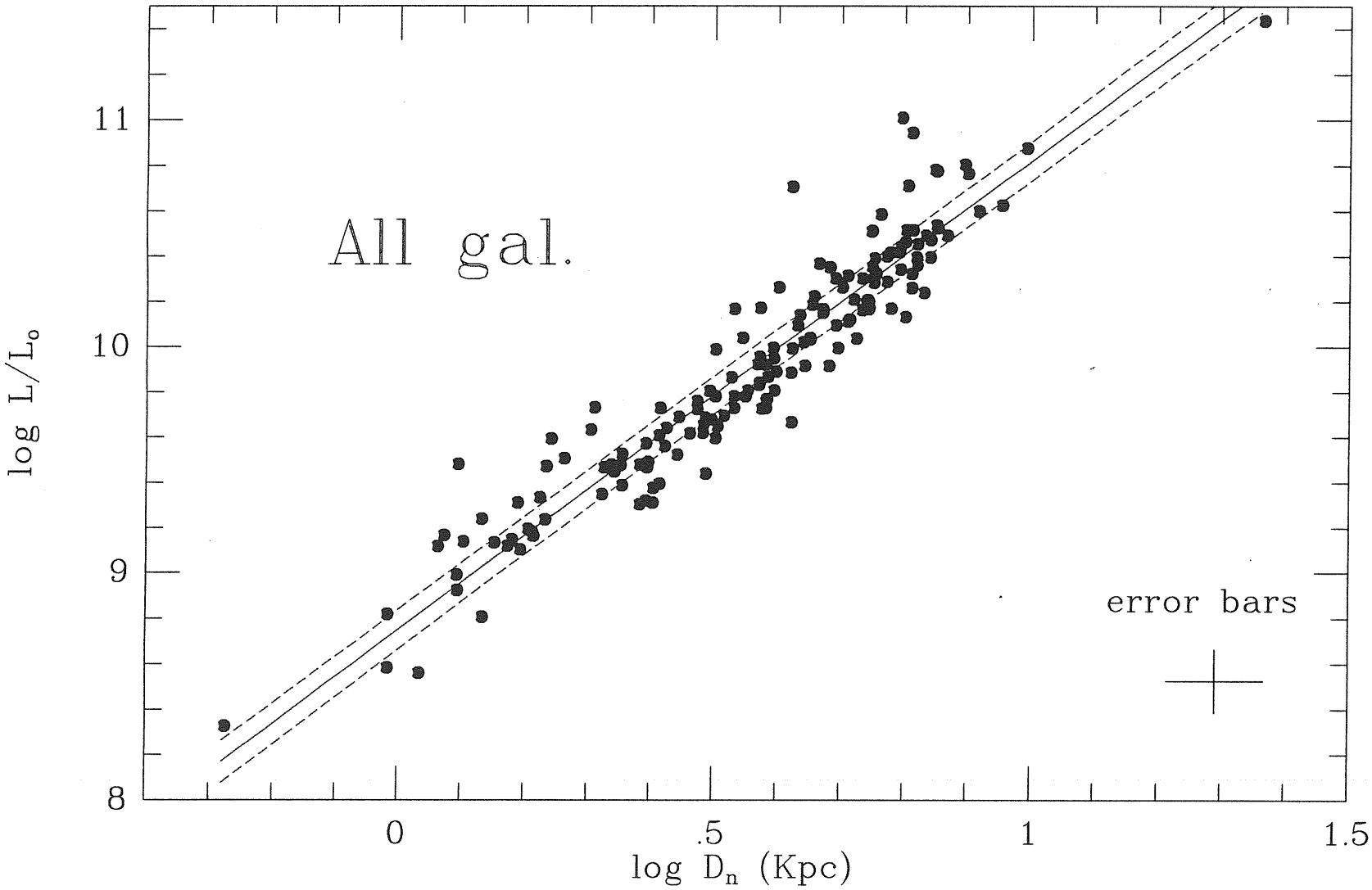

graph. C.18

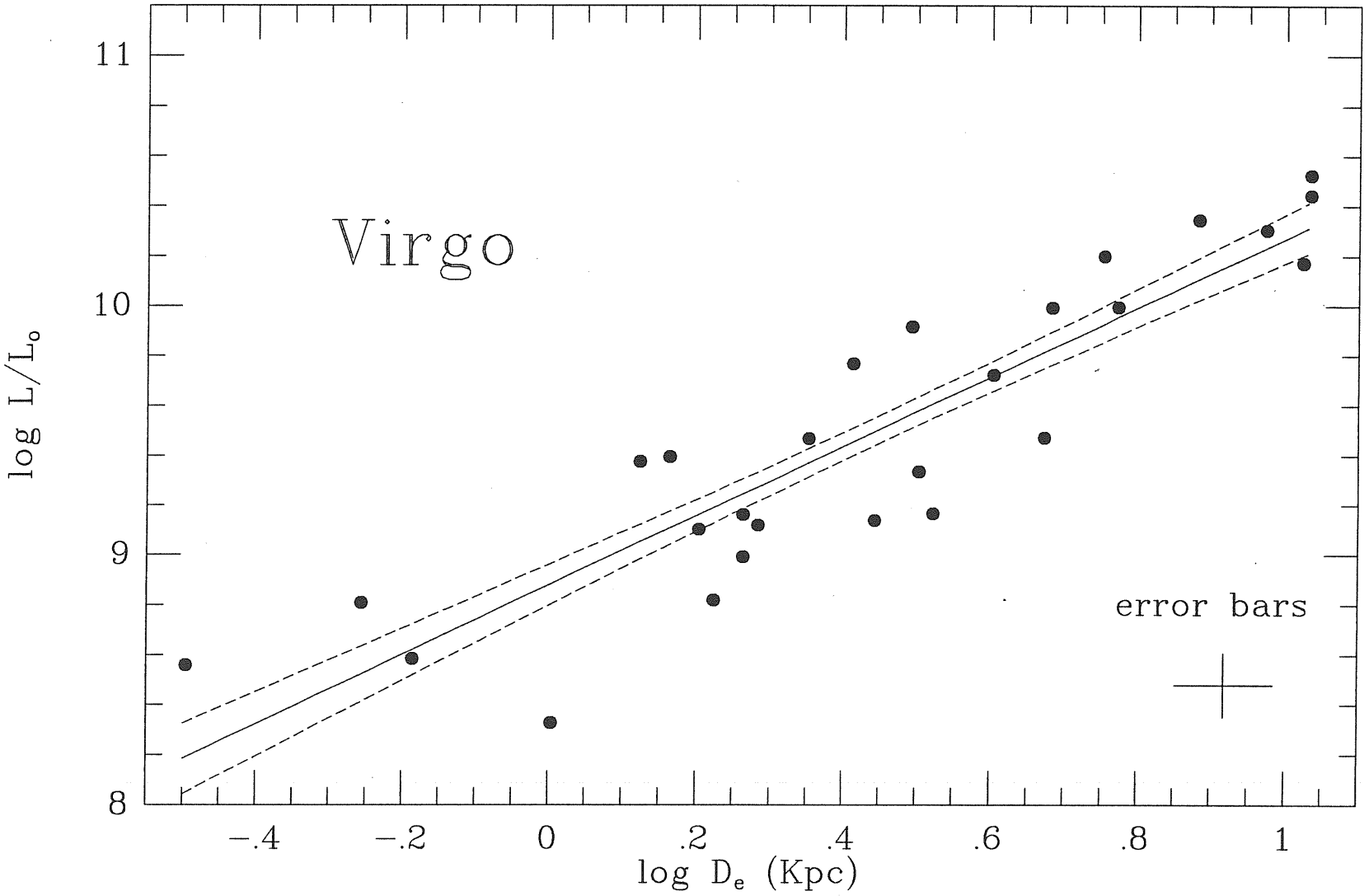

graph. C.19

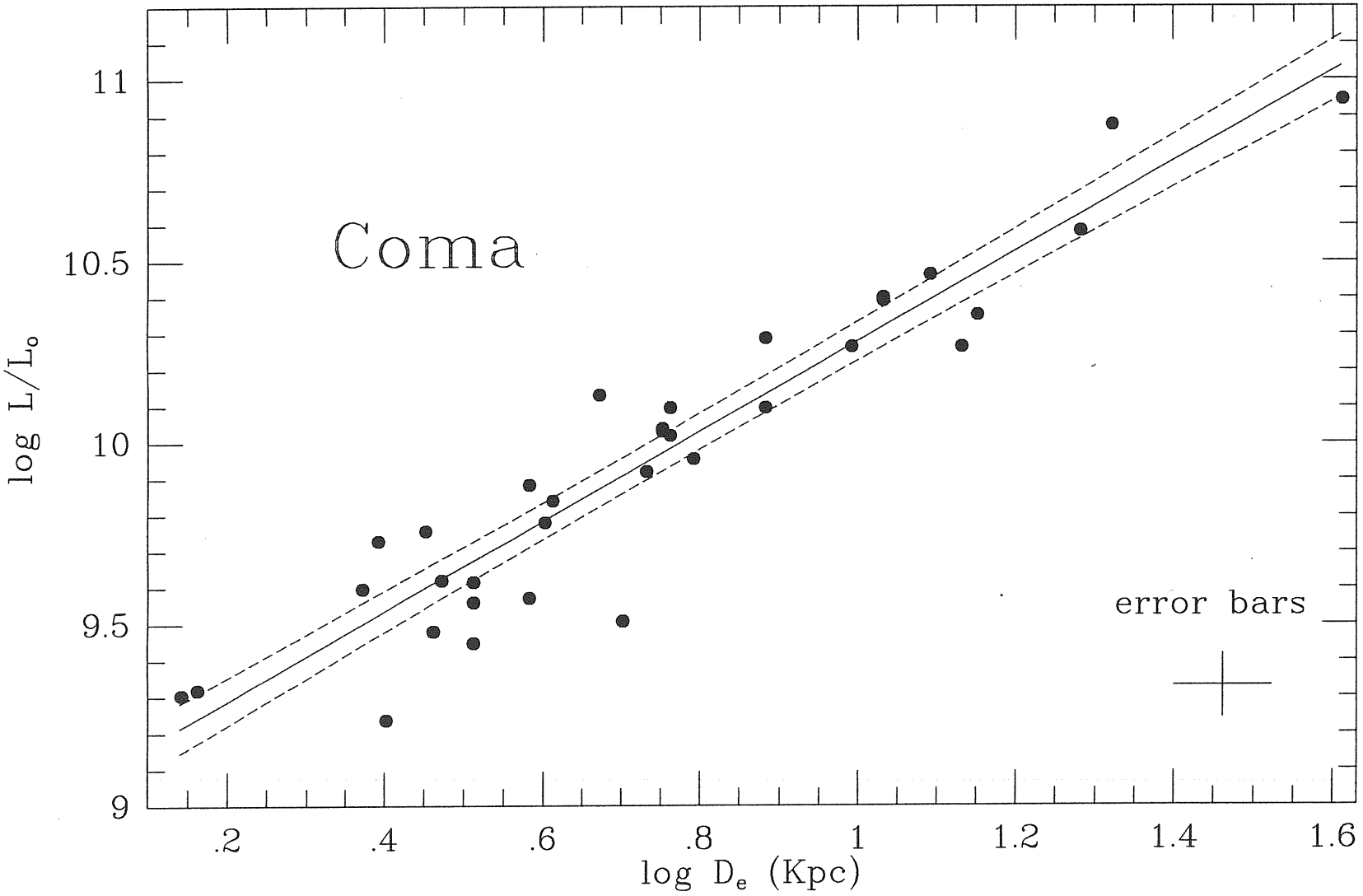

graph. C.20

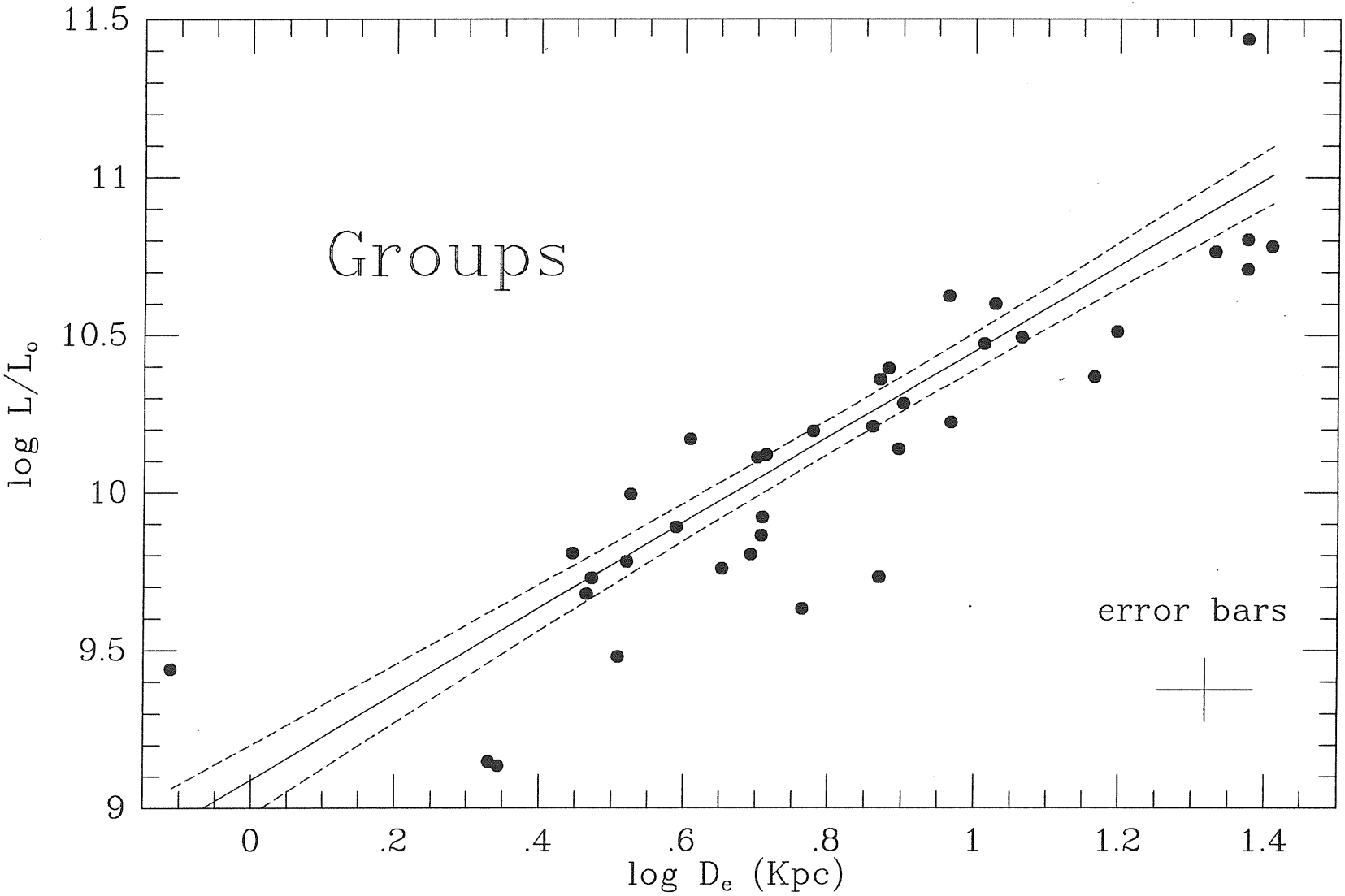
Groups
error bars
log L/L$_o$
log D$_e$ (Kpc)
11.5
11
10.5
10
9.5
9
0
.2
.4
.6
.8
1
1.2
1.4

graph. C.21

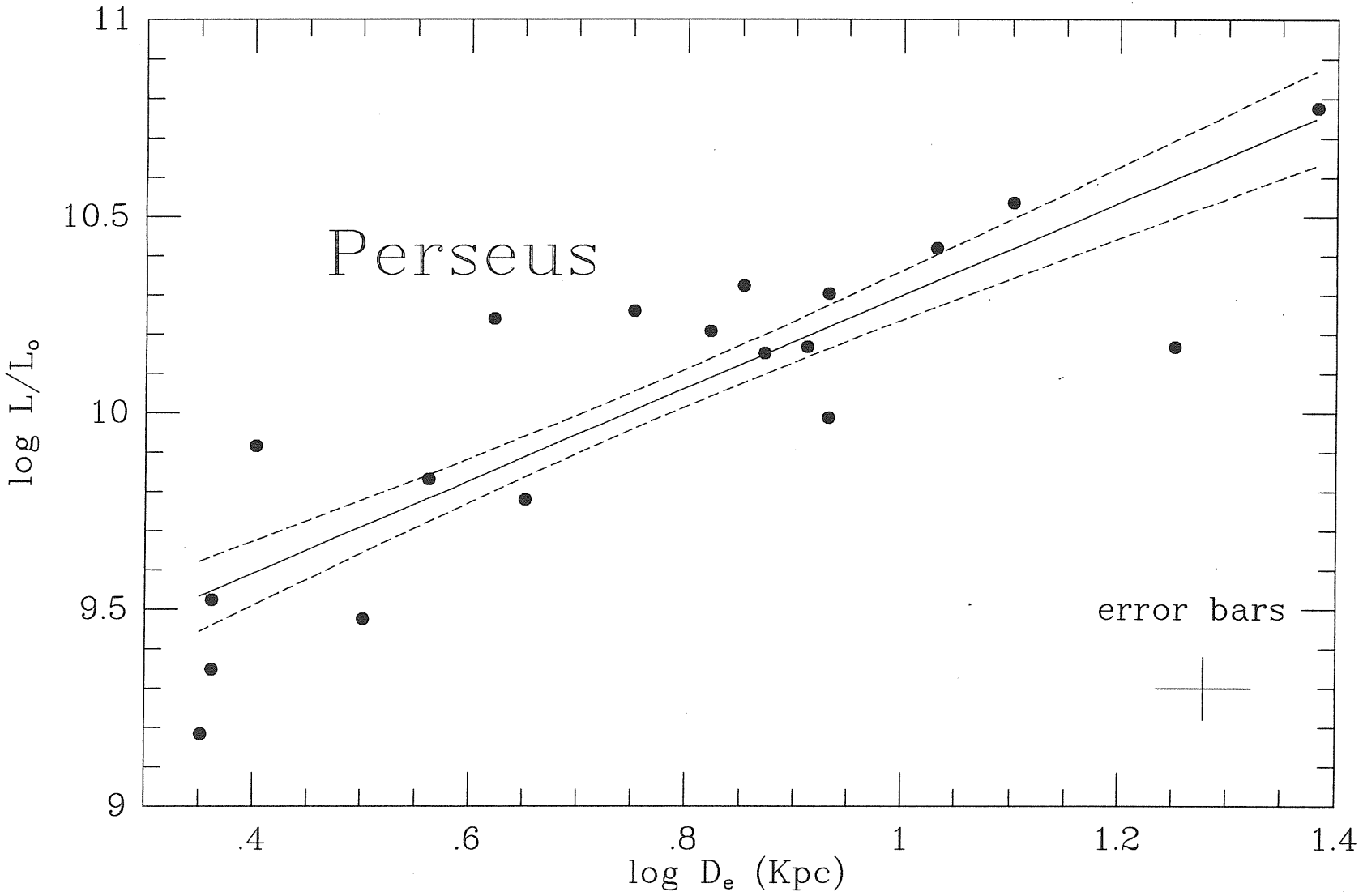

graph. C.22

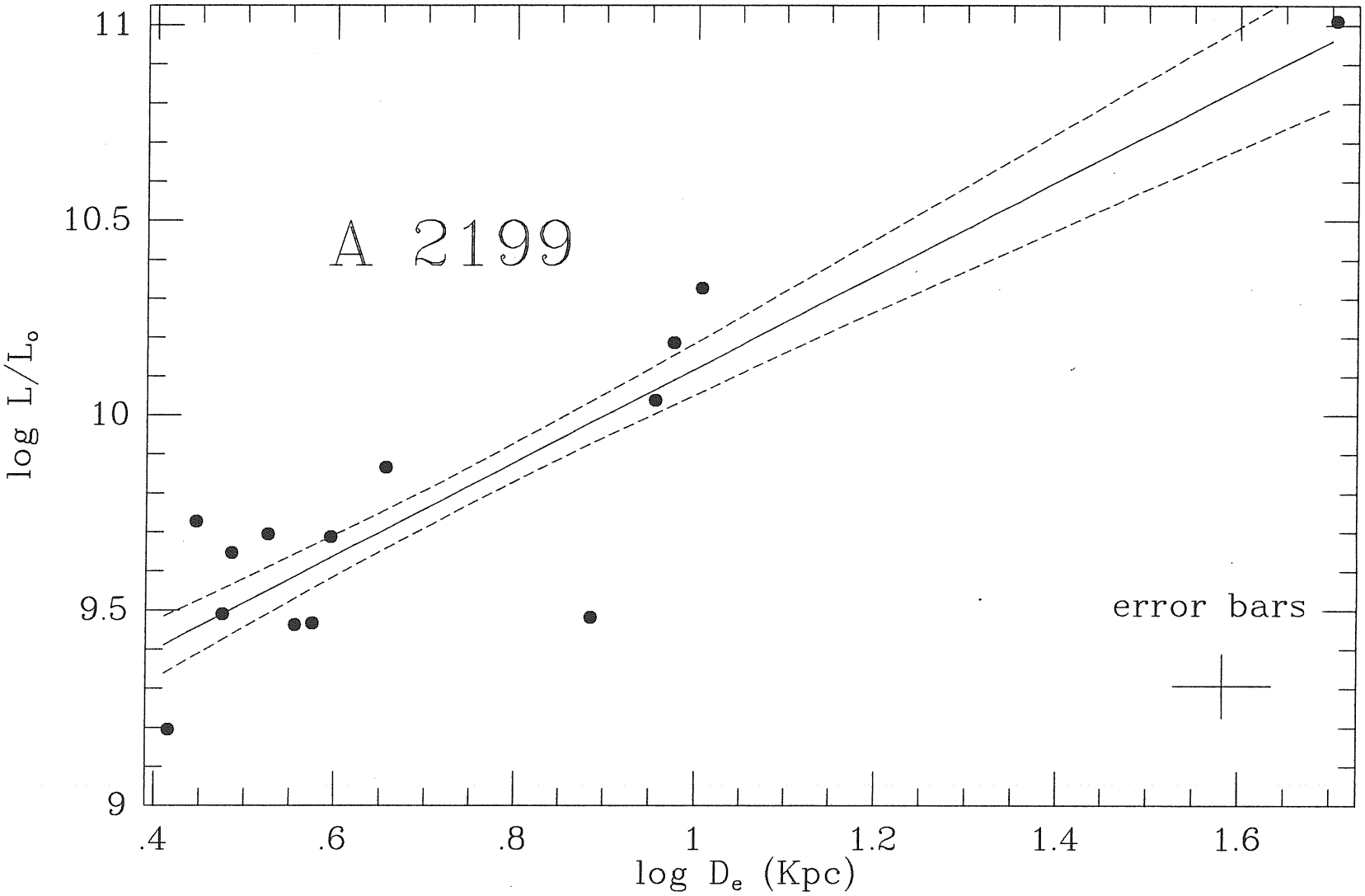

graph. C.23

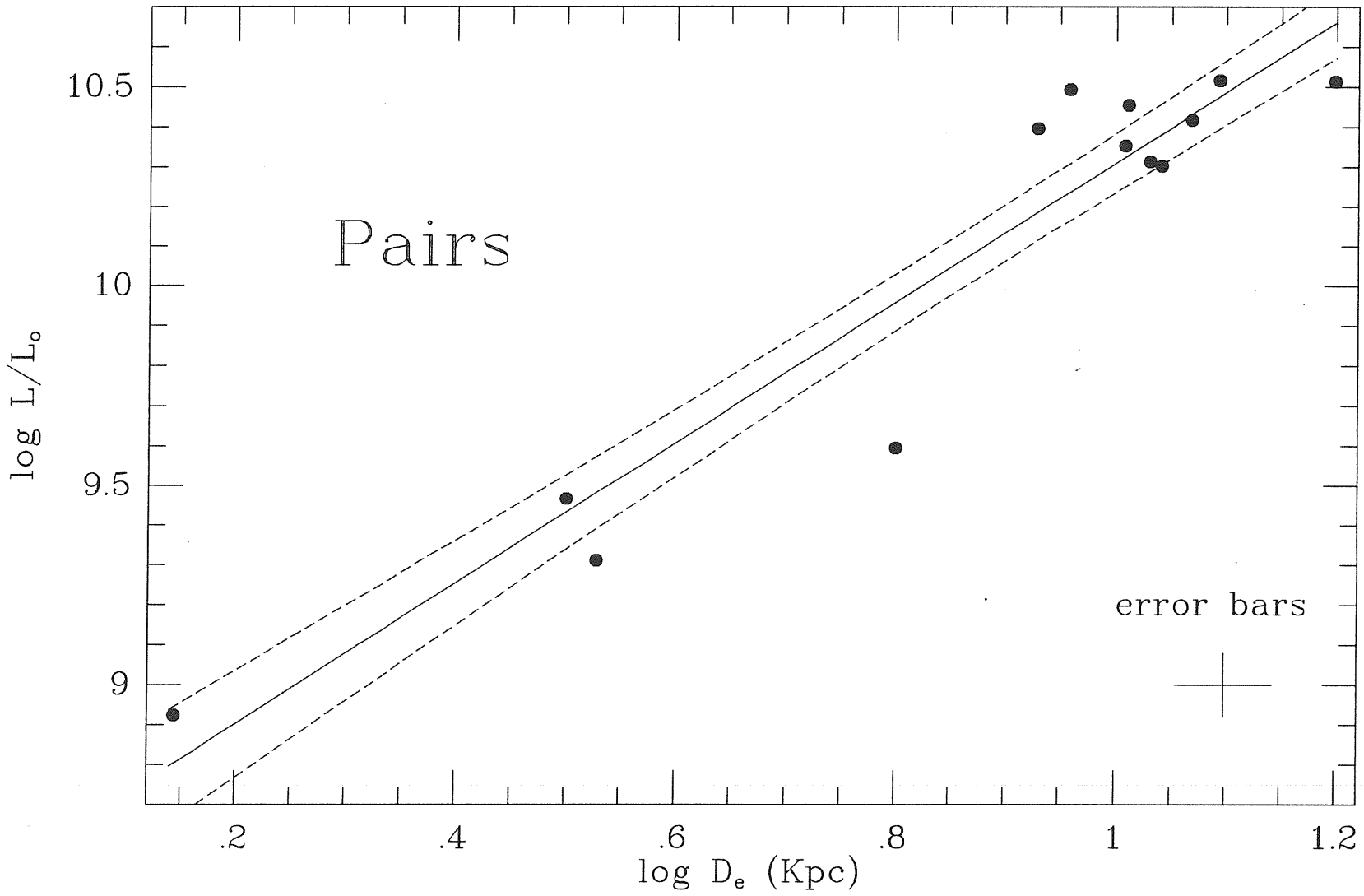

graph. C.24

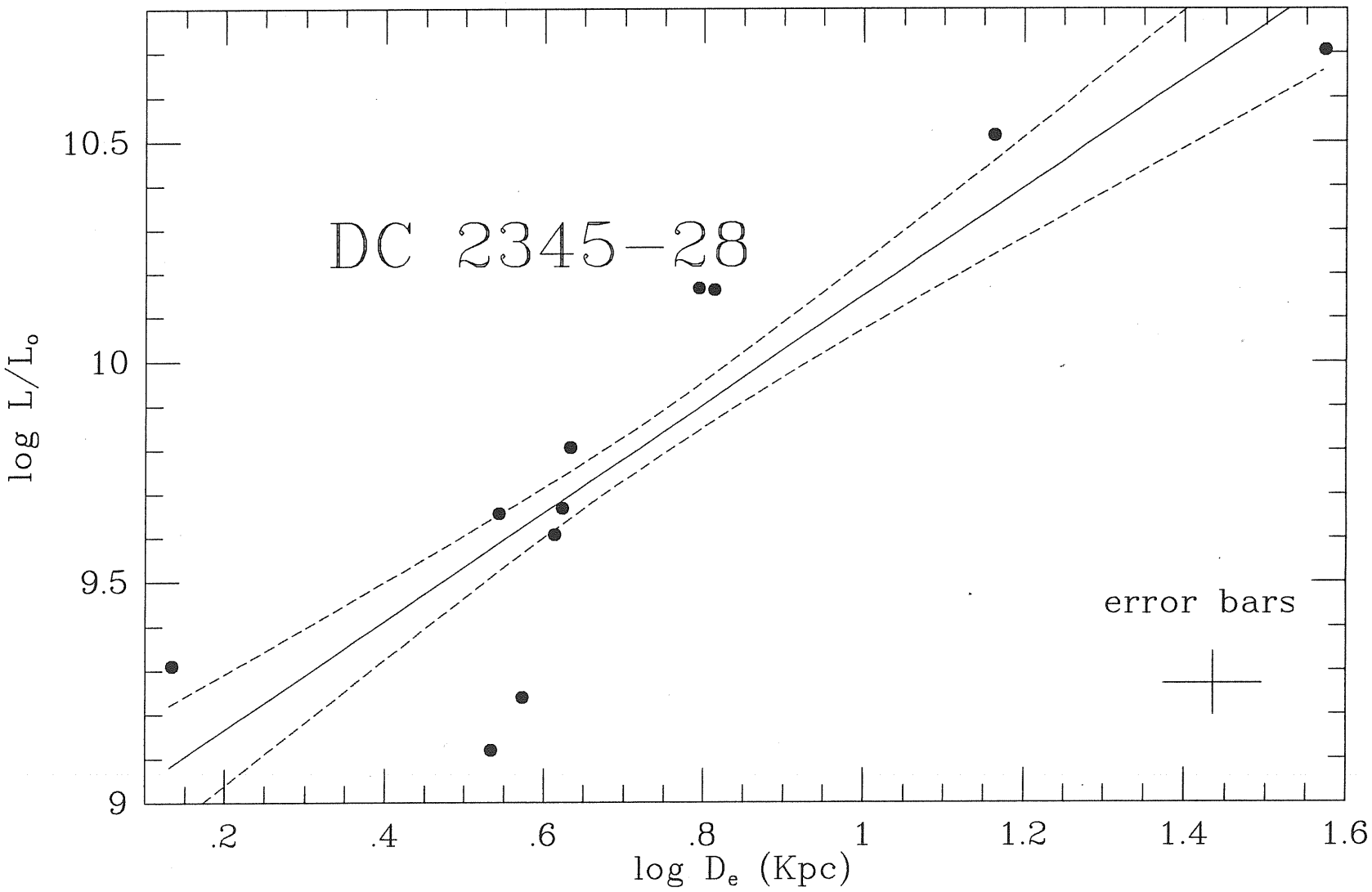
DC 2345−28
error bars
log L/L$_o$
log D$_e$ (Kpc)
10.5
10
9.5
9
.2
.4
.6
.8
1
1.2
1.4
1.6

graph. C.25

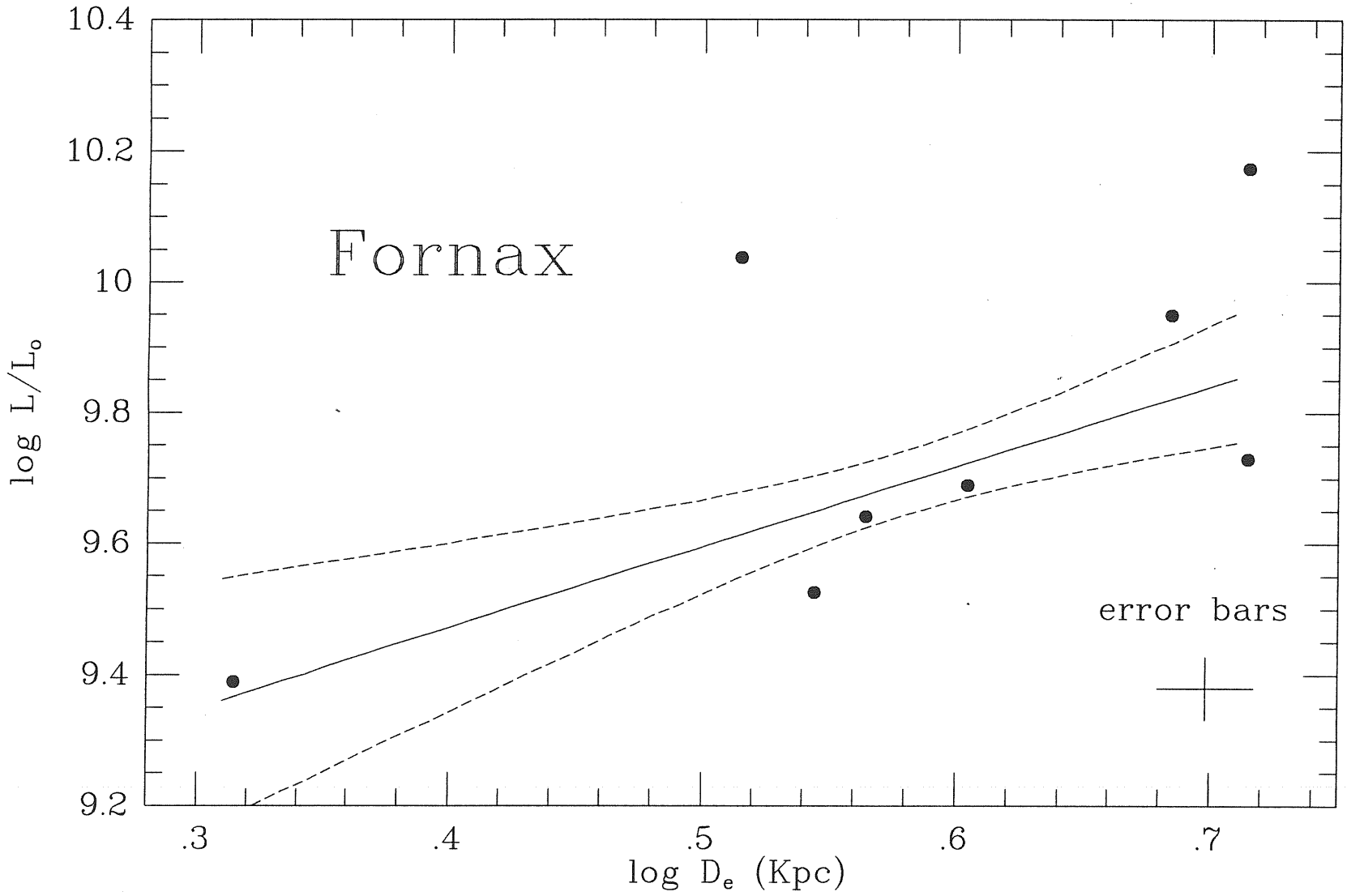
Fornax
error bars
10.4
10.2
10
9.8
9.6
9.4
9.2
log L/L$_o$
.3
.4
.5
.6
.7
log D$_e$ (Kpc)

graph. C.26

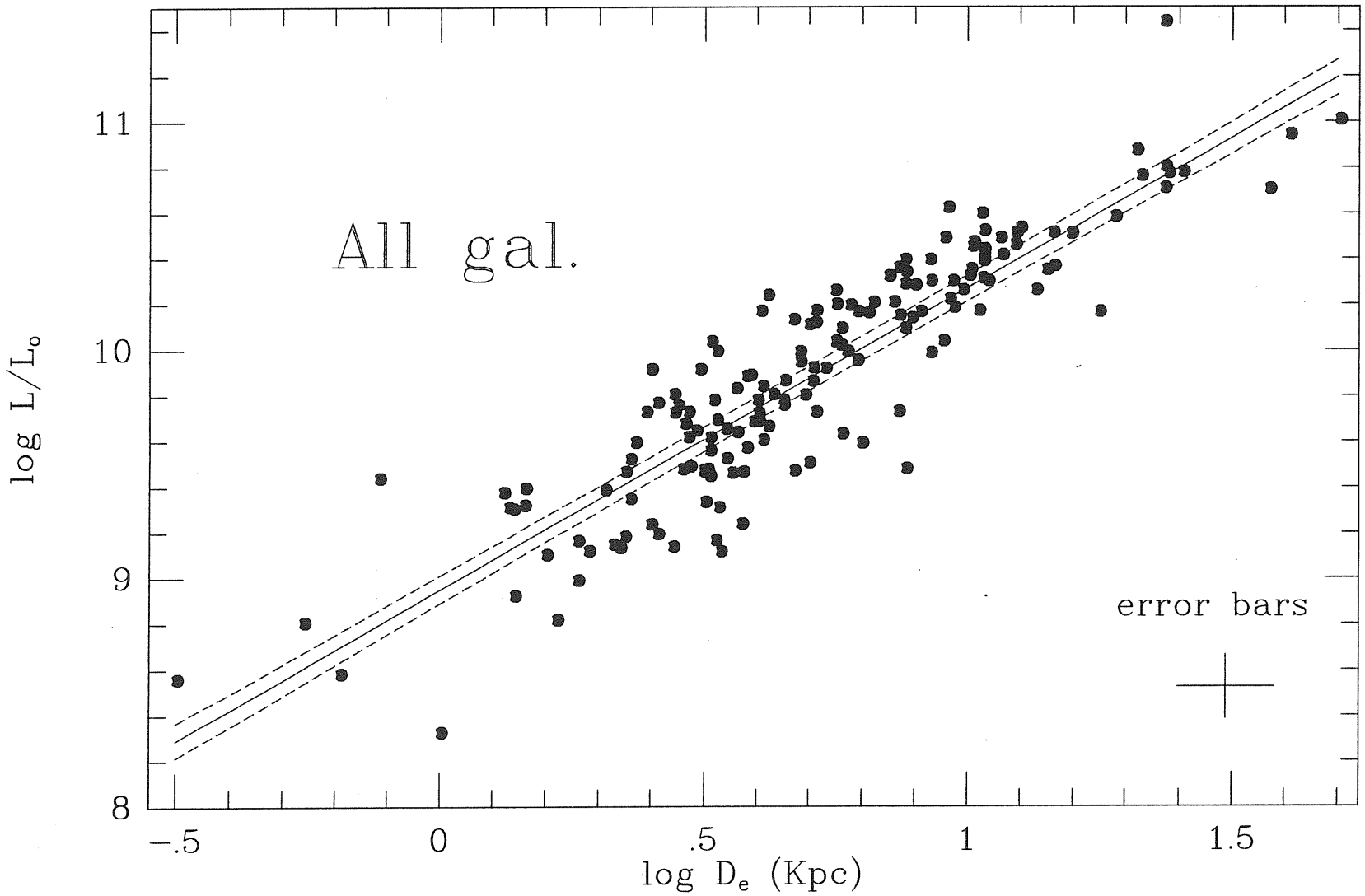

graph. C.27

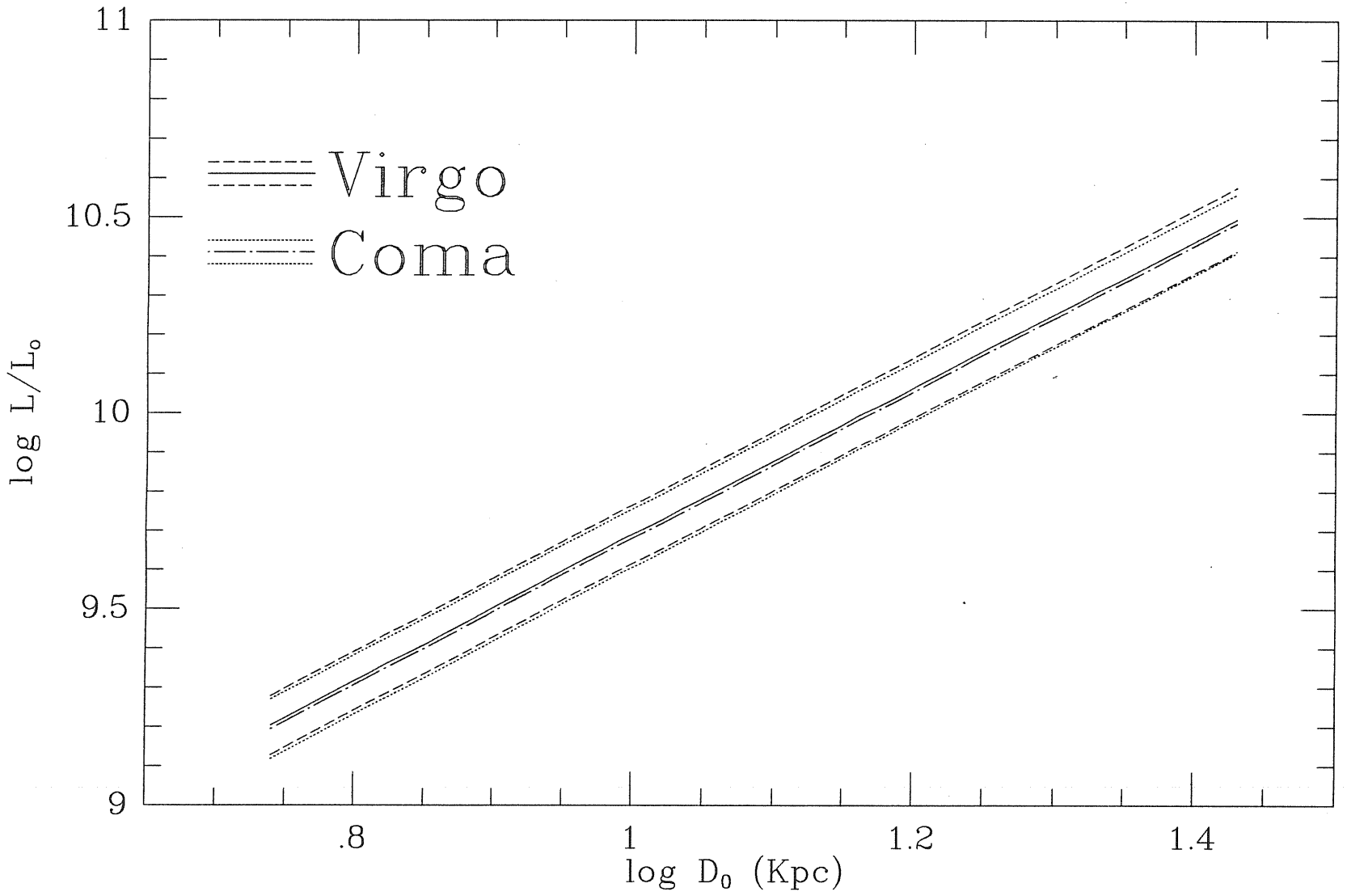

graph. C.28

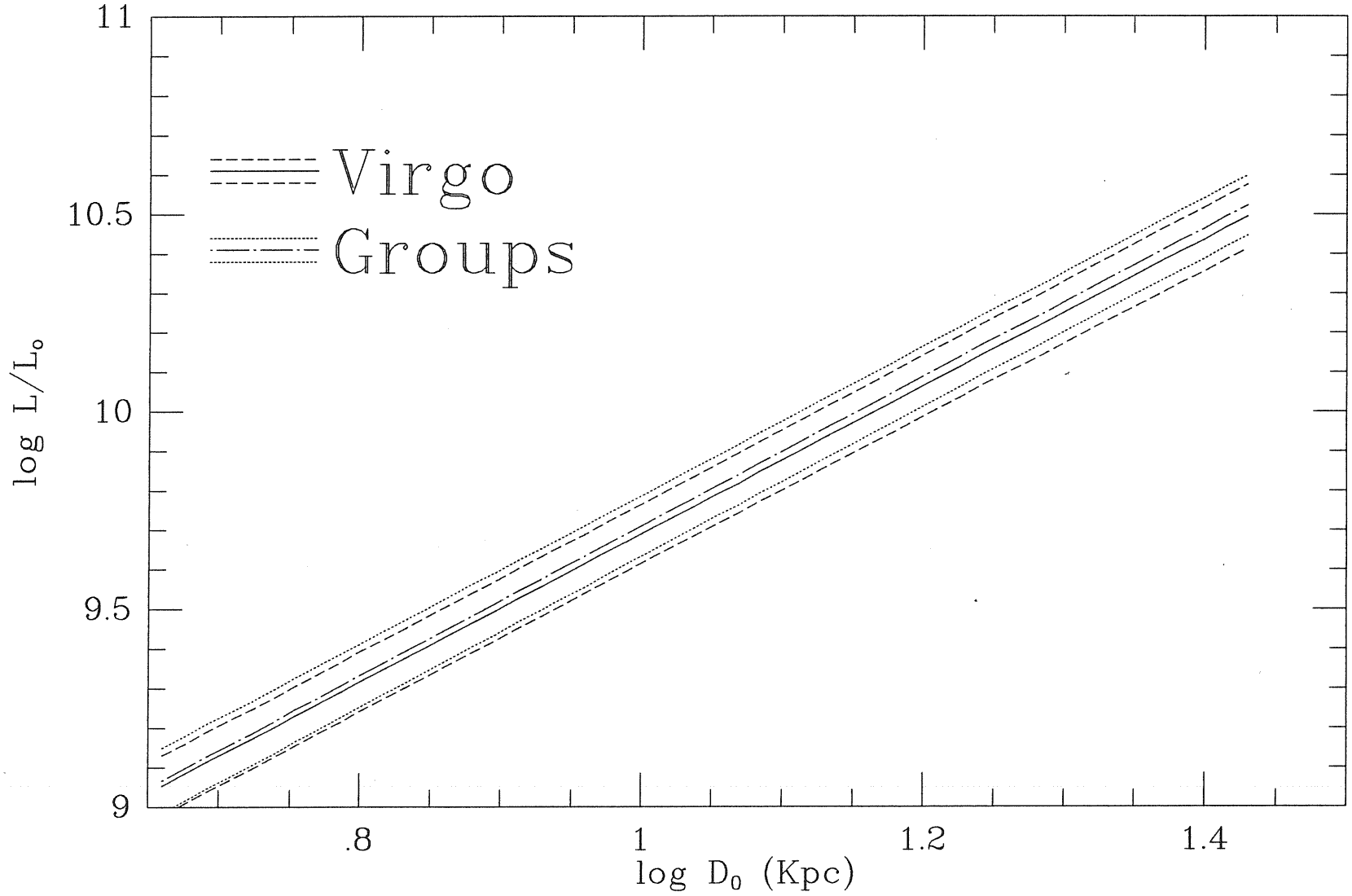

graph. C.29

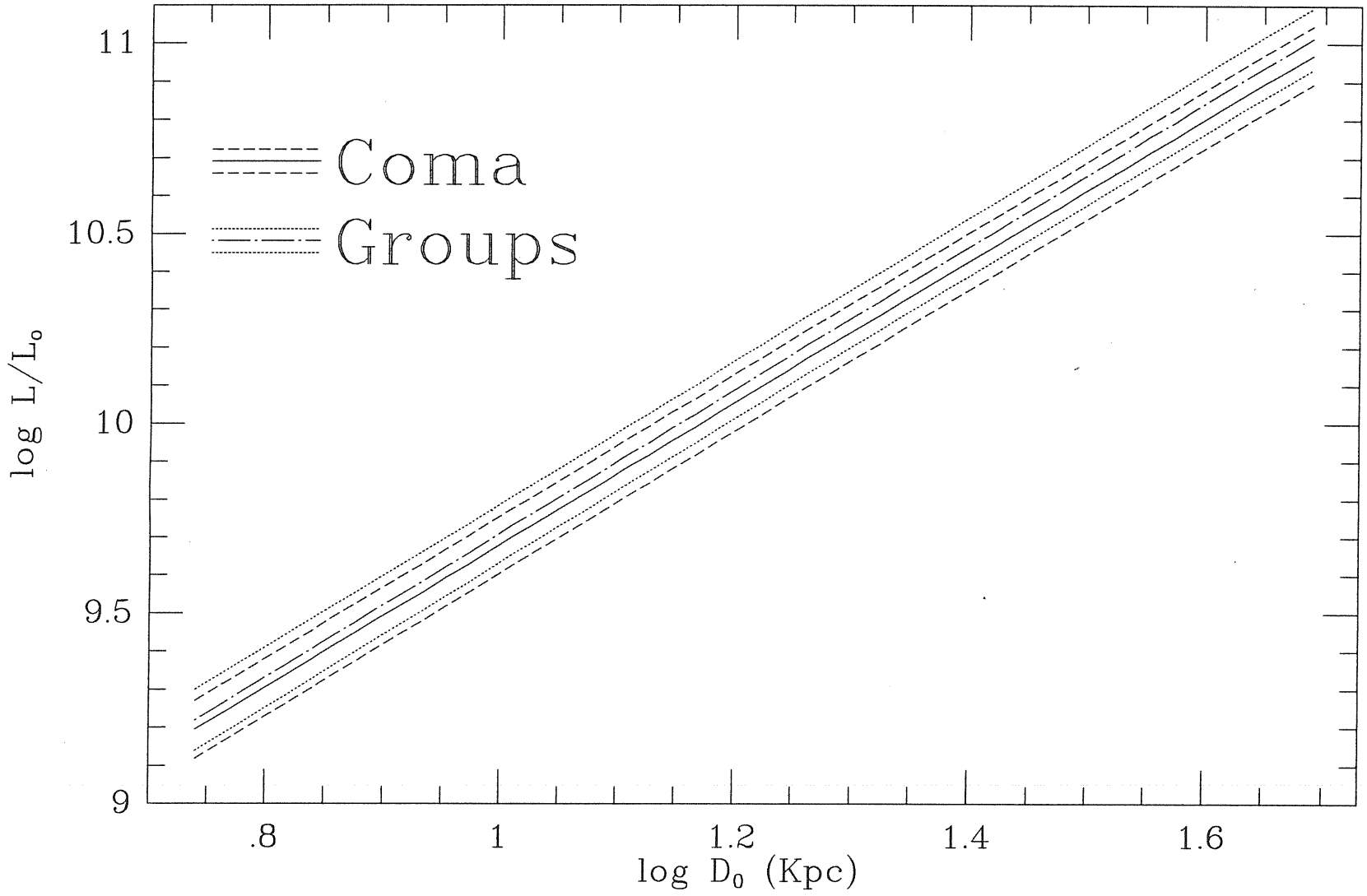

graph. C.30

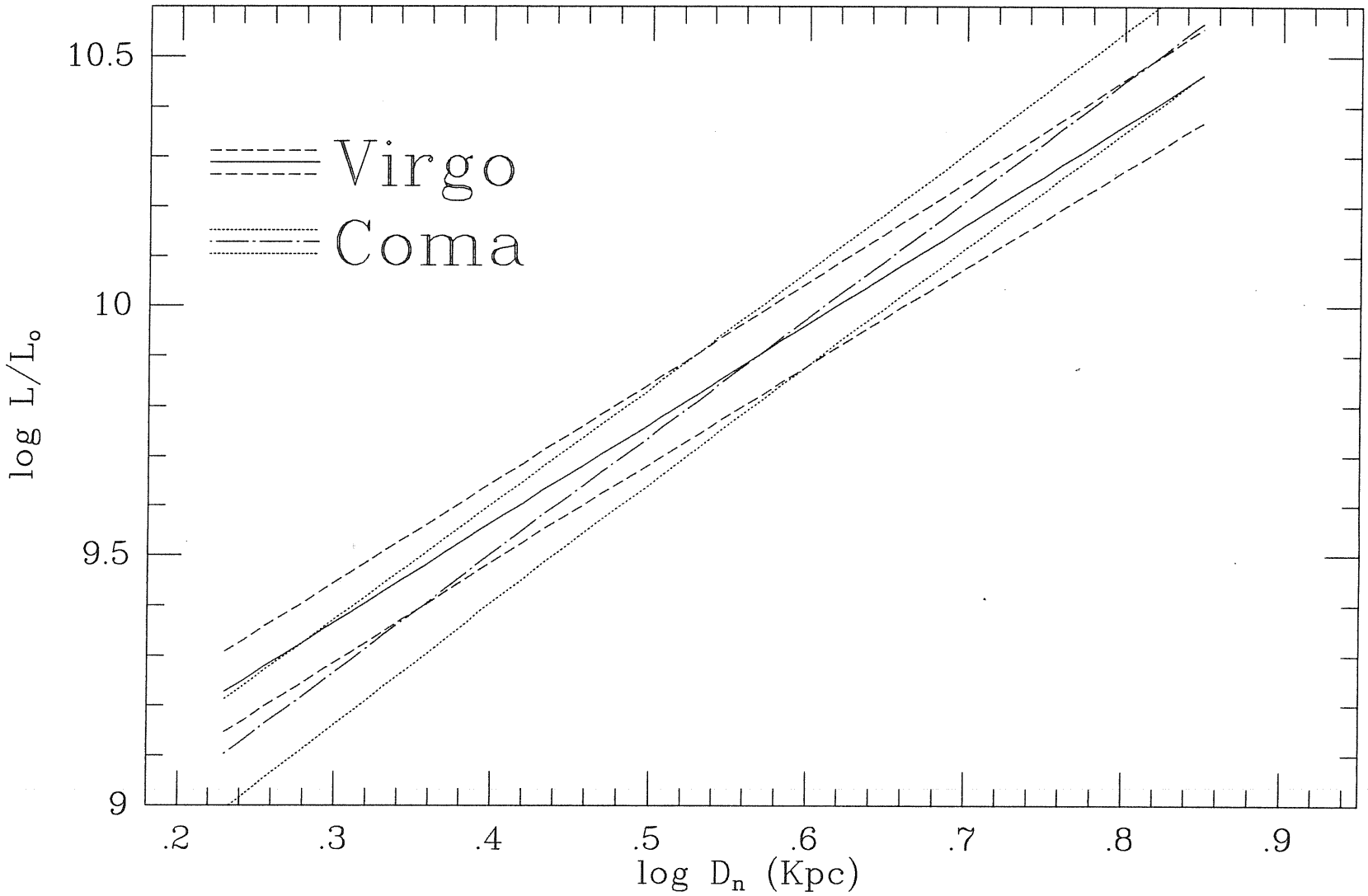

graph. C.31

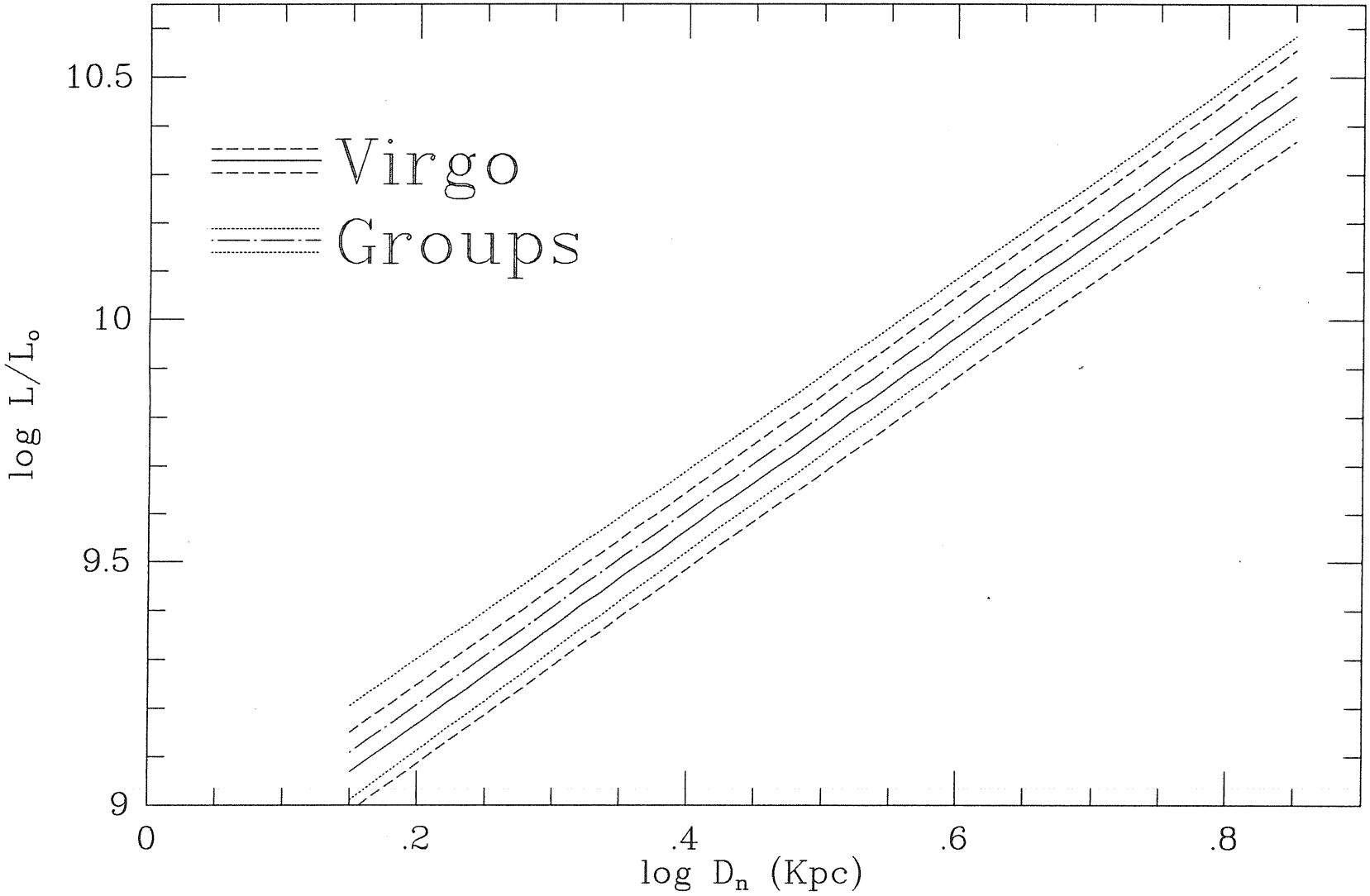

graph. C.32

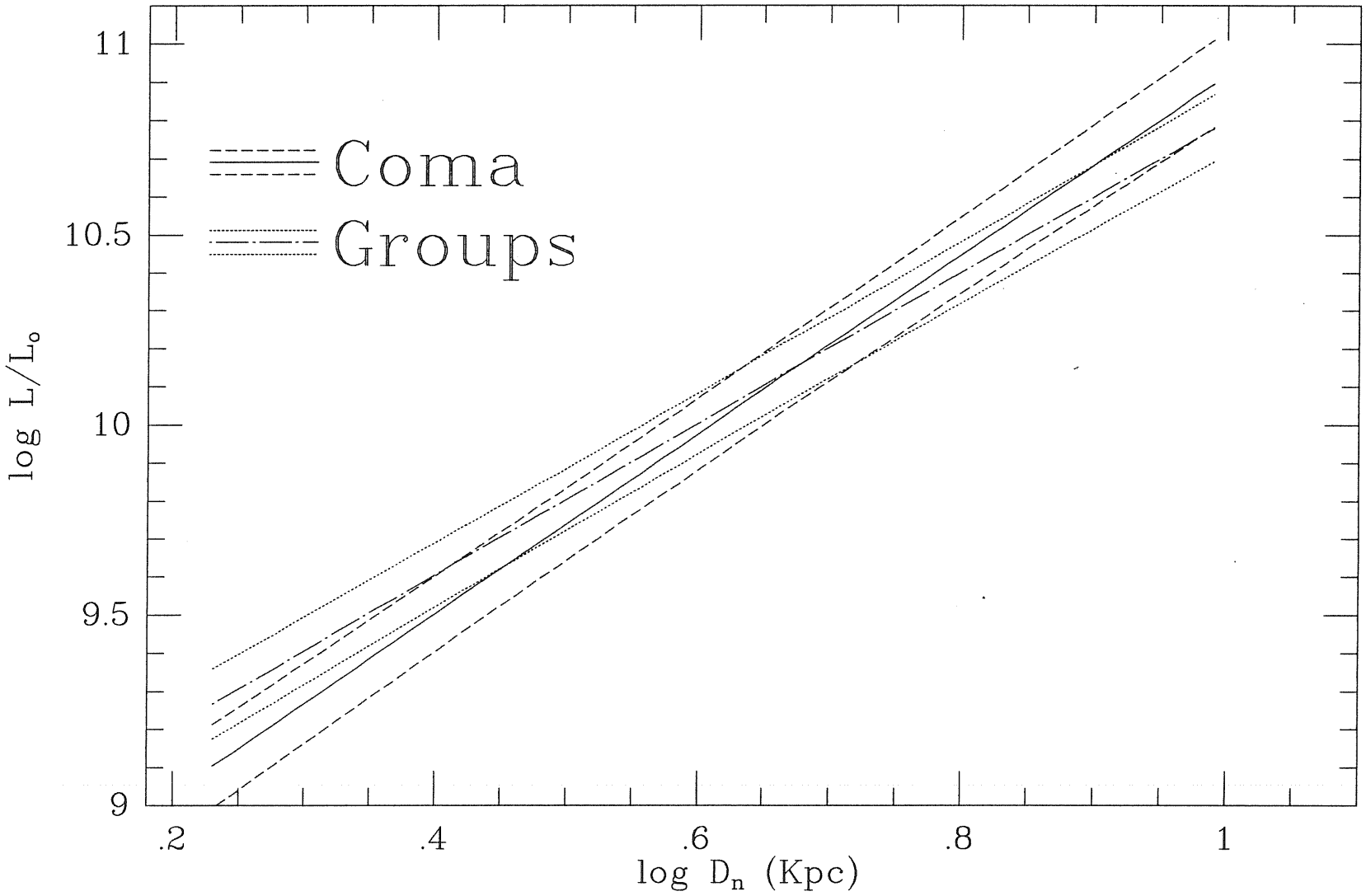

graph. C.33

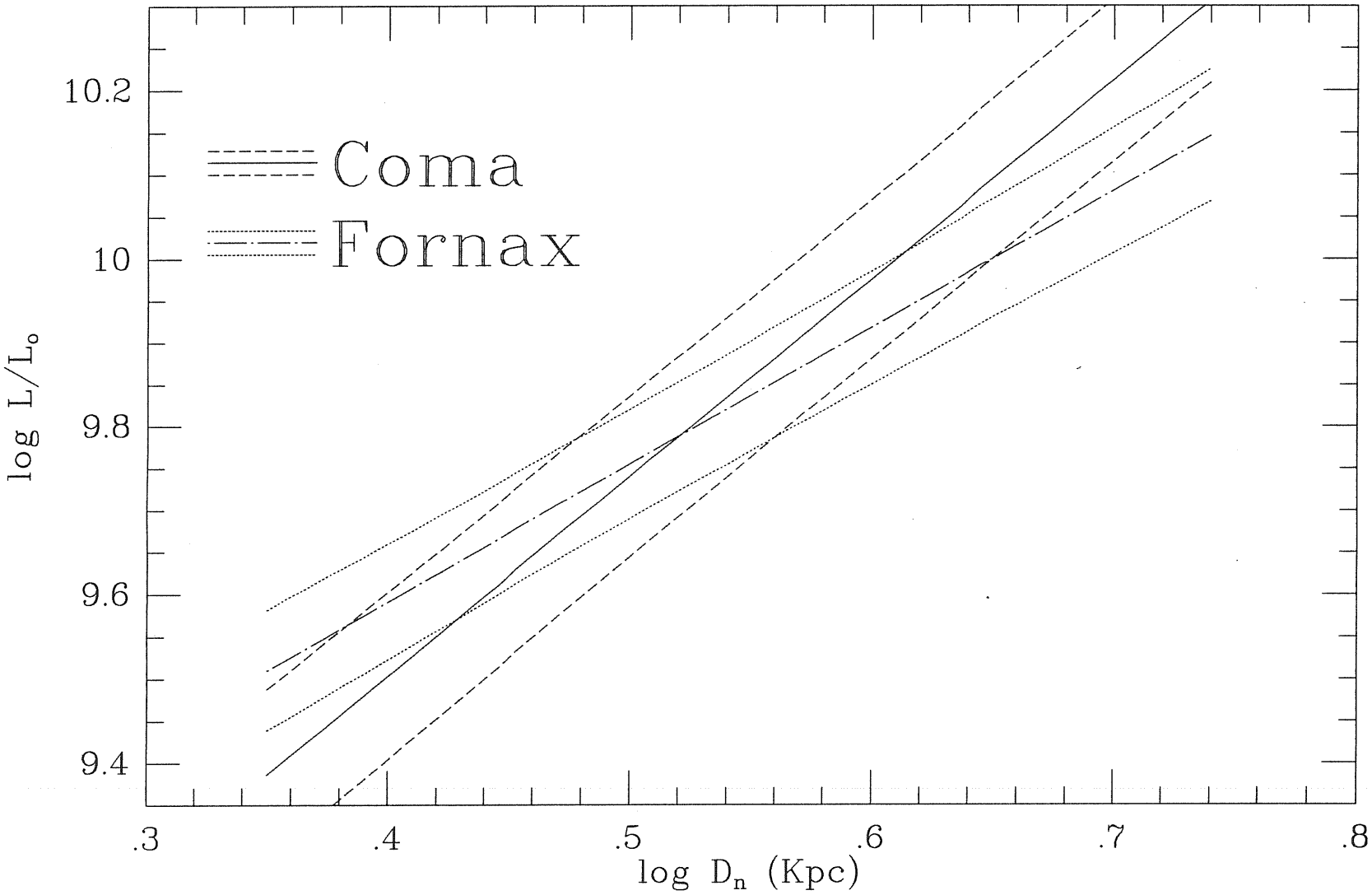

graph. C.34

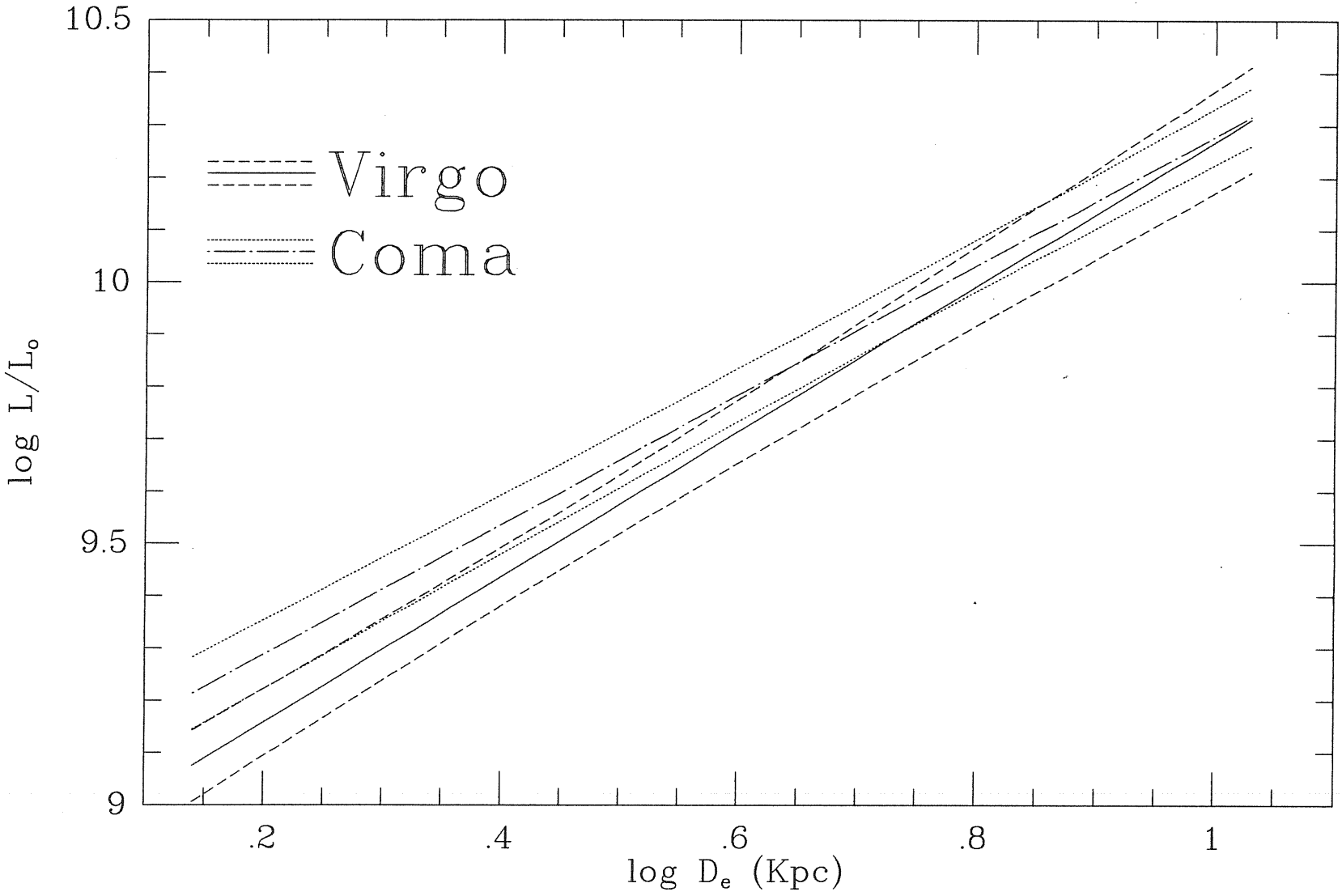

graph. C.35

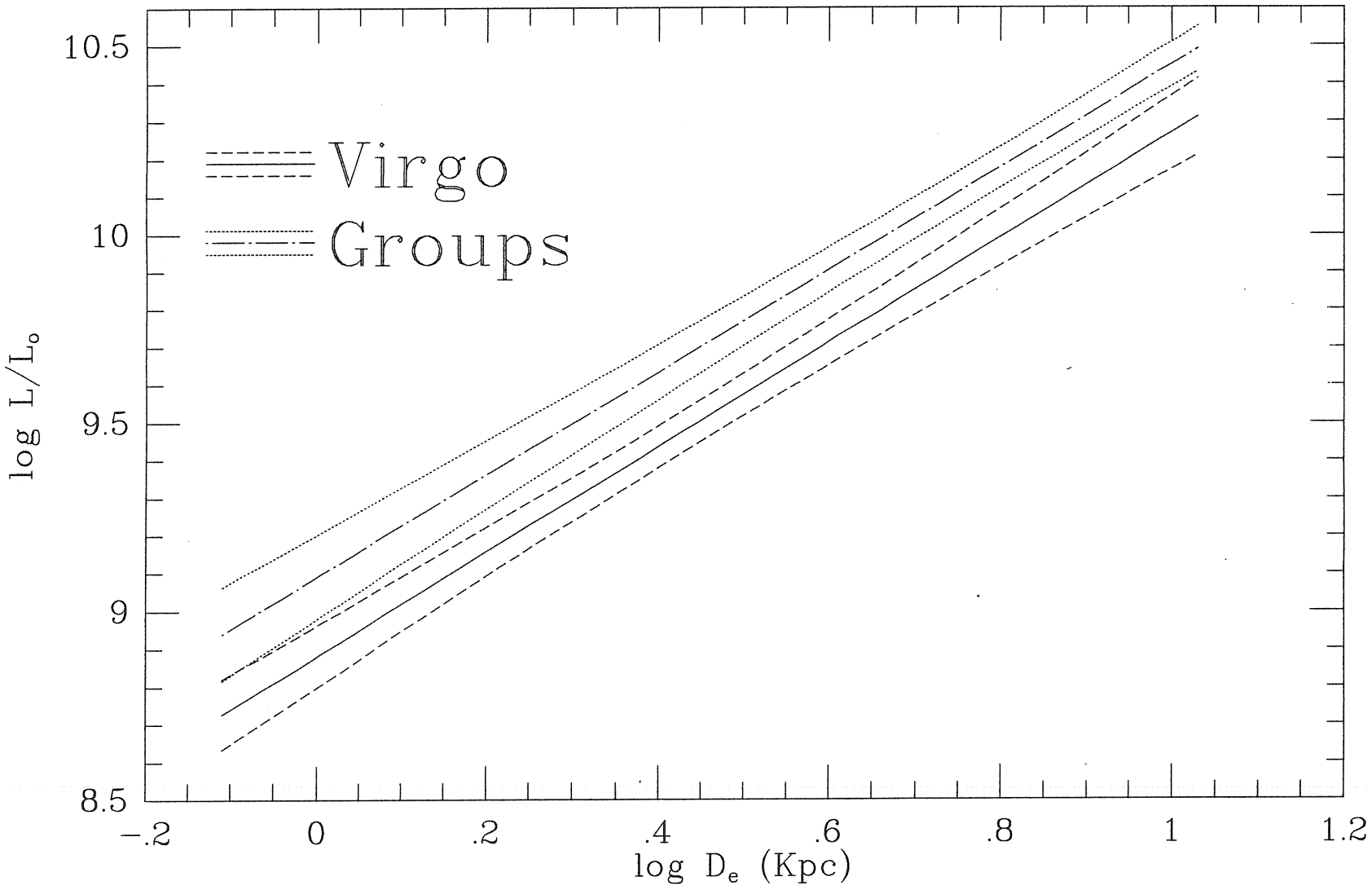

graph. C.36

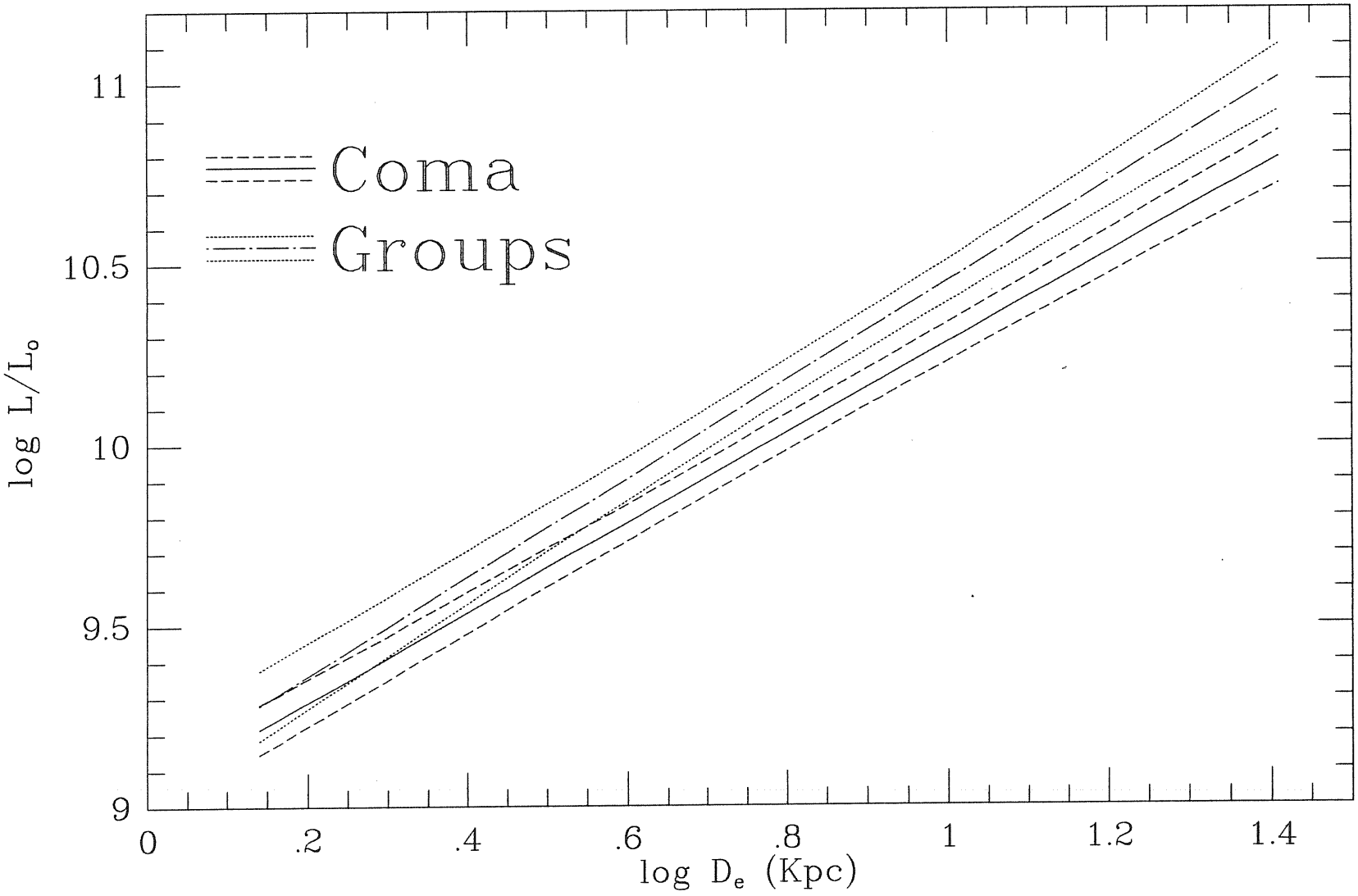

graph. C.37

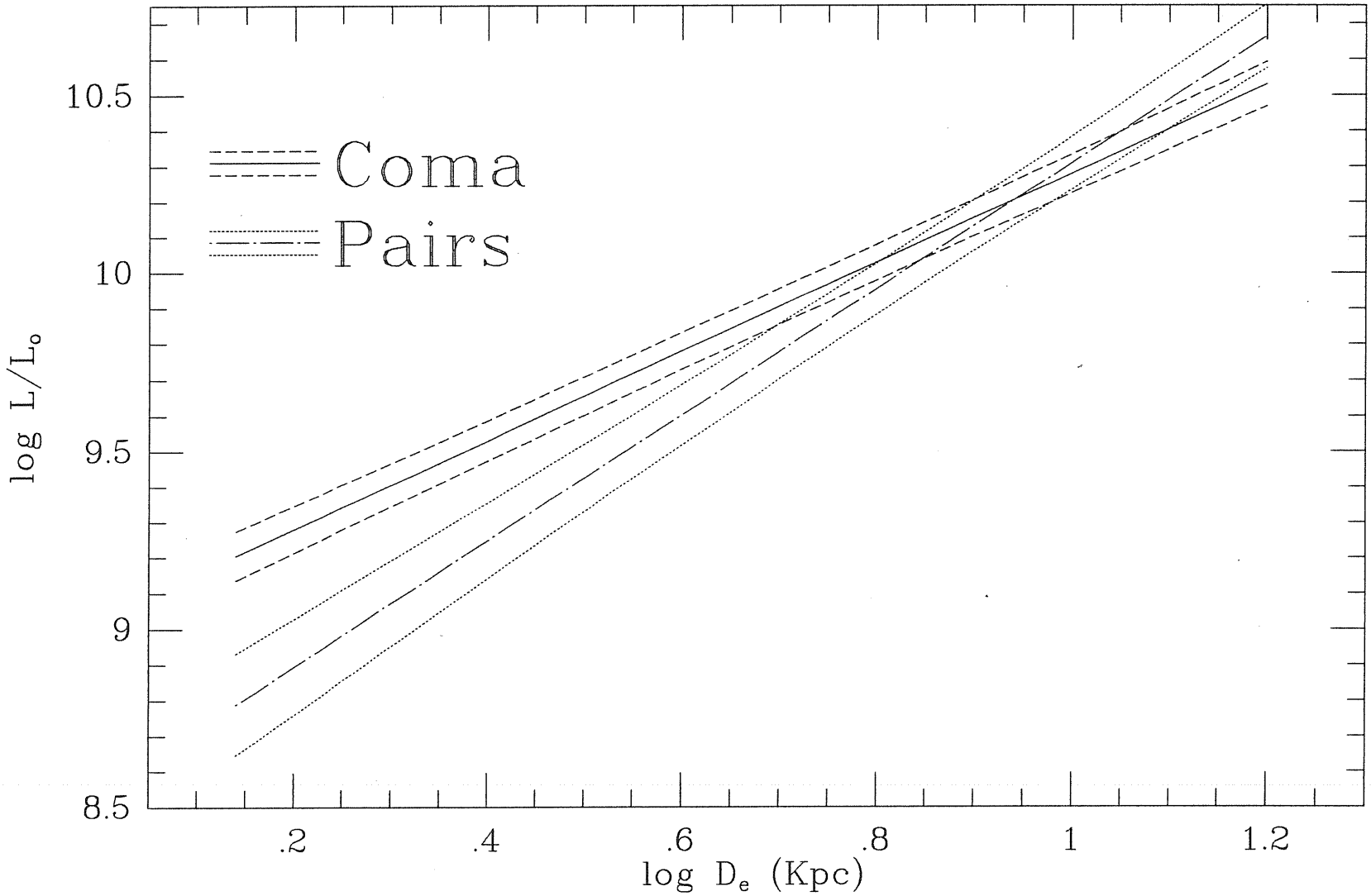

graph. C.38

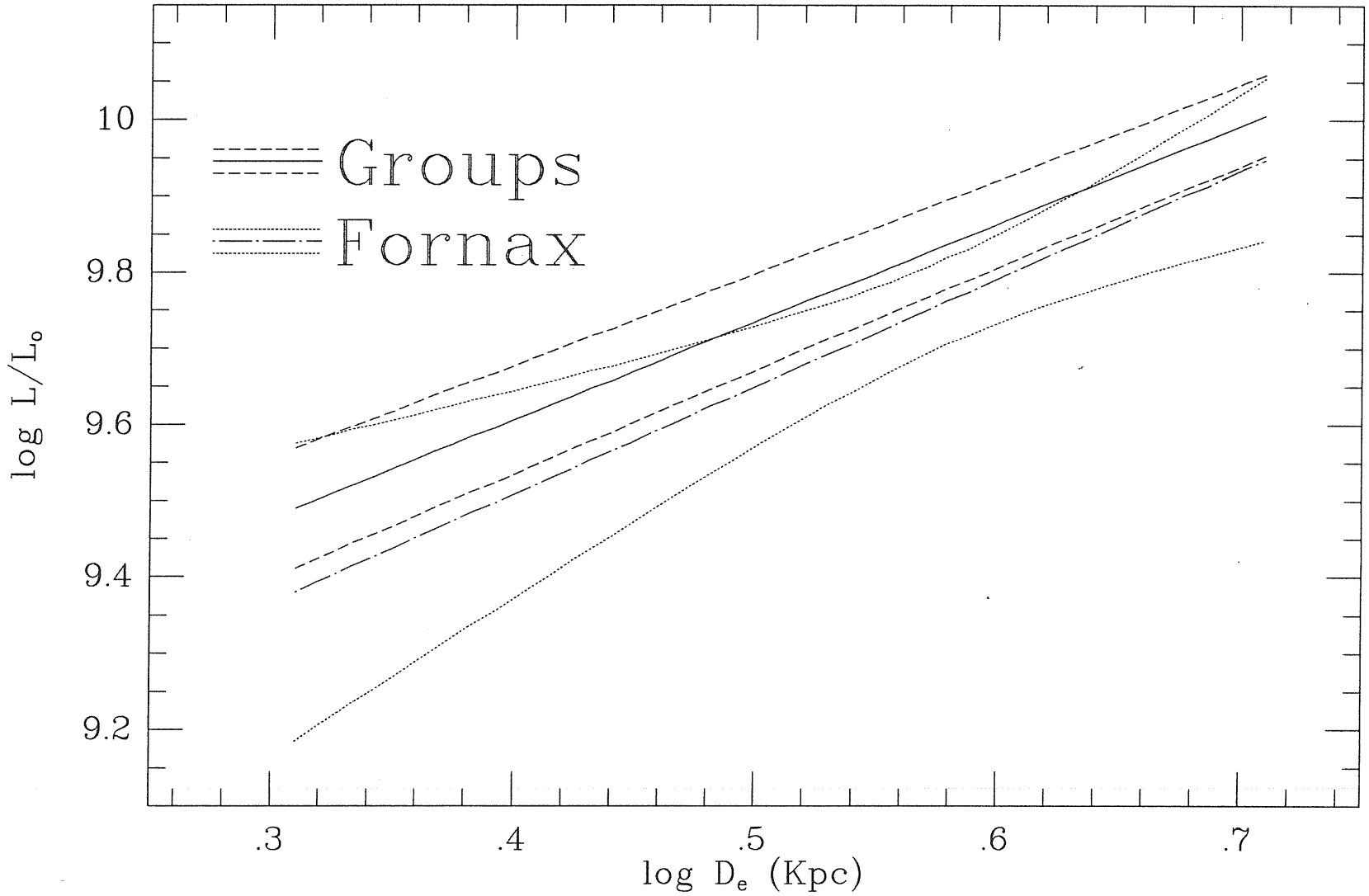

graph. C.39

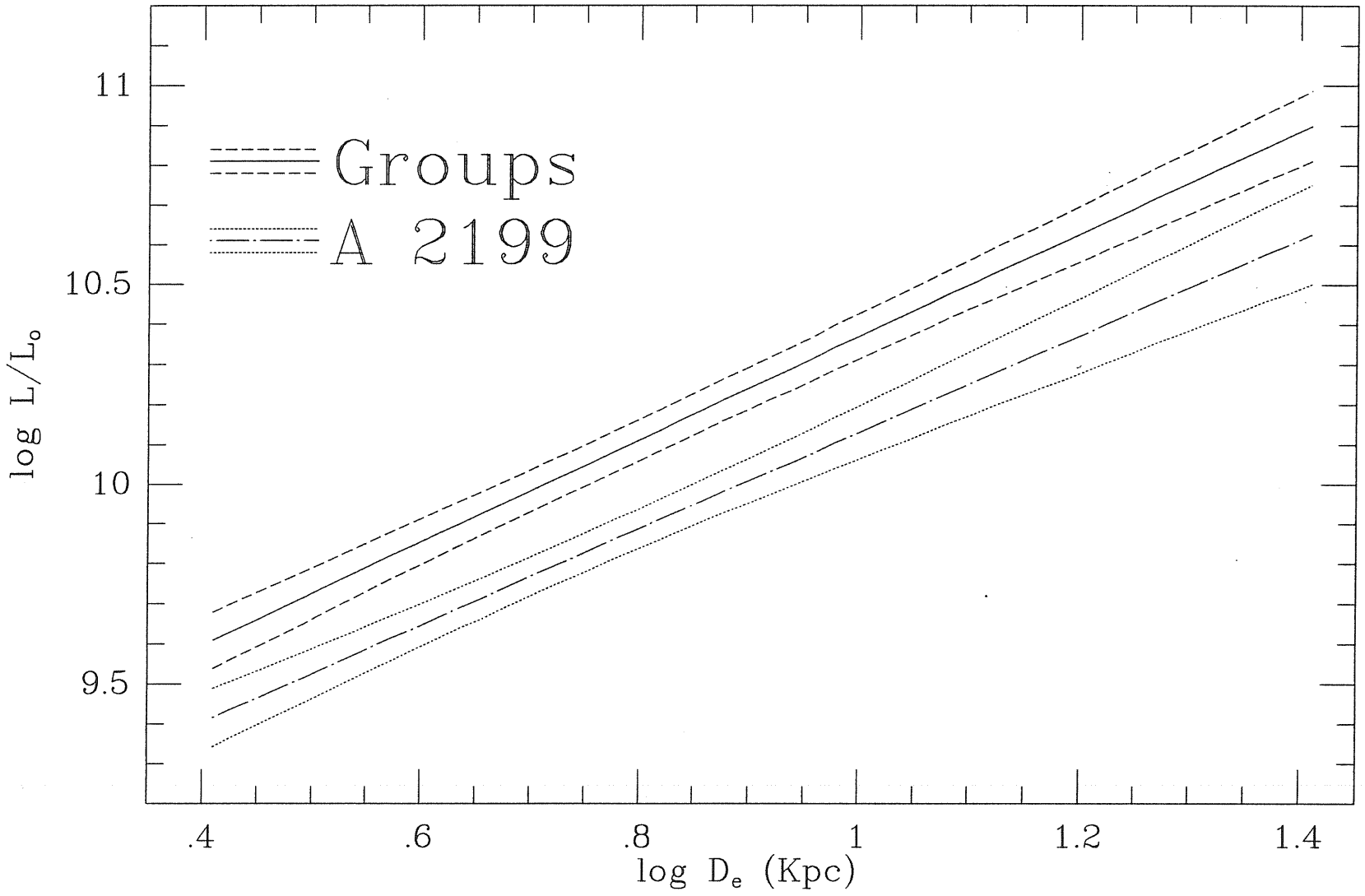

graph. C.40

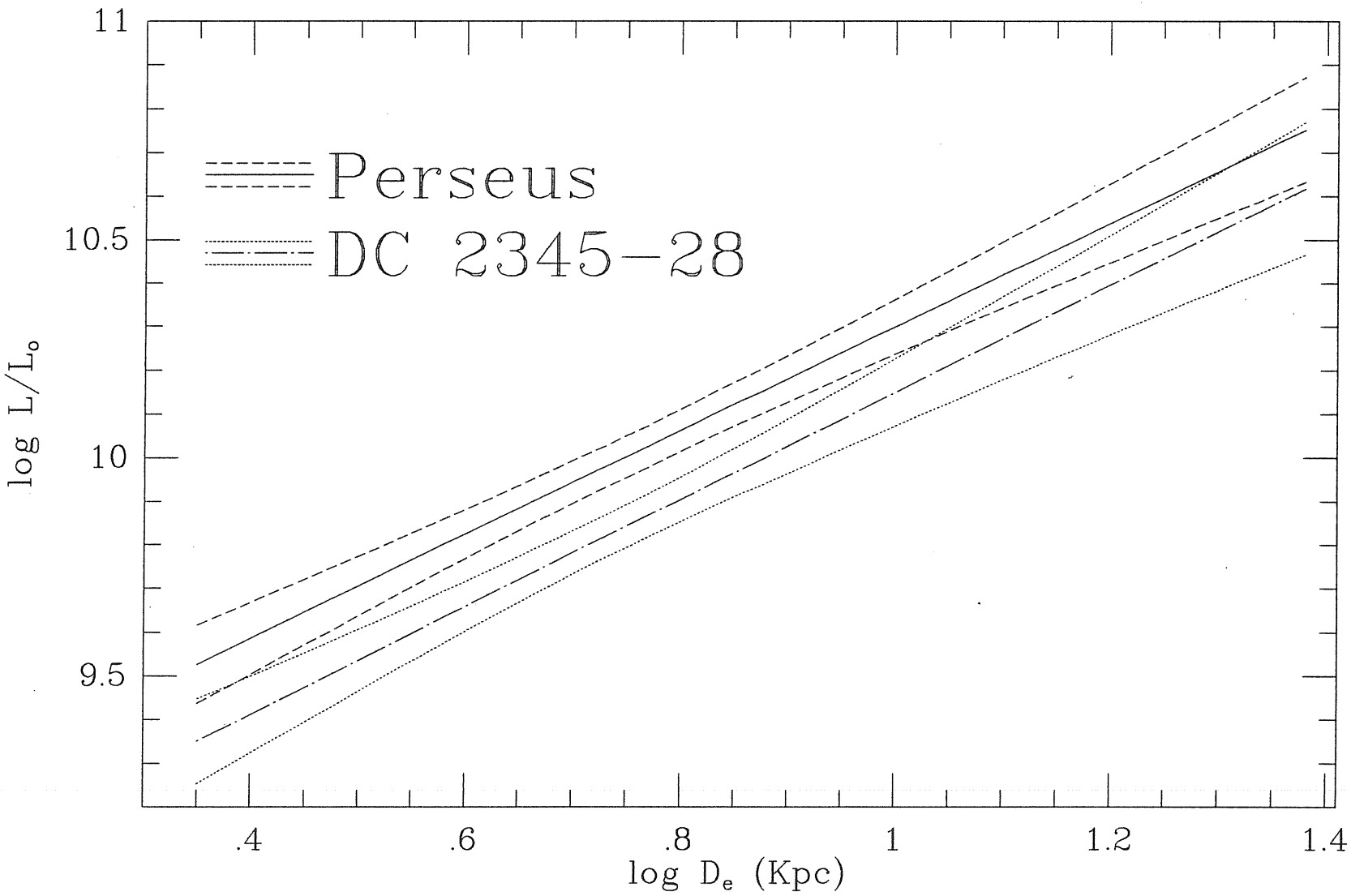

graph. C.41

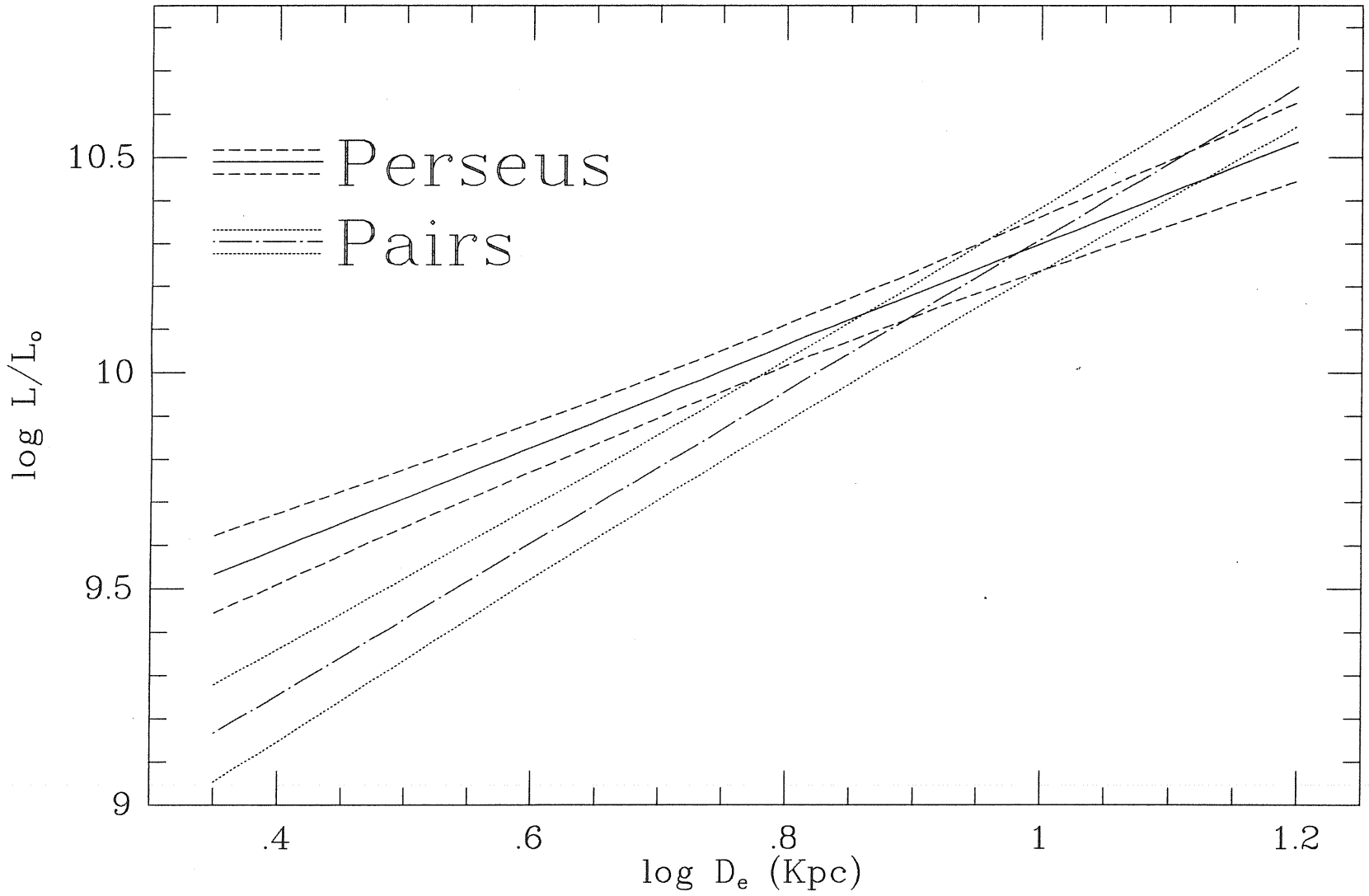

graph. C.42

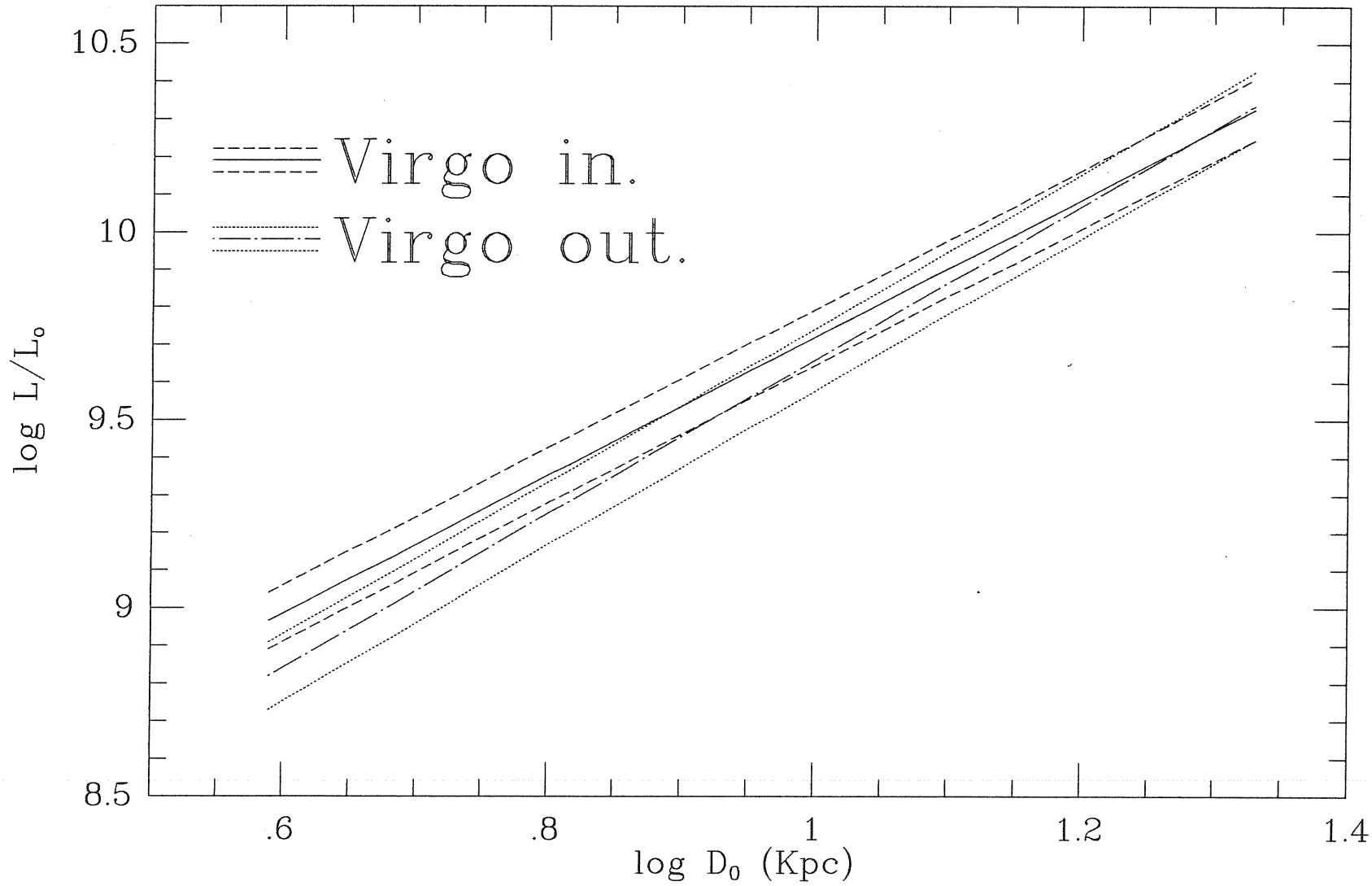

graph. C.43

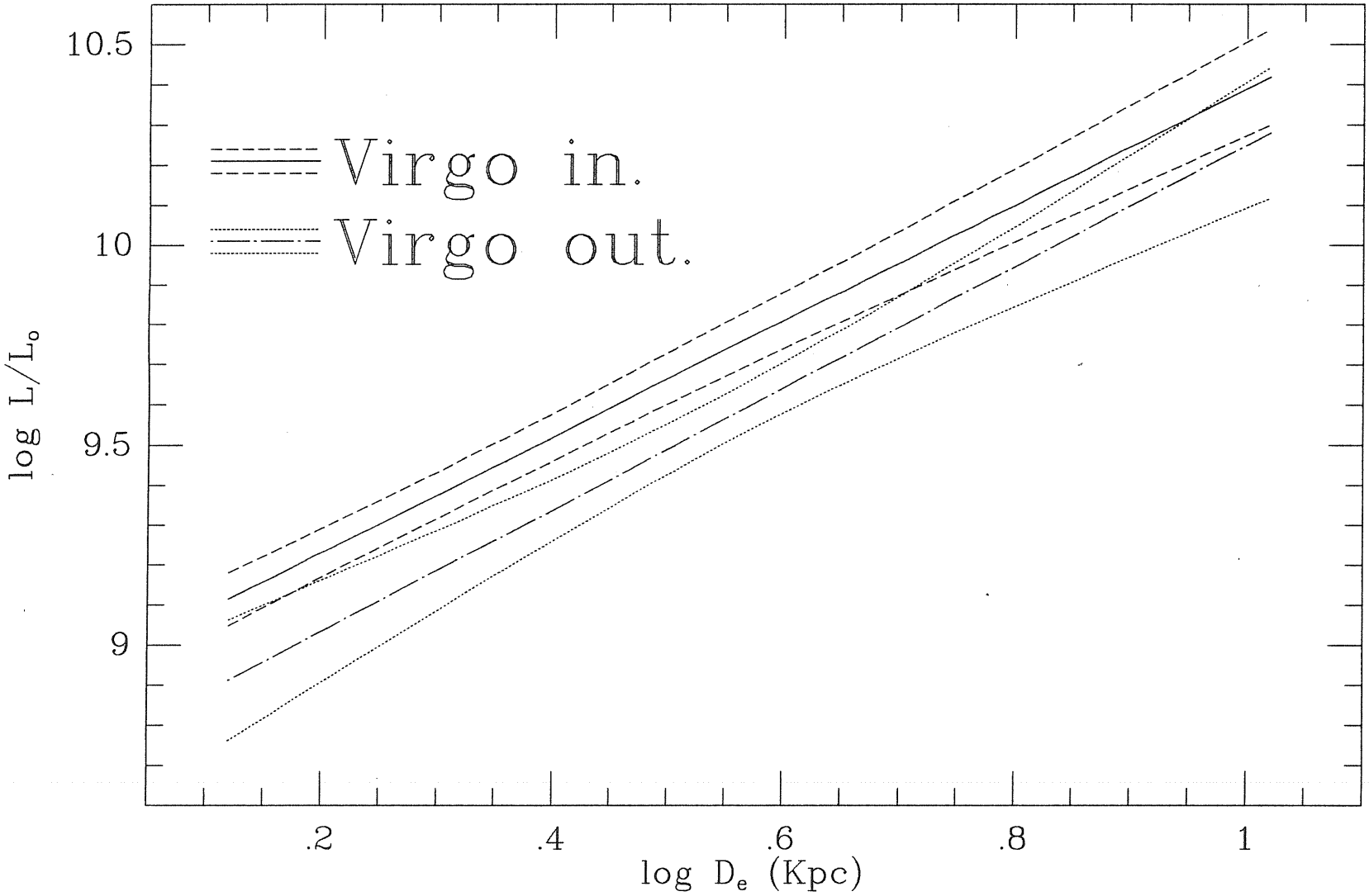

graph. C.44

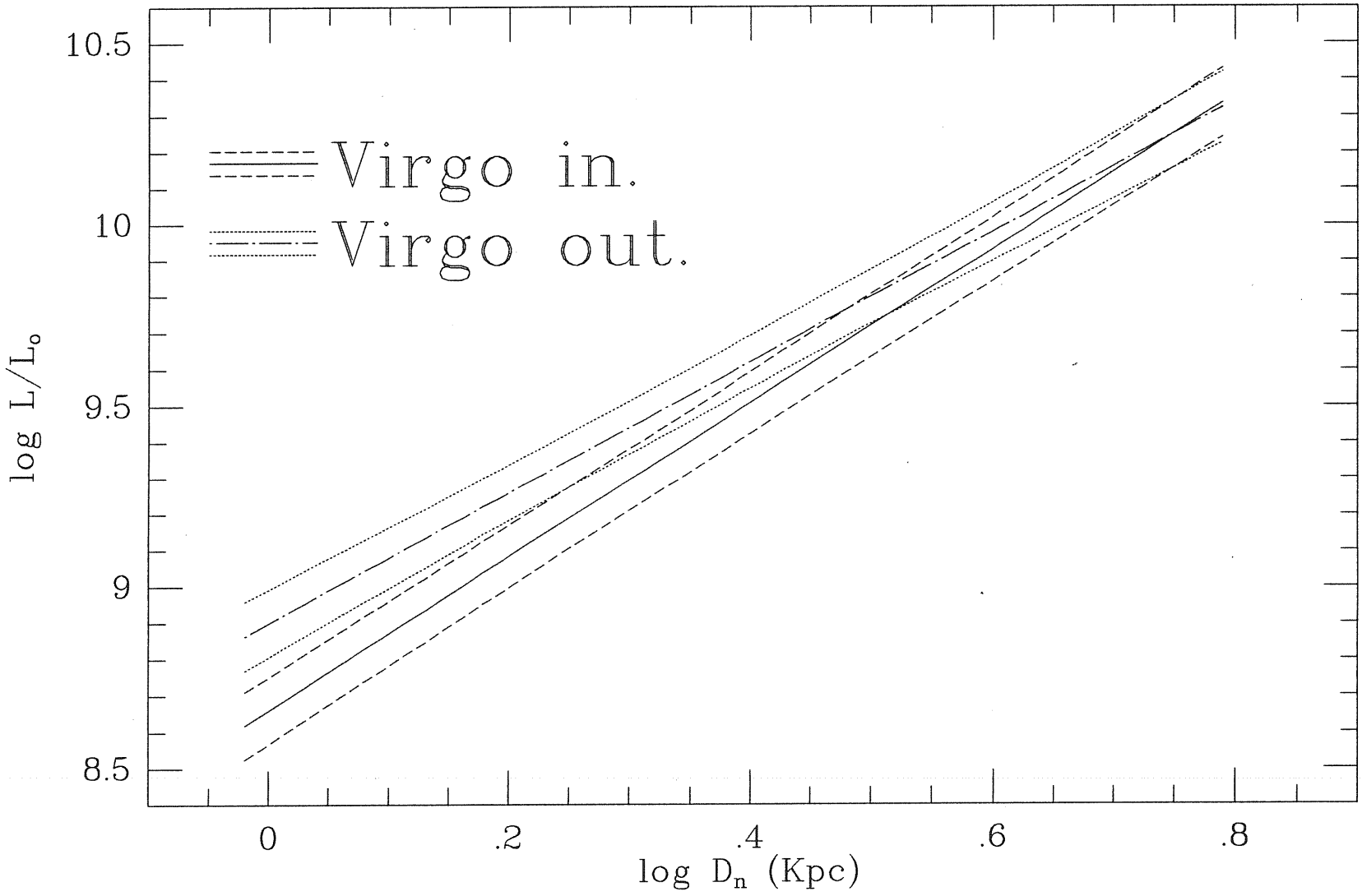

graph. C.45

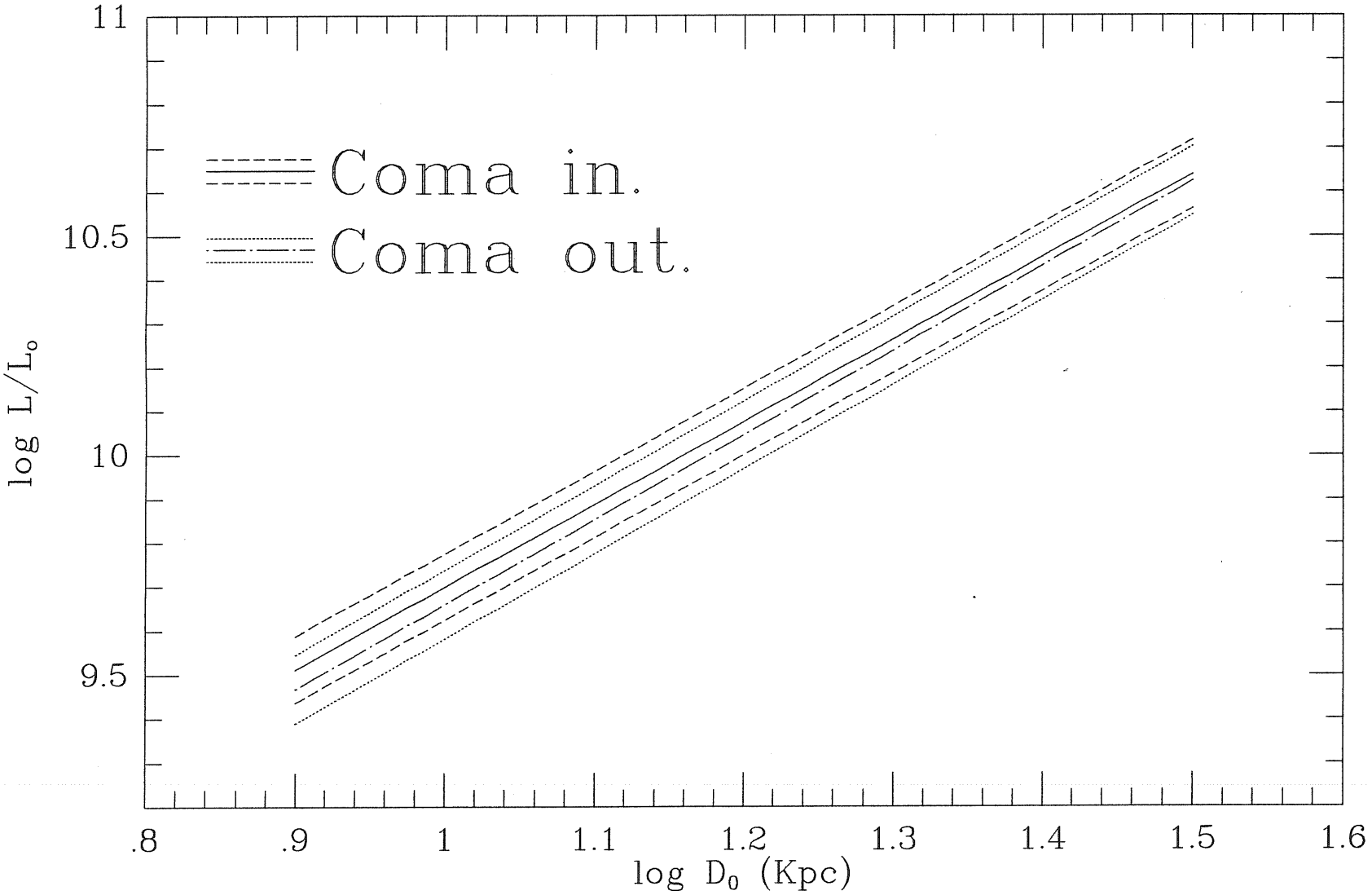
Coma in.
Coma out.
11
10.5
10
9.5
log L/L$_o$
.8
.9
1
1.1
1.2
1.3
1.4
1.5
1.6
log D$_0$ (Kpc)

graph. C.46

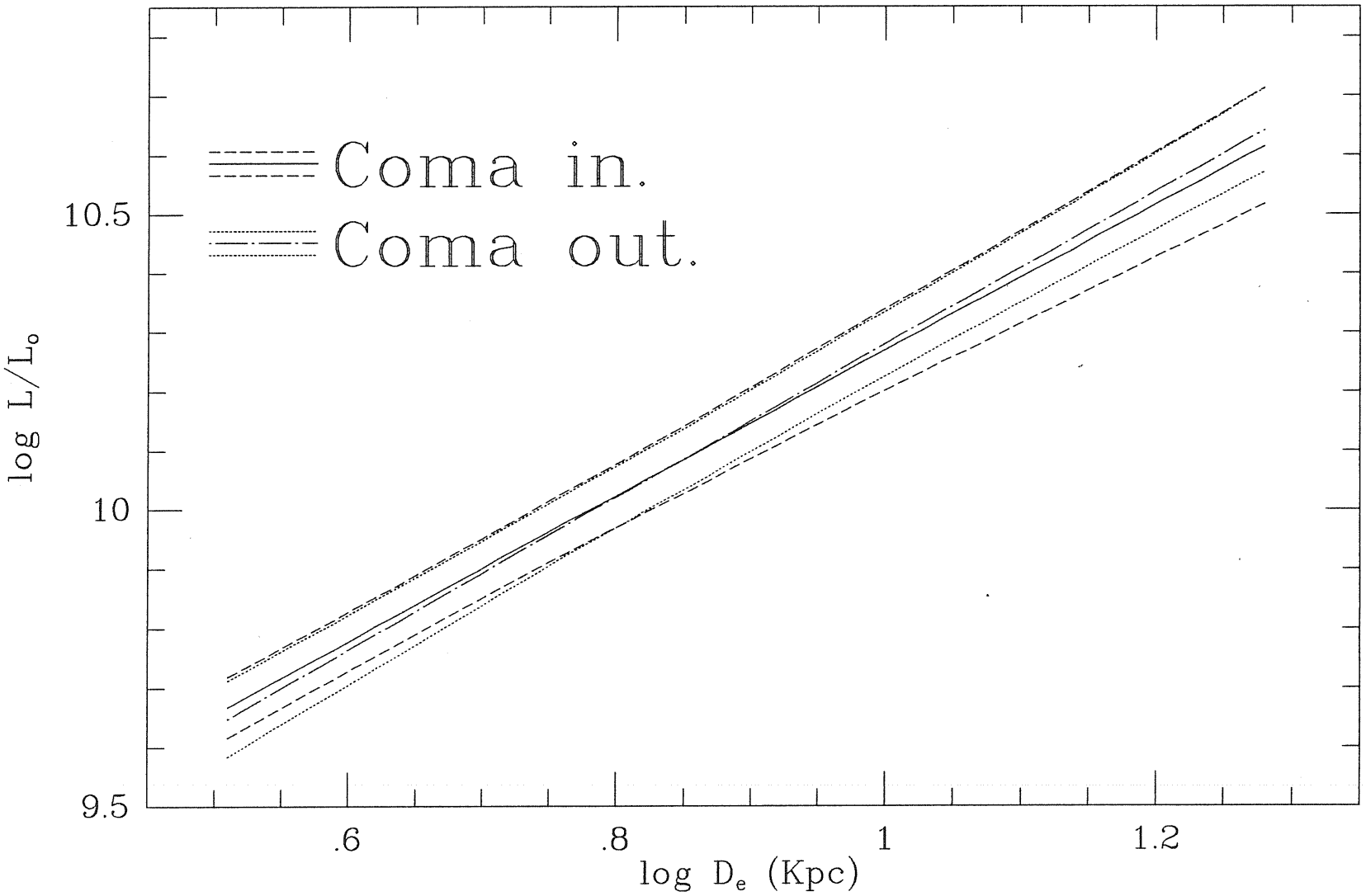

graph. C.47

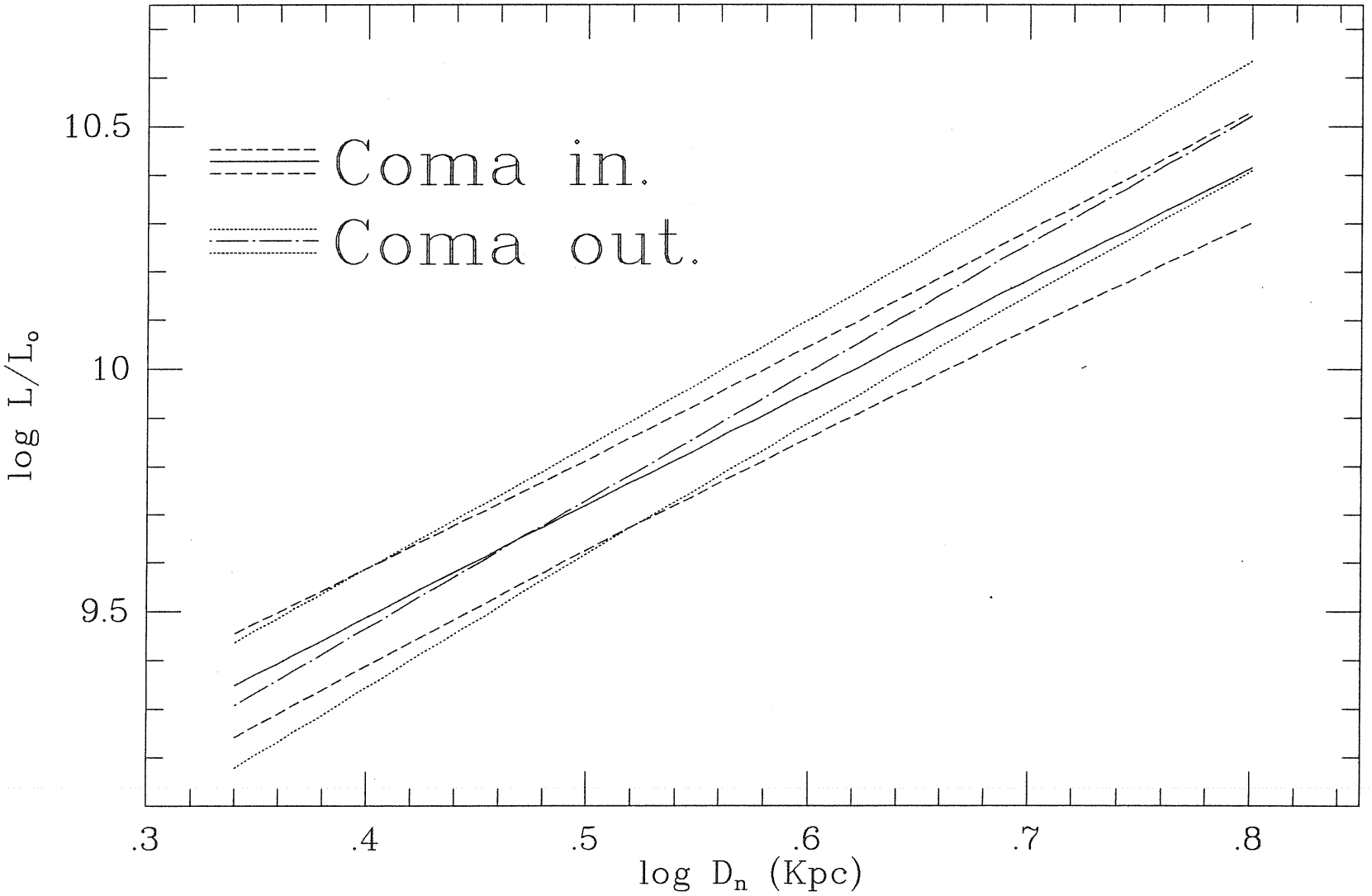

graph. C.48

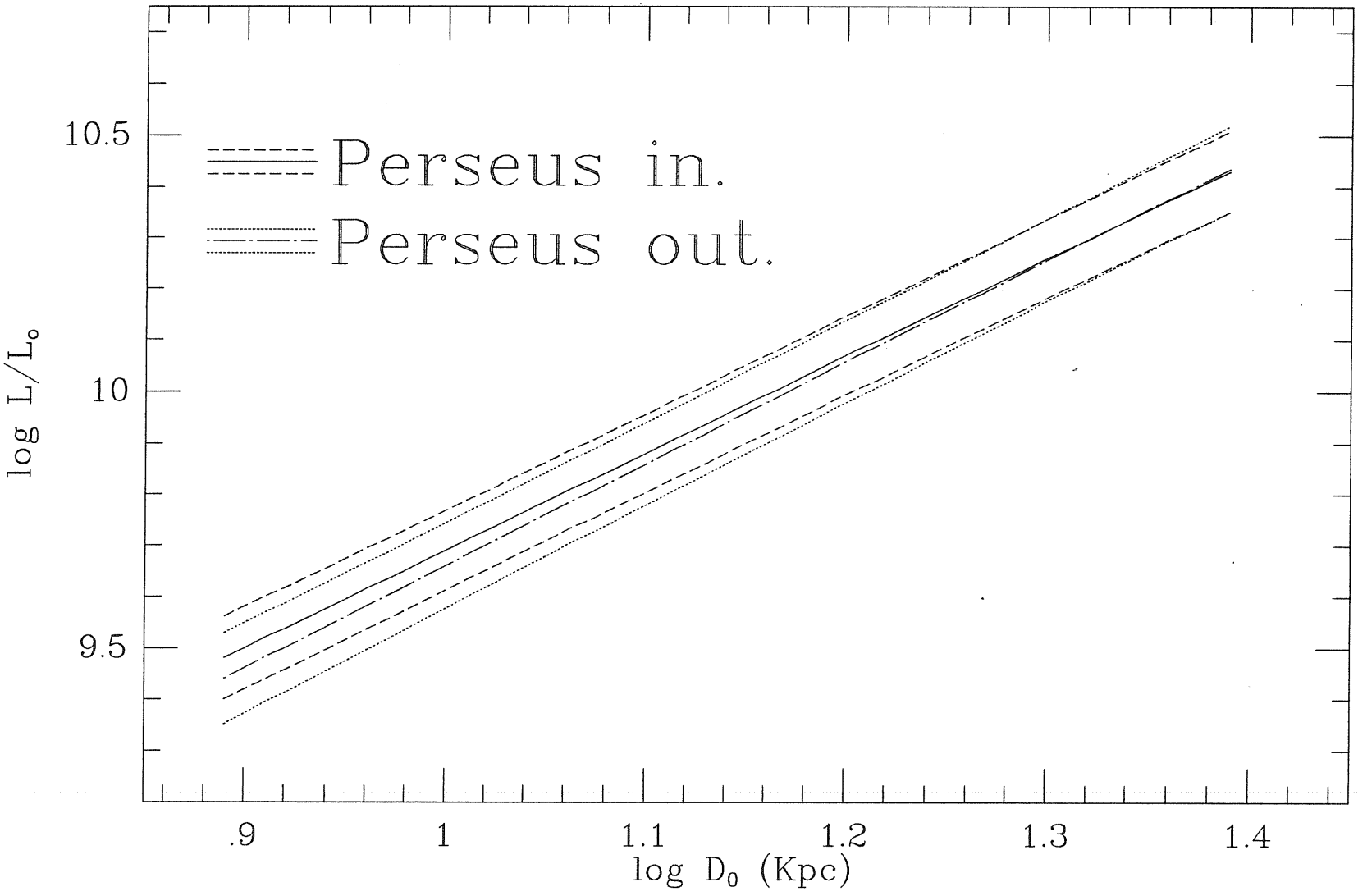
Perseus in.
Perseus out.
10.5
10
9.5
log L/L$_o$
.9
1
1.1
1.2
1.3
1.4
log D$_0$ (Kpc)

graph. C.49

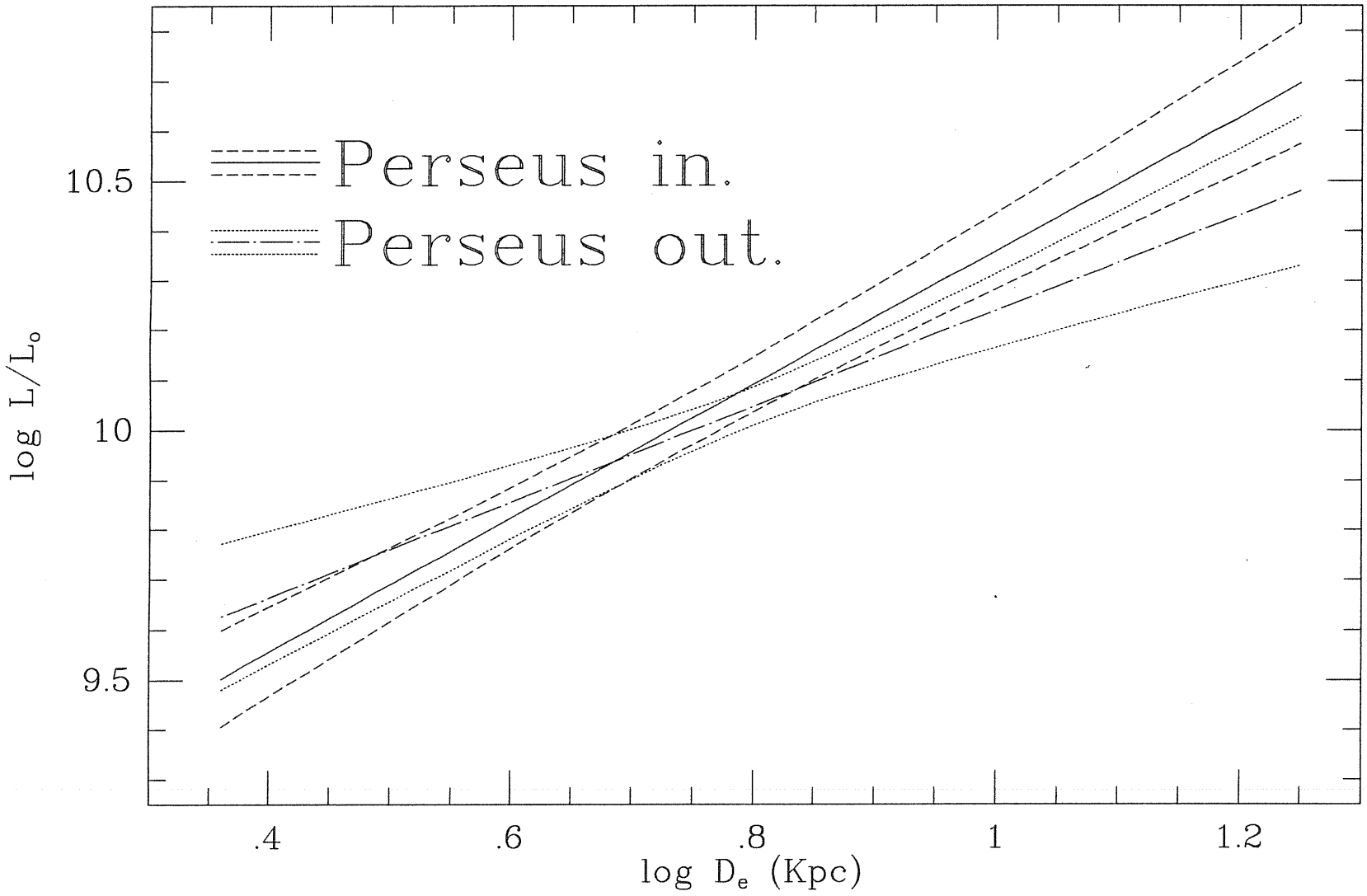

graph. C.50

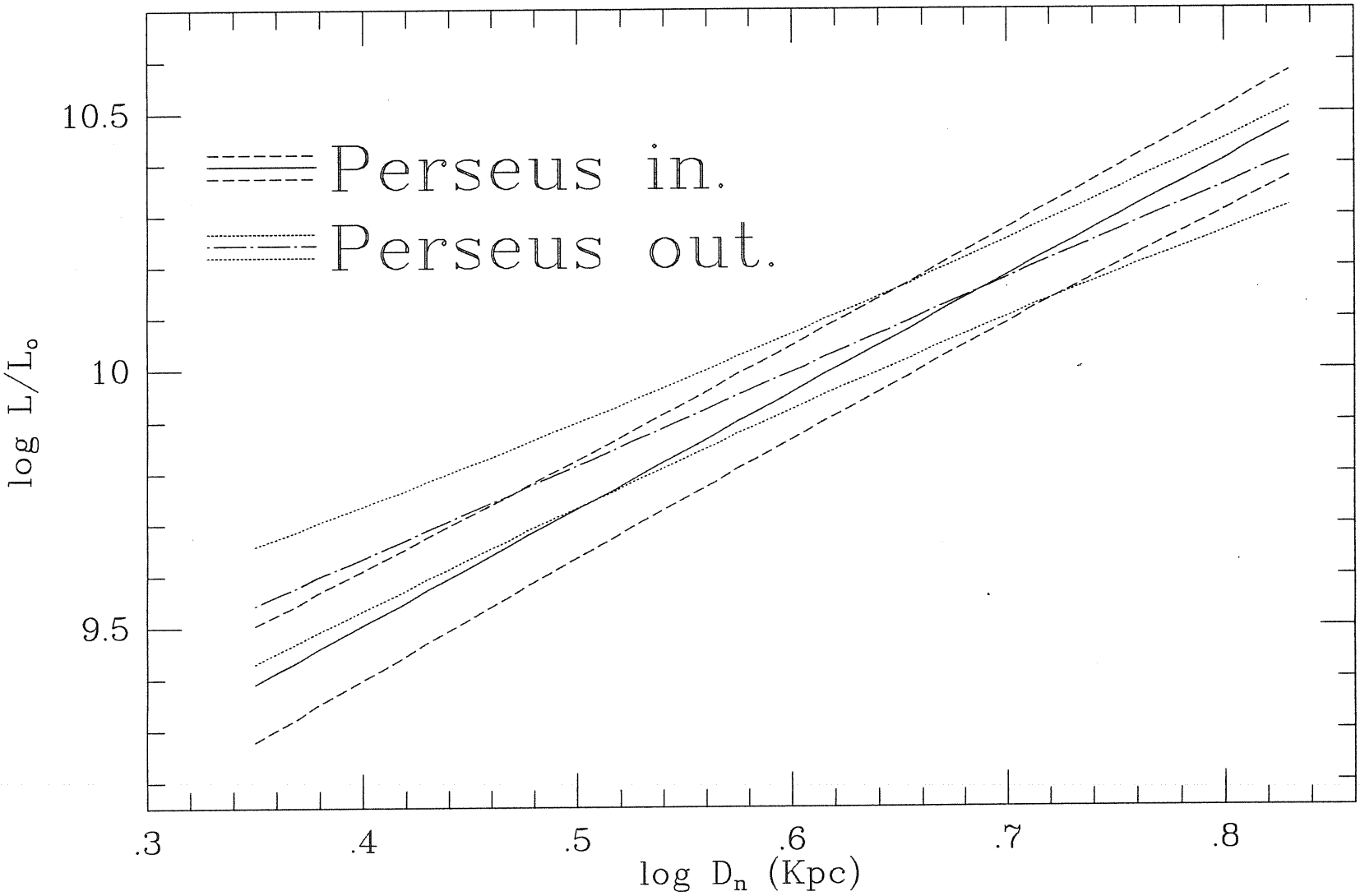

graph. C.51

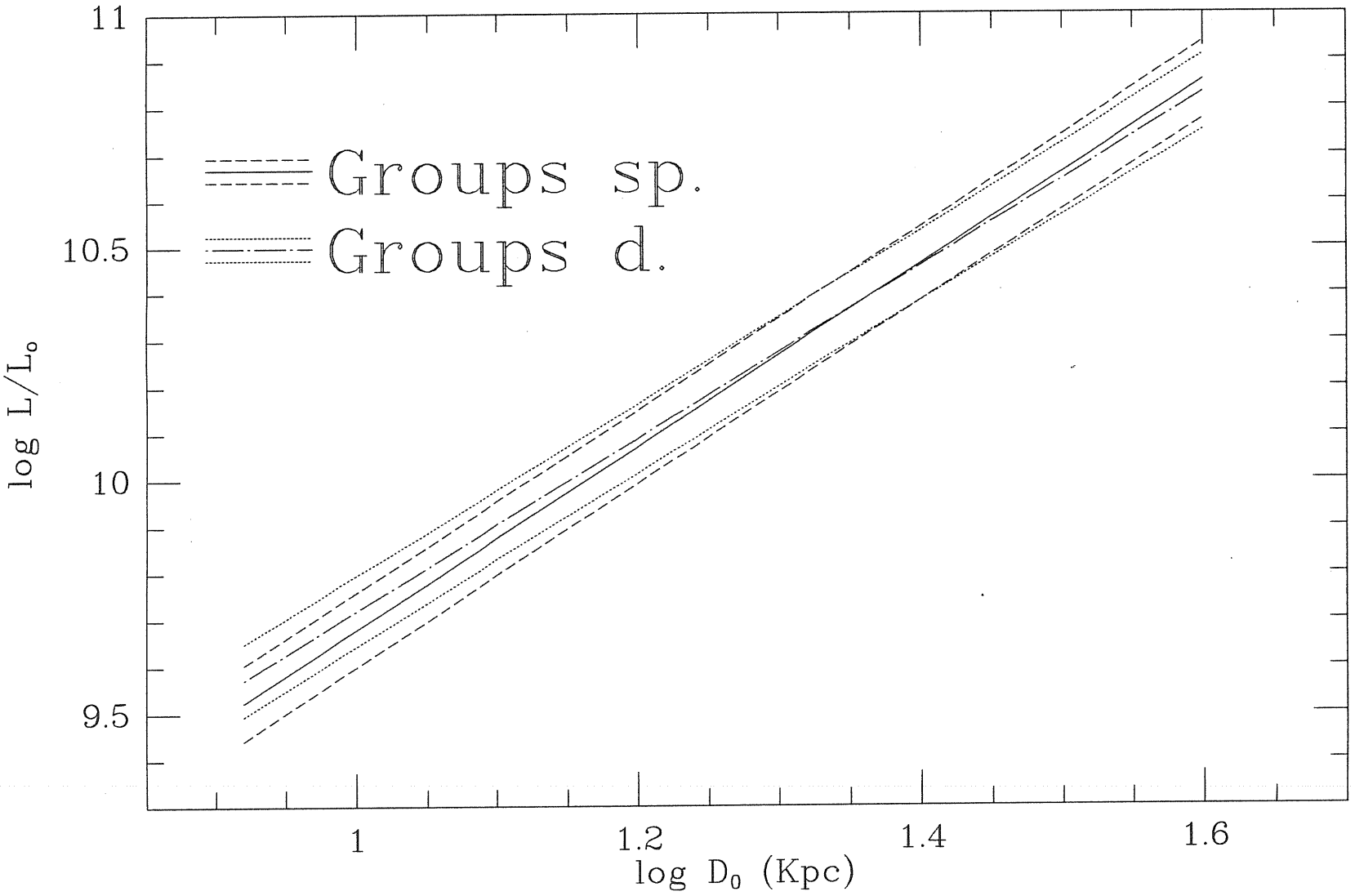

graph. C.52

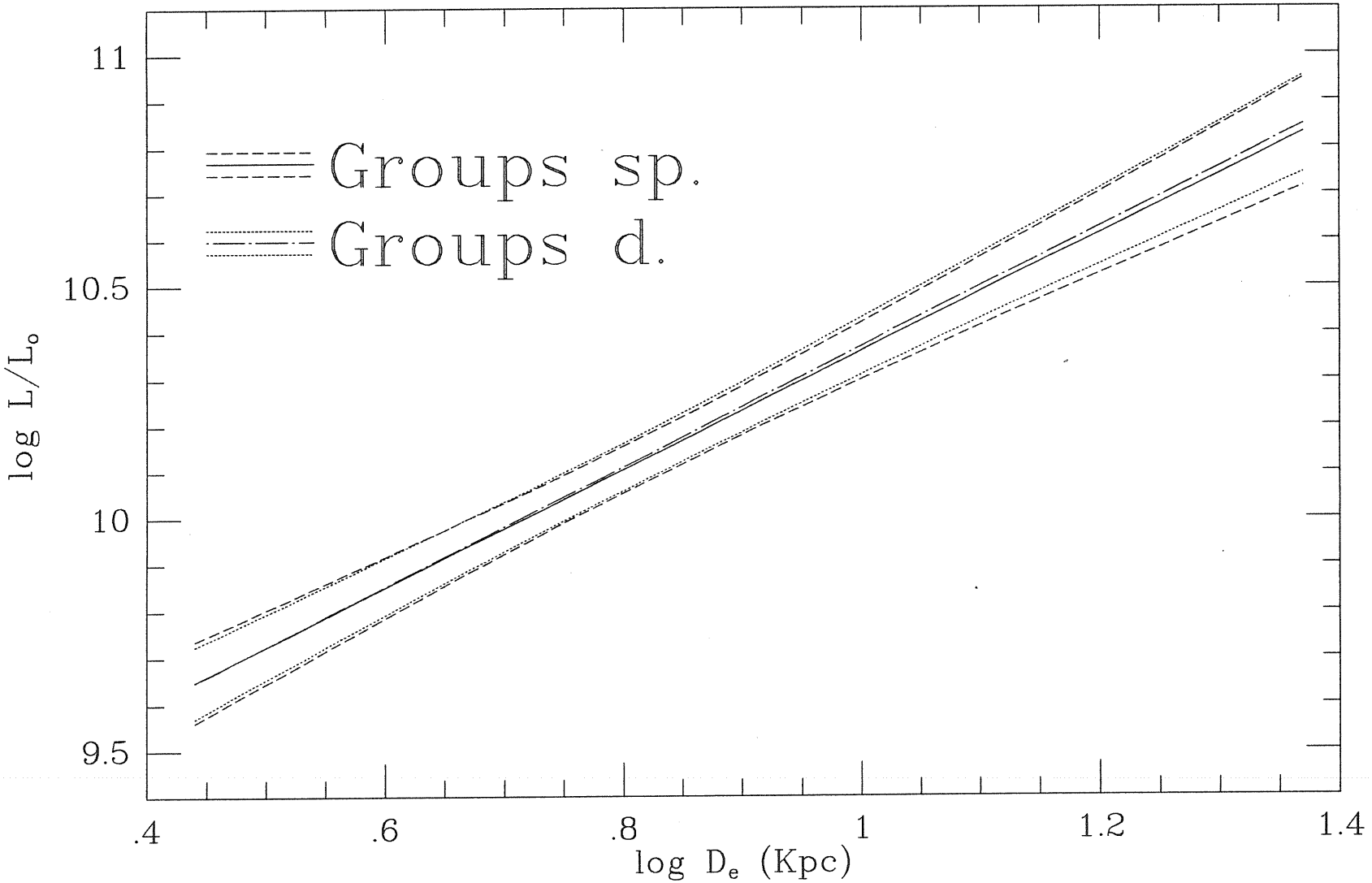

graph. C.53

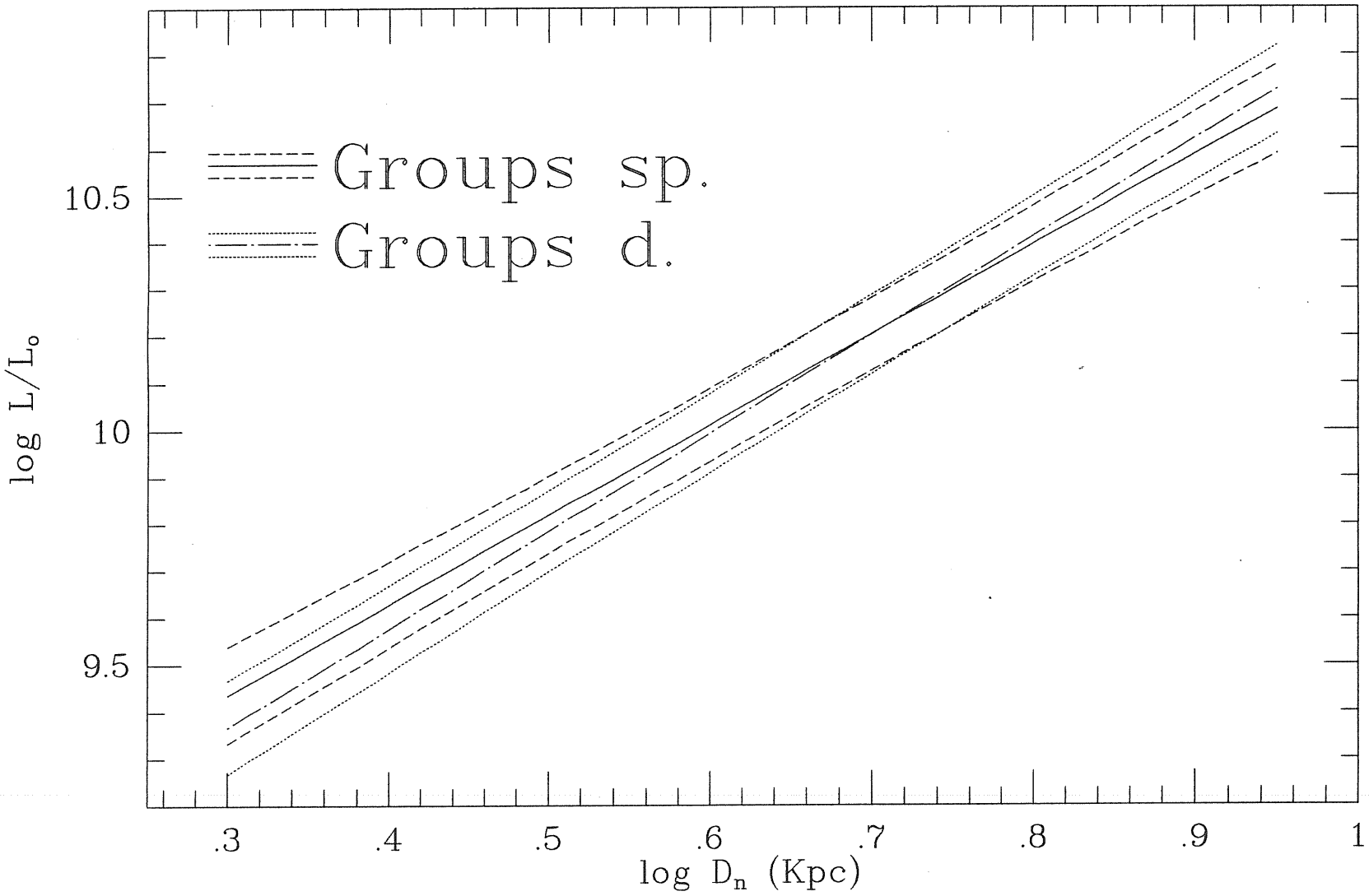

graph. C.54

Bibliography

[1] Aarseth S.J. and Fall S.M. 1980: *Ap. J.;* **236**, *43.*

[2] Aguilar L.A. and White S.D.M. 1985: *Ap. J.;* **295**, *374.*

[3] Alladin S.M. 1965: *Ap. J.;* **141**, *768.*

[4] Alladin S.M., Potdar A. and Sastry K.S. 1075: in *Dynamics of Stellar Systems*; ed. A.Hoyle, p.167.

[5] Balcells M. and Quinn P.J. 1988: *Evolutionary Phenomena in Galaxies.* (I.A.C. conference) in press.

[6] Binggeli B. et al. 1984 *Astron. J.;* **89**, *64.*

[7] Binney J. 1977: *M.N.R.A.S.;* **181**, *735.*

[8] Binney J. and Cowie L.L. 1981: *Ap. J.;* **247**, *464.*

[9] Binney J. and Silk J. 1979: *M.N.R.A.S.;* **188**, *273.*

[10] Burstein D., Davies R.L., Faber S.M., Stone R.P.S., Lynden-Bell D., Terlevich R.J. and Wegner G. 1987 (7S.III): *Ap. J. Suppl. Series;* **64**, *601.*

[11] Burstein D. and Heiles C. 1982: *Astron. J.;* **87**, *1165.*

[12] Burstein D. and Heiles C. 1984: *Ap. J. Suppl. Series;* **54**, *33.*

[13] Capaccioli M. and deVaucouleurs G. 1983 *Ap. J. Suppl. Series;* **52**, *465.*

[14] Capaccioli M. 1987 in *Structure and Dynamics of Elliptical Galaxies.* 47-61. T. de Zeeuw (ed.) I.A.U. Symposium Nr. 127.

[15] Chandrasekar S. 1942: *Principle of Stellar Dynamics*; Dover.

[16] Chandrasekar S. 1969: *Ellipsoidal Figures of Equilibrium*, New York.

[17] Cowie L.L. and Binney J. 1977: *Ap. J.;* **215**, *723.*

[18] Cowie L.L. and McKee C.F. 1977: *Ap. J.;* **211**, *135.*

[19] Cowie L.L. and Sonaglia A. 1977: *Nature;* **266**, *501.*

[20] Cowsik R. and Ghosh P. 1987: *Ap. J.;* **317**, *26.*

[21] Davis R.L., Efstathiou G., Fall M.S., Illigworth G. and Schechter P.I. 1983: *Ap. J.;* **266**, *41.*

[22] Davoust E. P. and Pence W. D. 1982 *Astron. and Astrophys. Suppl Series;* **49**, *517.*

[23] Dekel A., Lecar M. and Shaham J. 1980: *Ap. J.;* **241**, *946.*

[24] deVaucouleurs G. 1948: *Ann. d'Ap.;* **11**, *247.*

[25] deVaucouleurs G. 1958 *Ap. J.;* **128**, *65.*

[26] deVaucouleurs G. 1959: in *Hanbuch der Physik*, vol. 53, S. Flugge ed.; Berlin-Gottingen, Springer-Verlag, p.311.

[27] deVaucouleurs G. 1977: *Ap. J. Suppl. Series;* **33**, *21.*

[28] deVaucouleurs G. and Capaccioli M. 1979: *Ap. J. Suppl. Series;* **40**, *699.*

[29] deVaucouleurs G. and Corwin H. G. 1977 *Ap. J. Suppl. Series;* **33**, *219.*

[30] deVaucouleurs G., deVaucouleurs A. and Corwin H.R. 1976: *Second Reference Catalog of Bright Galaxies*, Austin: University of Texas (RC2).

[31] Djorgowski S. 1986: *Ph. D. Thesis, University of California at Berkeley.*

[32] Dressler A., Faber S.M., Burstein D., Davies R.L., Lynden-Bell D., Terlevich R.J. and Wegner G. 1987 (7S.IV): *Ap. J. Lett.,* **313**, *L37.*

[33] Dressler A., Lynden-Bell D., Burstein D., Davies D., Faber S.M., Terlevich R.J. and Wegner G. 1987 (7S.I): *Ap. J.,* **313**, *42.*

[34] Dressler A. 1984: *Ap. J.;* **281**, *512.*

[35] Efstathiou G. and Jones B.J.T. 1979: *M.N.R.A.S.;* **186**, *133.*

[36] Efstathiou G. and Silk J. 1983: *Found. of Cosmic Phys.;* **9**, *1.*

[37] Fabian A.C. and Nulsen P.E.J. 1977: *M.N.R.A.S.;* **180**, *479.*

[38] Farouki R.T. and Salpeter E.E. 1982, preprint.

[39] Gallagher J.S. and Ostriker J.P. 1972: *Astron. J.;* **77**, *288.*

[40] Gerhard O.E. 1981: *M.N.R.A.S.;* **197**, *179.*

[41] Gherard O.E. and Fall S.M. 1982: preprint.

[42] Giuricin G., Mardirossian F., Mezzetti M., Ramella M. and Pisani A. 1988: in *Evolutionary Phenomena in Galaxies*, I.A.C. conference; in press.

[43] Griersmith D. 1980 *Astron. J.;* **85**, *789.*

[44] Guest P.G. 1963: *Numerical Methods of Curve Fitting*; Cambridbe University Press.

[45] Gunn J.E. and Gott J.R. 1972: *Ap. J.;* **176**, *1.*

[46] Henon M. 1973: in *Dynamical Structure and Evolution of Stellar Systems*; eds. L.Martinet & M.Mayor, p.224.

[47] Hoel P.J. 1971: *Introduction to Mathematical Statistics*, 4^{th} ed. Jhon Wiley & Sons.

[48] Holmberg E. 1958: *Medd. Lunds Astron. Obs. Series*; 2, No. 136.

[49] Hoessel J.G., Oegerle W.R. and Schneider D.P. 1987: *Astron. J.;* **94**, *1111.*

[50] Hoyle F. 1949: *Problems of Cosmological Aerodynamics*, Int. Union Th. & Appl. Mech. &I.A.U. p.195.

[51] Hubble E.P. 1930: *Ap. J.;* **214**, *359.*

[52] Hubble E.P. and Tolman R.C. 1935: *Ap. J.;* **82**, *302.*

[53] Humason M.L., Mayall N.U. and Sandage A.R. 1956: *Astron. J.;* **61**, *97.*

[54] Jedrzejewski R.I. 1987: in *Structure and Dynamics of Elliptical Galaxies*, ed. T. de zeew, I.A.U. Symp. Nr. 127, p. 37.

[55] Jones W.B. et al. 1967 *Publ Dept. Astron. Univ. of Texas*, Austin; ser.2, **1**, No. 8.

[56] Kalnajs A. 1970: in *Gravitational N-body Problem*; ed. Lecar L., p. 13.

[57] Kandrup H.E. 1980: *Phys. Reports;* **63**, *1.*

[58] Keenan D.W. 1981: *Astron. and Astrophys.;* **95**, *340.*

[59] Kent 1984: *Ap. J. Suppl. Series;* **56**, *105.*

[60] Kent S.M. and Gunn J.E. 1982: *Astron. J.*, **87**, *945.*

[61] Kent S.M. and Sargent W.L.W. 1983: *Astron. J.*, **88**, *697.*

[62] King I.R. 1962: *Astron. J.;* **67**, *471.*

[63] King I.R. 1966: *Astron. J.;* **71**, *64.*

[64] Knobloch E. 1978: *Ap. J.;* **222**, *779.*

[65] Kormendy J. 1984: *Ap. J.;* **287**, *577.*

[66] Lake G. 1979: in *Photometry, Kinematics and Dynamics of Galaxy*; D.S. Evans ed., Univerity of Texas Press, Austin, p.381.

[67] Lauer 1985 *Ap. J. Suppl. Series;* **57**, *473.*

[68] Lecar M. 1975:in *Dynamics of Stellar Systems*; ed. A.Hoyle, p.161.

[69] Lynden-Bell D., Faber S.M., Burstein D., Davies R.L., Terlevich R.J. and Wegner G. 1988 (7S.V): *Ap. J.,* **326**, *19.*

[70] Malumuth and Kirshner 1984: *Ap. J.;* **291**, *8.*

[71] Marchant A.B. and Olson D.W. 1979: *Ap. J. Lett.;* **230**, *L157.*

[72] Mattews T.A., Morgan W.W. and Schmidt M. 1964: *Ap. J.;* **140**, *35.*

[73] McKee C.F. and Ostriker J.P. 1977: *Ap. J.;* **218**, *148.*

[74] Merritt D. 1982: preprint.

[75] Merritt D. 1983: *Ap. J.;* **264**, *24.*

[76] Mezzetti M., Pisani A., Giuricin G. and Mardirossian F. 1985: *Astron. and Astrophys.;* **143**, *188.*

[77] Mihalas and Binney 1981: *Galactic Astronomy*; 2^{nd} ed. Freeman & Co., San Francisco.

[78] Nieto J.L. 1987: *Second Extragalactic Astronomy Regional Meeting*; Cordoba, Argentina (preprint).

[79] Nulsen P.E.J. 1982: *M.N.R.A.S.;* **198**, *1007.*

[80] Oemler 1976: *Ap. J.;* **209**, *693.*

[81] Ostriker P. and Cowie L.L. 1981: *Ap. J. Lett.;* **243**, *L127.*

[82] Ostriker J.P. and Tremaine S.D. 1975: *Ap. J. Lett.;* **202**, *L113.*

[83] Peebles P.J.E. 1969: *Ap. J.;* **155**, *393.*

[84] Peebles P.J.E. 1980: *The Large-Scale Structure of the Universe*, Princeton University Press.

[85] Pence W.D. 1976: *Ap. J.;* **203**, *39.*

[86] Pence W.D. and Davoust E. 1985: *Astron. and Astrophys. Suppl. Series;* **49**, *631.*

[87] Richstone D.O. 1975: *Ap. J.;* **200**, *535.*

[88] Richstone D.O. 1979: *Ap. J.;* **234**, *825.*

[89] Sadler E.M. 1984 *Astron. J.;* **89**, *34.*

[90] Sandage A. 1973 *Ap. J.;* **183**, *711.*

[91] Sandage A., Binggeli B. and Tarenghi M. 1982: *Canergie Institution of Washington Yearbook*; **81**, 623.

[92] Sandage A. and Visvanathan N. 1978 *Ap. J.;* **232**, *352.*

[93] Silk J. and Norman C.A. 1981: *Ap. J.;* **247**, *59.*

[94] Spinard H., Smith H.E. and Taylor D.J. 1972: *Ap. J.;* **175**, *649.*

[95] Spitzer L. 1958: *Ap. J.;* **127**, *17.*

[96] Spitzer L. 1962: *Physics of Fully Ionized Gas*; Wiley.

[97] Spitzer L. and Baade W. 1951: *Ap. J.;* **113**, *413.*

[98] Strom S.E. et al. 1976 *Ap. J.;* **204**, *684.*

[99] Strom S.E. et al. 1978 *Astron. J.;* **83**, *73.*

[100] Struck-Marcell C. 1981: *M.N.R.A.S.;* **197**, *487.*

[101] Thuan T.X. and Kormendy J. 1977: *Publ. A.S.P.;* **89**, *466.*

[102] Thuan T.X. and Romanishin W. 1981: *Ap. J.;* **248**, *439.*

[103] Tinsley B.M. and Larson R.B. 1979: *M.N.R.A.S.;* **186**, *503.*

[104] Toomre A. 1977: in *Evolution of Galaxies and Stellar Population*; Eds. Larson R.B.M. and Tinsley M.M., p.401.

[105] Toomre A. and Toomre A. 1972: *Ap. J.;* **178**, *623.*

[106] Tremaine S.D. 1981: in *The Structure and Evolution of Normal Galaxies*; eds. Fall S.M. & Lyndenn-Bell D., p.67.

[107] Tremaine S.D., Ostriker J.P. and Spitzer L. 1975: *Ap. J.;* **196**, *407.*

[108] Weimberg S. 1972: Gravitation and Cosmology, Jhon Wiley & Sons, New York.

[109] White S.D.M. 1976a: *M.N.R.A.S.;* **174**, *19.*

[110] White S.D.M. 1976b: *M.N.R.A.S.;* **174**, *467.*

[111] White S.D.M. 1977: *M.N.R.A.S.;* **184**, *185.*

[112] White S.D.M. 1982: in *Environmental Influences on Galaxy Structure*, eds. L. Martinet & M. Mayor.

[113] White S.D.M. and Rees M.J. 1978: *M.N.R.A.S.;* **183**, *341.*

[114] White S.D.M. and Silk J. 1980: *Ap. J.;* **241**, *864.*

[115] Wirth A. and Gallagher J.S.III 1984: *Ap. J.;* **282**, *85.*

[116] Zel'dovich Ya. B. 1970: *Astron. and Astrophys.;* **5**, *84.*